THE ASTROPHYSICAL JOURNAL

AN INTERNATIONAL REVIEW OF SPECTROSCOPY AND ASTRONOMICAL PHYSICS

VOLUME 86 DECEMBER 1937 NUMBER 5

THE CONTOURS OF $H\gamma$ AND $H\delta$ IN δ CEPHEI

C. J. KRIEGER

ABSTRACT

The contours of $H\gamma$ and $H\delta$ were measured on twenty-five spectrograms and were found to vary within wide limits throughout the period. The half-widths are greatest shortly before maximum light and smallest near minimum light.

With an adopted value of $\log g$ the temperature variation of the atmosphere is determined from Verweij's tables on the Stark Effect. Different temperatures result from half-widths taken at different residual intensities. This discrepancy is attributed to the fact that the variation of the temperature with the depth in the atmosphere was neglected. At residual intensity 0.9 the temperature variation is about 5800°–7100° K, as compared with 5100°–6600°, the average by seven other methods.

I. OBSERVATIONAL MATERIAL AND MEASUREMENTS

The observational material consisted of twenty-five one- and three-prism spectrograms placed at the writer's disposal by the Lick and the Yerkes observatories. Twenty of these spectrograms were used in a previous study[1] and are listed there in Table 1. The additional plates are:

Plate	Date U.T.	J.D.	Phase
IR 9912 (Yerkes)	1931 Oct. 18.218	2426632.718	2.02
IR 9917 (Yerkes)	19.047	2426633.547	2.85
IR 9927 (Yerkes)	21.279	2426635.779	5.09
IR 9929 (Yerkes)	21.402	2426635.902	5.21
17547 (Lick)	1930 Aug. 27.513	2426217.013	4.90

[1] *Ap. J.*, **85**, 304, 1937.

The contours were drawn on microphotometer tracings having a scale of about 3 mm/A near $H\gamma$, and the half-widths were measured at residual intensities $r = 0.9, 0.8, 0.7, 0.6, 0.5, 0.4, 0.3$, and 0.2.

The probable error is estimated to be between 5 and 10 per cent, largely due to the uncertainty involved in drawing the continuous background and the contour itself, especially at the higher residual intensities.

II. VARIATION OF HALF-WIDTHS AT VARIOUS RESIDUAL INTENSITIES

The results of the measurements are collected in Table 1, where the headings of columns 3–10 indicate residual intensities. The symbol x indicates that the measurement is unreliable because the toe or shoulder of the deflection-intensity curve would have to be used. Absence of an entry indicates that measurements were not possible because the contour did not extend to the residual intensity given in the column heading.

In Figures 1 and 2 the half-widths of $H\gamma$ and $H\delta$ at various residual intensities are plotted against phase, while in Figures 3 and 4 the half-contours are shown for various phases. The contours and, of course, the half-widths are largest near phase 5.25, i.e., shortly before maximum light, and smallest near phase 3.5, i.e., near minimum light. The half-widths decrease slowly from maximum to minimum and increase somewhat more rapidly to maximum from minimum. A general agreement with F. L. Whipple's[2] curves in his Figure 5 is noted. He used a smaller number of spectrograms and did not draw smooth curves through the observed points.

III. VARIATION OF TEMPERATURE BASED ON VERWEIJ'S THEORY OF THE STARK EFFECT OF HYDROGEN IN STELLAR SPECTRA

Verweij's[3] work makes it possible to derive the stellar temperature from measured half-widths, provided the surface gravity g is known. The latter is readily calculated if a mean radius R, a pulsational variation ΔR, and the mass μ are available.

[2] *Lick Obs. Bull.*, **16**, 1, 1932.

[3] *Pub. Astr. Inst. Amsterdam*, No. 5, 1936.

TABLE 1

HALF-WIDTHS OF $H\gamma$ AND $H\delta$ IN δ CEPHEI

Phase	Plate No.	0.9	0.8	0.7	0.6	0.5	0.4	0.3	0.2	No. of Tracings
					$H\gamma$					
0.25	17521	8.19	5.2	3.84	2.63	1.68	1.09	.72	.37	1
0.69	IR 9933	8.4	3.9	1.9	1.0	.65	.4	x	x	1
1.32	17482	6.25	4.0	2.5	1.8	1.35	1.0	.55	.15	1
1.84	IR 9910	5.40	3.5	2.4	1.5	.9	.4	0	.....	1
2.02	IR 9912	4.01	2.85	1.91	1.33	.80	.45	x	.....	3
2.29	17484	4.68	2.43	1.93	1.54	1.24	1.04	.62	.....	1
2.81	17539	3.35	2.4	1.75	1.2	.75	.42	.20	.....	1
2.85	IR 9917	4.01	2.82	1.98	1.38	.94	.76	.38	.....	2
2.94	IR 9945	4.40	3.4	2.7	2.1	1.4	.8	.4	.....	1
3.10	IR 9919	3.90	2.9	2.0	1.3	.75	.4	x	.....	1
3.76	IR 9903	3.30	2.3	1.57	.95	.50	x	.....	.....	1
4.05	IR 9954	3.30	2.30	1.65	1.05	.60	.35	.2:	.....	1
4.07	17588	4.75	3.8	2.7	1.95	1.25	.7	.25	.....	1
4.11	IR 9955	4.02	2.69	1.76	1.28	.94	.62	.35	x	3
4.83	IR 9950	5.0	3.42	2.00	1.15	.70	.35	.2	0	1
4.83	17546	5.27	3.29	2.23	1.63	1.21	0.99	0.72	0.25	1
4.90	17547	4.83	3.54	2.62	1.88	1.44	.99	.64	.35	1
4.99	IR 9925	6.5	3.9	2.45	1.55	.90	.5	.3	x	1
5.03	IR 9926	9.58	4.26	2.00	1.03	x	x	x	x	3
5.05	17464	9.34	5.42	3.15	1.97	1.45	1.04	.54	.17	1
5.09	IR 9927	x	3.05	1.85	1.32	1.10	.82	.40	.....	2
5.15	IR 9928	7.97	3.90	2.53	1.77	1.33	1.02	x	.....	2
5.21	IR 9929	12.9	7.58	4.82	3.16	2.08	1.25	x	x	3
5.28	IR 9938	12.2	7.5	4.75	3.25	2.2	1.25	.55	x	1
5.33	17596	10.47	6.79	4.28	2.68	1.60	1.02	.55	.08	1
					$H\delta$					
0.69	IR 9933	4.58	2.64	1.44	.65	x	.....	.....	.....	1
1.32	17482	3.42	2.57	1.81	1.25	.80	.52	.31	.20	1
1.84	IR 9910	2.98	1.87	1.22	.78	.48	.13	.....	.....	1
2.02	IR 9912	3.88	2.44	1.31	.71	.45	.30	x	x	3
2.29	17484	2.89	2.00	1.48	1.09	.84	.78	.37	.....	1
2.81	17539	3.32	2.52	1.65	1.14	.72	.40	.17	0	1
2.85	IR 9917	3.16	2.52	1.76	1.30	.94	.64	.46	x	2
2.94	IR 9945	3.22	2.05	1.64	.94	.60	.32	.10	.03	1
3.10	IR 9919	3.59	2.82	2.04	1.30	.61	x	x	x	1
3.76	IR 9903	3.70	2.86	1.96	1.40	.92	.56	.24	.08	1
4.05	IR 9954	2.60	1.42	.80	.34	0	.....	.....	.....	1
4.07	17588	2.72	2.02	1.48	1.01	.65	.32	.06	.....	1
4.11	IR 9955	3.93	2.62	1.65	1.00	.71	.46	x	x	3
4.83	IR 9950	4.58	2.48	1.44	.85	.52	.26	.....	.....	1
4.83	17546	3.85	3.04	2.32	1.61	1.00	0.56	.37	.28	1
4.90	17547	3.98	3.08	2.22	1.57	1.08	.74	.54	.28	1
4.99	IR 9925	6.09	3.45	2.02	1.22	.72	.46	.20	x	1
5.03	IR 9926	6.57	3.21	1.51	.83	.47	x	x	x	3
5.05	17464	7.60	5.04	3.32	2.03	1.24	.95	.53	.32	1
5.09	IR 9927	5.60	3.23	2.28	1.48	.96	.61	.30	.....	2
5.15	IR 9928	7.76	4.38	2.78	1.65	.88	.46	x	.....	3
5.21	IR 9929	7.46	4.08	2.59	1.68	.92	.45	x	x	2
5.33	17596	7.68	4.54	2.44	1.63	1.12	.70	.36	.08	1

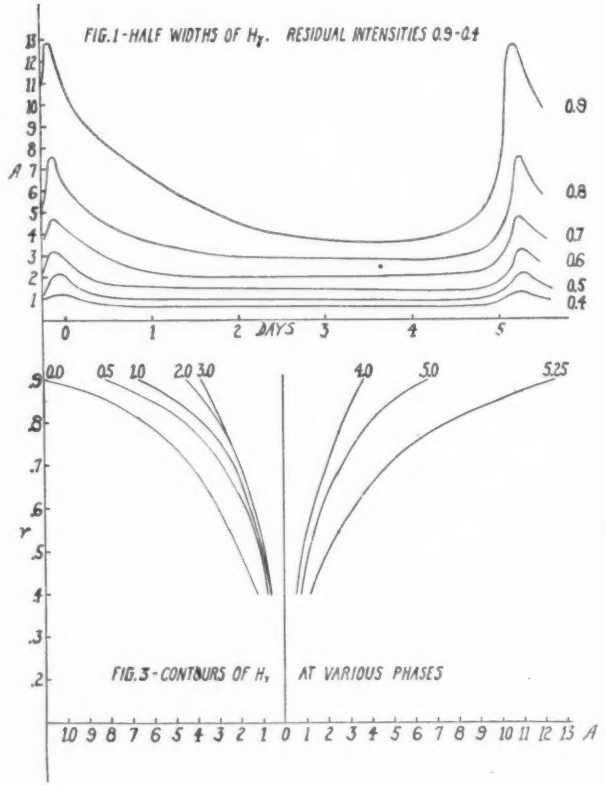
FIG. 1 - HALF WIDTHS OF H_γ. RESIDUAL INTENSITIES 0.9-0.1
A
DAYS
0.9
0.8
0.7
0.6
0.5
0.4
FIG. 3 - CONTOURS OF H_γ AT VARIOUS PHASES
0.0 0.5 1.0 2.0 3.0 4.0 5.0 5.25
Y
A

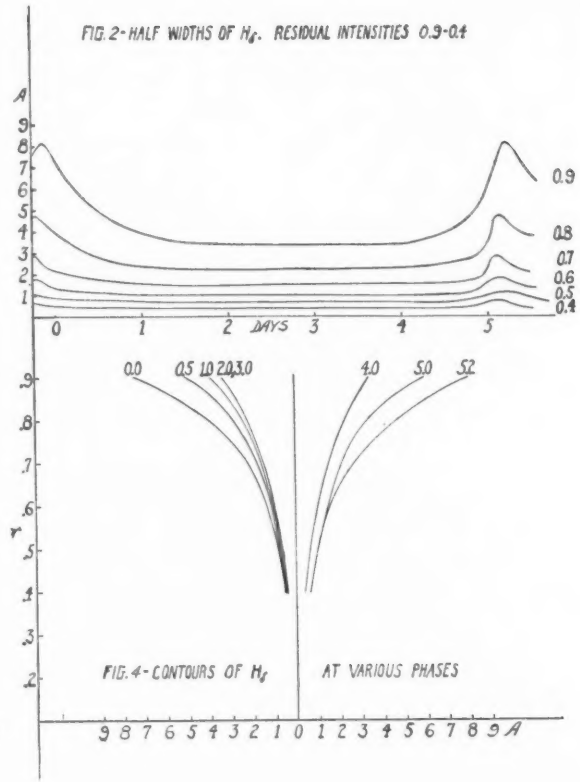
FIG. 2 - HALF WIDTHS OF H_δ. RESIDUAL INTENSITIES 0.9-0.1
A
DAYS
0.9
0.8
0.7
0.6
0.5
0.4
FIG. 4 - CONTOURS OF H_δ AT VARIOUS PHASES
0.0 0.5 1.0 2.0 3.0 4.0 5.0 5.2
Y
A

A mean radius R of 33.9⊙,[4] a variation ΔR of 5⊙, and a mass of 10.5⊙[5] were used, and a mean log g = 2.36 cm/sec² was found. Due to the variation of R, log g varies from 2.30 for maximum radius to 2.43 for minimum radius.

From Verweij's Table 11, families of curves were drawn showing the half-widths of $H\gamma$ and $H\delta$ against the temperature with various surface gravities (log g) and residual intensities. By simple graphical interpolation, using the mean value of 2.36 for log g, the tempera-

TABLE 2

VARIATION OF TEMPERATURE

PHASE	$H\gamma$						$H\delta$						AVERAGE*
	0.9	0.8	0.7	0.6	0.5	0.4	0.9	0.8	0.7	0.6	0.5	0.4	
0.0	7000	6650	6400	6250	6150	5800	6700	6300	5900	5800	5650	(5500)	6280
0.5	6500	6200	6050	5850	5650	5600	6150	6050	5800	5700	5600	(5500)	5950
1.0	6300	6000	5850	5800	5600	5550	5950	5850	5750	5650	5600	(5400)	5830
2.0	5950	5900	5800	5700	5600	5550	5850	5800	5700	5650	5550	(5400)	5750
3.0	5850	5850	5800	5700	5600	5550	5850	5800	5700	5650	5550	(5400)	5730
3.5	5800	5800	5800	5700	5600	5550	5850	5800	5700	5650	5550	5400	5720
4.0	5800	5800	5800	5700	5600	5550	5850	5850	5700	5650	5550	(5400)	5730
4.5	5900	5900	5800	5700	5600	5550	5950	5850	5750	5650	5600	(5400)	5770
5.0	6300	6100	6000	5850	5750	5650	6300	6100	5900	5850	5650	5550	5980
5.25	7400	6950	6550	6350	6150	5800	6850	6350	6000	5900	5700	5550	6420
Amplitude	1600	1150	750	650	550	250	1000	550	300	250	150	(150)	700

* Average from residual intensities 0.9 to 0.5, $H\gamma$ and $H\delta$ (r=0.4 excluded).

tures in Table 2 were found. It was unnecessary to take into account the slight variation of log g, as its effect on the half-width is negligible at the temperatures involved here.

Using residual intensities 0.9–0.5 in both $H\gamma$ and $H\delta$, a mean

[4] Hopmann (*A.N.*, **222**, 1, 1924) ..... 12.5⊙
Pettit and Nicholson (*Mt. W. Contr.*, No. 369, 1928) 15.5
Whipple (*Lick Obs. Bull.*, **16**, 1, 1932) 10.5
Sampson (*M.N.*, **85**, 240, 1925) 52.5
Pannekoek and Ressinck (*B.A.N.*, **3**, 46, 1925) 80.5
Shapley (*Star Clusters*, p. 139) 24.0
Ludendorff (*Handbuch der Astrophysik*, **6**, Part II, 217) 50.0
Russell, Dugan, and Stewart (*Astronomy* **2**, 768, 1927) 25.9

[5] Russell, Dugan, and Stewart, *loc. cit.*

variation from 6420° to 5720° is found. The maximum value is in fair agreement with other determinations, but the minimum value is higher than that derived by most other methods.

The amplitude of the temperature variation depends very decisively on the residual intensity at which the half-width is measured. Higher temperatures and larger amplitudes follow from half-widths measured at the higher residual intensities as compared with measurements at the lower residual intensities. Verweij has himself pointed out that the variation of the temperature with the depth in the atmosphere should be taken into account, although his Table 11 is constructed for constant temperatures.

TABLE 3

r	0.95	0.90	0.80	0.70	0.60	0.50
$\Delta\lambda$.....	8.5	5.4	2.9	1.9	1.4	0.9
T.....	6110°	6000°	5780°	5700°	5620°	5500°

TABLE 4

r	0.95	0.90	0.80	0.70	0.60	0.50
$\Delta\lambda$ observed by Unsöld..	3.9	2.9	2.0	1.5	0.9	0.5
$\Delta\lambda$ predicted by Verweij for $T=5600°$.....	4.0	2.9	2.1	1.6	1.3	1.1

Since the core of the line (small residual intensity) is, in general, formed in layers of small depth, lower temperatures will be found from half-width measurements at $r = 0.4$ and 0.5, as compared with those derived from large residual intensities (0.9 and 0.8), since in this case the active part of the atmosphere lies at a greater depth.

In his Figure 6 Verweij plots an unpublished profile of $H\gamma$ in the sun, measured by Minnaert at the Heliophysical Institute at Utrecht. Table 3 shows the dependence of the temperature on the residual intensity, as determined from Verweij's tables.

Unsöld's observations, listed in Verweij's Table 17, are, at least in the wings, in good agreement with a temperature of 5600°, although in the core the same tendency noted above appears (Table 4).

Verweij's attempt to calculate the contour of $H\gamma$ in the sun with an effective temperature $T_1 = 6300°$, taking into account the variation of the temperature with the depth, is successful only in the sense that the profile so calculated is similar to the one observed, but the half-widths are too large throughout (Table 5).

TABLE 5

r	0.90	0.80	0.70	0.60	0.50
$\Delta\lambda$ observed by Minnaert	5.4	2.9	1.9	1.4	0.9
$\Delta\lambda$ observed by Unsöld	2.9	2.0	1.5	0.9	0.5
$\Delta\lambda$ calculated by Verweij for $T_1=6300°$	10.0	5.3	3.0	1.8	1.3

In view of the disagreements between theory and observation for the sun, no importance is attached to the temperatures given in Table 2 for δ Cephei. They are rather intended to illustrate the power of the methods and at the same time the limitations to which they are subject at present.

I am indebted to Dr. O. Struve and to Dr. H. N. Russell for several valuable suggestions they made when reading the manuscript.

St. Louis University
St. Louis, Missouri
August 14, 1937

PHOTOGRAPHIC STUDIES OF NEBULAE*

FIFTH PAPER

JOHN C. DUNCAN

ABSTRACT

Photographs of nebulae, diffuse and planetary, are *reproduced*. The dark nebulae *Barnard 92 and 93 Sagittarii*, photographed with the 100-inch telescope, show *no change* in an interval of fourteen years. Seventeen bright planetary nebulae were photographed with both short and long exposures. *Faint envelopes* surrounding the Ring Nebula in Lyra and NGC 6826 Cygni are displayed. Four other planetary nebulae exhibit various interesting features.

I. DIFFUSE NEBULAE

Of a number of photographs of diffuse nebulae which have been made since the publication of the fourth paper* of this series, those mentioned below perhaps possess the greatest interest.

Northern Portion of the Nebulous Wreath in Cygnus

$\alpha = 20^h45^m$, $\delta = +31°.7$ (1930.0)

This exceedingly faint, filamentous nebulosity lies near the beautiful and famous "veil" nebulae in Cygnus, NGC 6960 and 6992, being slightly north of them and of intermediate right ascension. The photograph here reproduced as Plate XII covers a part of the field of the excellent 14-hour plate made at Forcalquier by De Kerolyr[1] and has the advantages of somewhat greater scale and resolving power.

Obscured Region in Vulpecula

$\alpha = 19^h39^m$, $\delta = +27°.2$ (1930.0)

The bright star near the center of Plate XIII is BD+27°3471, magnitude 7.1. No luminous nebulosity is noticeable on the plate. The obscuring mass, especially just north of the star referred to, is

* *Contributions from the Mount Wilson Observatory, Carnegie Institution of Washington*, No. 579. Earlier papers are *Mt. W. Contr.*, Nos. 177, 209, 256, 303; *Ap. J.*, **51**, 4–12, 1920; **53**, 392–396, 1921; **57**, 137–148, 1923; **63**, 122–126, 1926.

[1] *L'Astronomie*, **48**, Pl. I, 1934.

PLATE XII

North

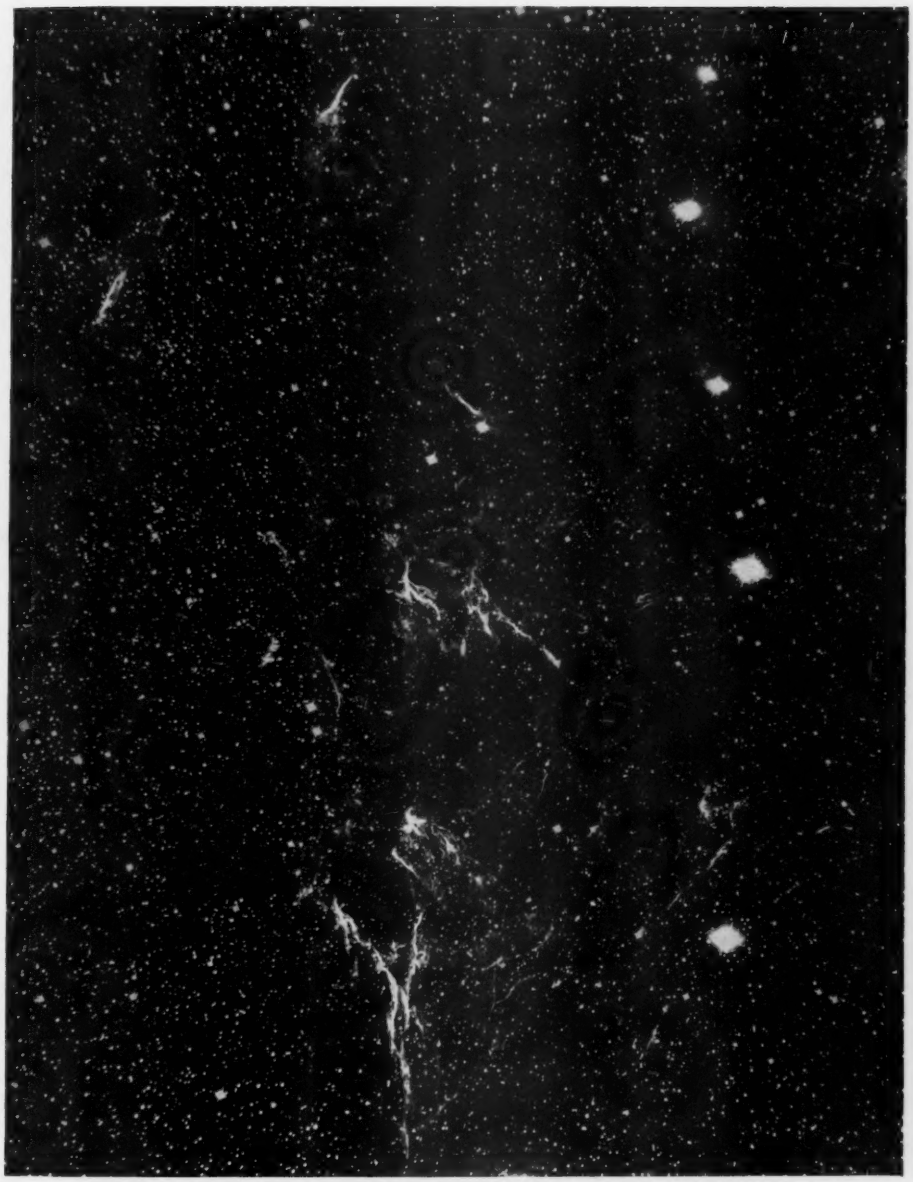

NORTHERN PORTION OF NEBULOUS WREATH IN CYGNUS

Negative Δ399. Photographed with the 100-inch Hooker telescope, August 9–10, 1929, with aperture reduced to 84 inches. Eastman 40 plate. Exposure, 9 hours. Scale: 1 mm = 17″.8.

PLATE XIII

North

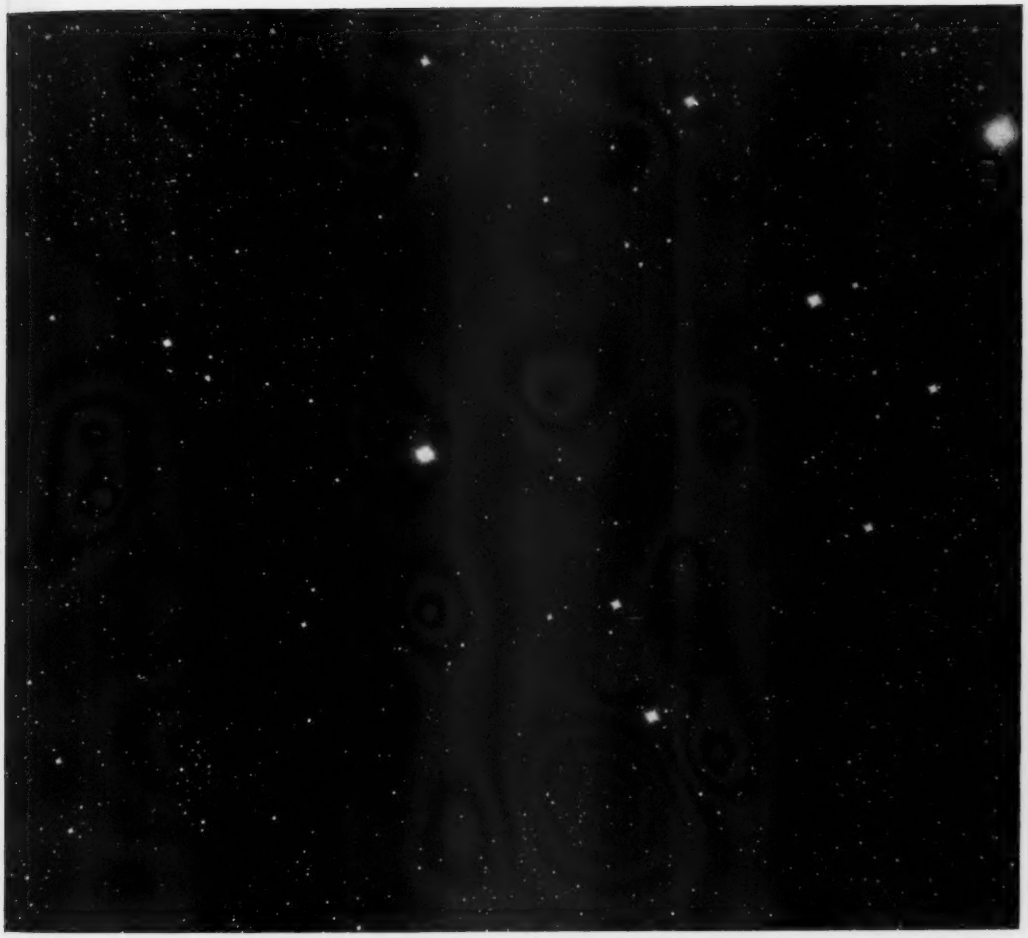

OBSCURED REGION IN VULPECULA

Negative Δ463. Photographed with the 100-inch Hooker telescope, August 19, 1931, with aperture reduced to 84 inches. Eastman Speedway plate. Exposure, 3 hours and 10 minutes. Scale: 1 mm = 21″.2.

North

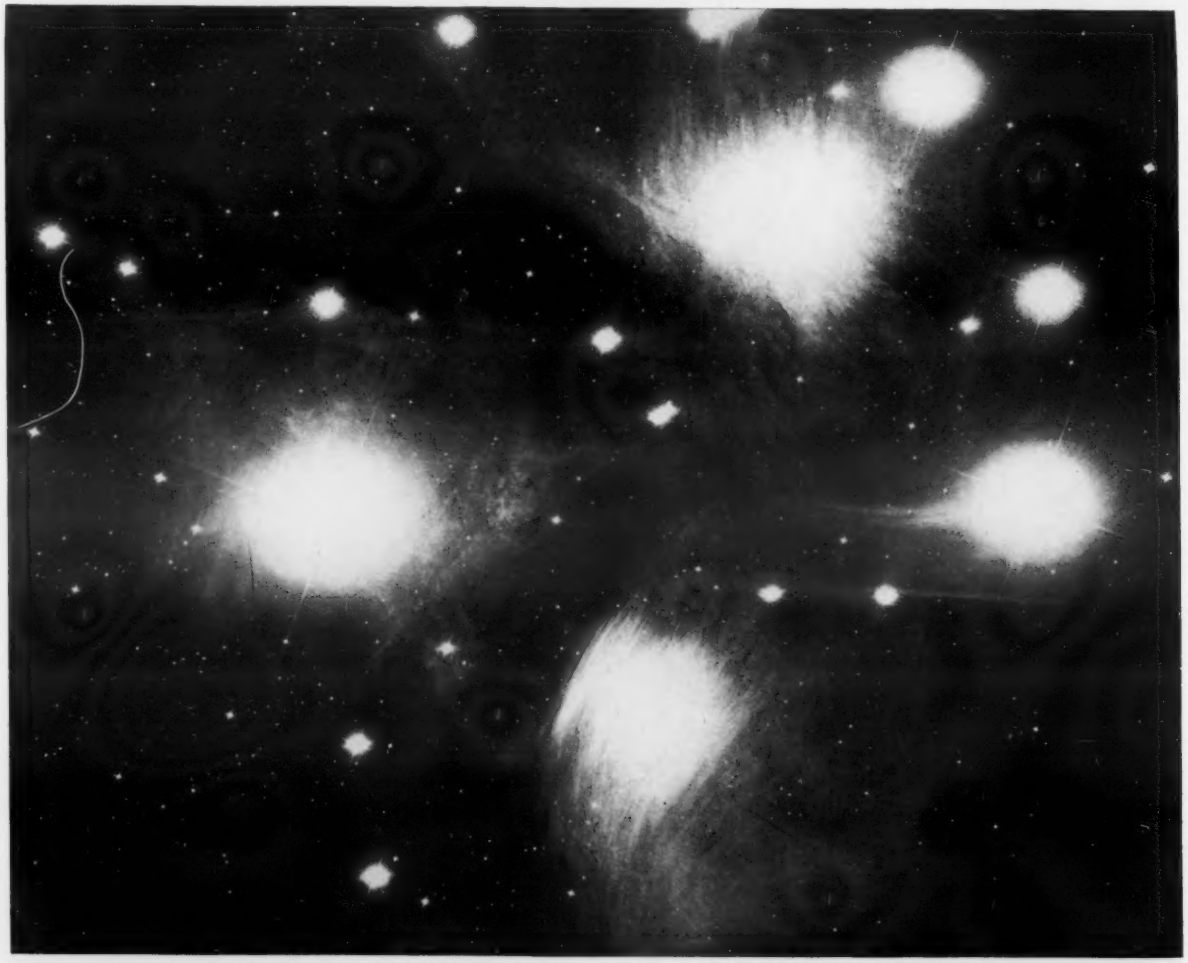

THE PLEIADES

Negative Δ548. Photographed with the 100-inch telescope (aperture reduced to 84 in.) and Ross zero-power correcting lens, August 20, 1933. Imperial Eclipse plate. Exposure, 2 hours and 10 minutes. Scale: 1 mm = 23″.7.

PLATE XV

North

a

b

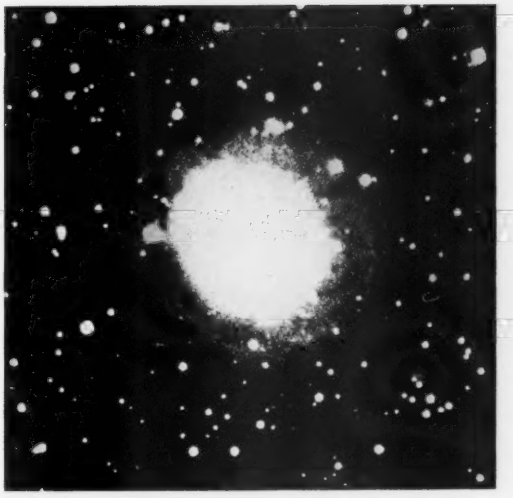

THE RING NEBULA IN LYRA

Photographed with the 100-inch Hooker telescope (aluminum-coated mirrors) and Imperial Eclipse plates. (*a*) Negative Δ554, aperture 84 inches, August 6, 1935; exposure, 15 minutes. (*b*) Negative Δ591, full aperture, August 13, 1936; exposure, 2 hours. Scale of both cuts: 1 mm = 5″.3.

PLATE XVI

North

a

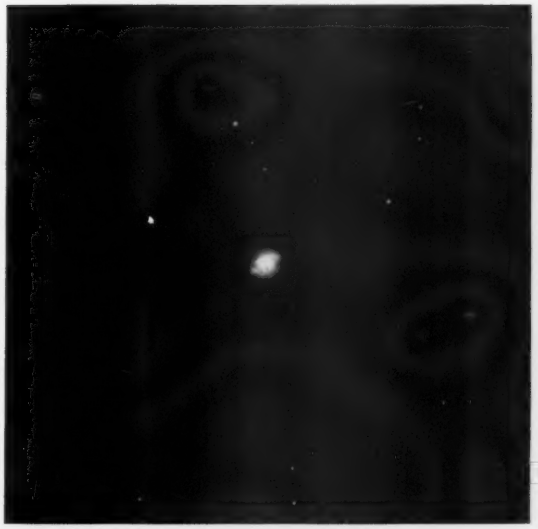

b

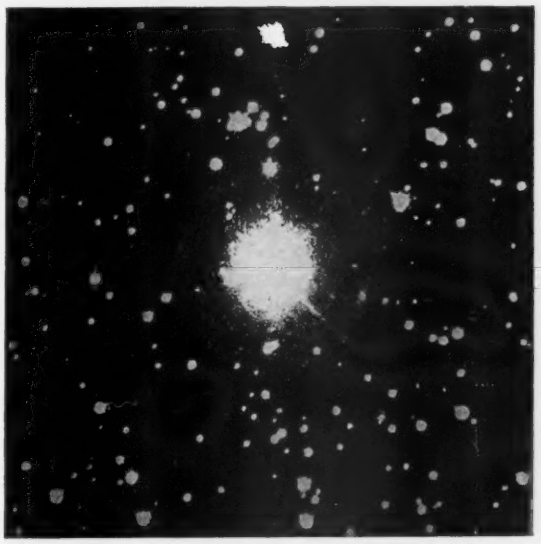

THE PLANETARY NEBULA NGC 6826 CYGNI

(*a*) Negative Δ586, 100-inch telescope, full aperture, August 21, 1936; exposure, 1 minute. Scale: 1 mm = 5″. (*b*) Negative Δ612, 60-inch telescope, full aperture, July 27, 1936; exposure, 1 hour. Scale: 1 mm = 4″.8.

PLATE XVII

North

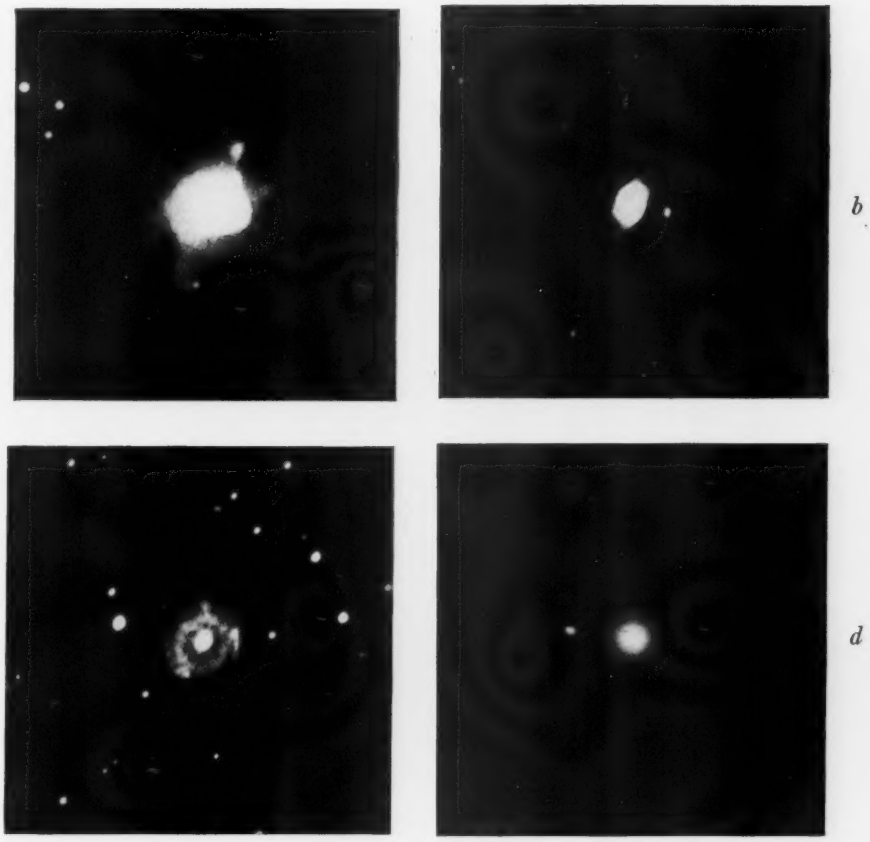

PLANETARY NEBULAE

(*a*) NGC 6210 Herculis (Σ5). Negative Δ564. 100-inch telescope, June 25, 1936. Imperial Eclipse plate. Exposure, 35 minutes. (*b*) IC 4634 Ophiuchi. Negative Δ633. 100-inch telescope, July 12, 1937. Imperial Eclipse plate. Exposure, 1 hour. (*c*) NGC 6751 Aquilae. Negative Δ634. 100-inch telescope, July 12, 1937. Imperial Eclipse plate. Exposure, 20 minutes. (*d*) IC 3568 Camelopardalis. Negative Δ669. 60-inch telescope, August 2, 1937. Eastman 33 plate. Exposure, 10 minutes. For all these photographs the telescopes were used at full aperture and all mirrors were aluminum-coated. The scale of each of the reproductions is 1 mm = 2″.

sharply defined on the following side. The appearance of the region is confirmed by negative Δ460, made the preceding night with an exposure of 3 hours.

The Pleiades

The picture reproduced in Plate XIV, owing to fine seeing and to the use of the Ross zero-power corrector, which improves the quality of off-axis images, is of unusually good quality.

Dark Nebulae Barnard 92 and 93 Sagittarii

Negative Δ568, made with the 100-inch Hooker telescope and an exposure of 2 hours on June 25, 1936, duplicates Δ207, which was made in 1922.[2] Owing to the use of rapid Imperial Eclipse plates and to the new aluminum surfaces of the mirrors, the later plate shows about the same details as the earlier, although made with only half the exposure time. A careful comparison of the two plates in the blink comparator detected no change in the dark nebulae in the fourteen-year interval.

II. PLANETARY NEBULAE

On August 6, 1936, a photograph of the Ring nebula in Lyra revealed a previously unsuspected faint envelope. This is fairly well shown in the lower cut of Plate XV, obtained with a longer exposure than that which was published at the time.[3]

As it seemed likely that this discovery was due partly to the use of the rapid Imperial Eclipse plates and especially to the new aluminum coatings of the mirrors, other bright planetary nebulae were studied to see if they possessed similar attachments. One was found[4] around NGC 6826 Cygni and is shown in the lower cut of Plate XVI. The envelope is sensibly circular, with a diameter of 110″. Its existence is confirmed by plate Δ594, obtained with the 100-inch telescope on August 13, 1936.

The fifteen nebulae listed in Table 1 were photographed with various exposures, including in each case an exposure much longer

[2] *Mt. W. Contr.*, No. 256, Pl. VI; *Ap. J.*, **57**, Pl. X, 1923.

[3] *Pub. A.S.P.*, **47**, 271, 1935.

[4] *Publications of the American Astronomical Society*, **8**, 241, 1936.

than is necessary to burn out all detail in the familiar bright parts; but no more faint envelopes were found. Interesting features were, however, disclosed in the four nebulae shown in Plate XVII.

NGC 6210 Herculis ($\Sigma 5$), on exposures of 35 minutes to 2 hours (100-inch), shows a bizarre form 47″ long. The extensions in p.a. 167°–347°, referred to by Curtis,[5] are not rings as he supposed, but look more like hooks, each ending in a nucleus, the southern one of which appears to be stellar.

TABLE 1

NGC	Longest Exposure	Telescope (Inches)	NGC	Longest Exposure	Telescope (Inches)
6210 Herculis	2^h	100	7008 Cygni	1^h50^m	60
6543 Draconis	1	60	7009 Aquarii	1 50	100
6572 Ophiuchi	0 30^m	100	7026 Cygni	1	60
6751 Aquilae	2	100	7027 Cygni	1	60
6804 Aquilae	2	60	7662 Andromedae	2 10	60
6818 Sagittarii	2	100	IC 4634 Ophiuchi	1	100
6891 Delphini	1 50	100	IC 3568 Camelopardalis	1	60
6905 Sagittae	2	60			

IC 4634 Ophiuchi, with long exposure, exhibits faint hooks, which give it the appearance of being crossed by an integral sign 22″ long.

NGC 6751 Aquilae consists clearly of two concentric rings, the outer one of which is broken up on the south-following side into minute knots or condensations.

IC 3568 Camelopardalis consists of a very bright circular disk 7″ in diameter surrounded concentrically by a faint disk of diameter 16″.

The quality of the illustrations in this *Contribution* is due largely to the skill of Messrs. Ferdinand Ellerman and Edison Hoge, each of whom prepared a number of the prints which were used for reproduction.

CARNEGIE INSTITUTION OF WASHINGTON
MOUNT WILSON OBSERVATORY
August 1937

[5] *Lick Obs. Pub.*, **13**, Pl. XIV, 1918.

THE EXCITATION OF EMISSION LINES IN LATE-TYPE VARIABLES*

A. D. THACKERAY

ABSTRACT

Twelve bright lines observed in Me variables are attributed to resonance excitation, chiefly by lines in the ultraviolet. In particular, *Mg* II 2795 and 2802 will account for *Fe* 4202, 4308, 3852, and *Ti* 4372.

The appearance of a bright line λ 3907 is attributed to excitation by a bright K line at low levels which is masked by an upper layer of absorption.

Five other lines are attributed to intercombination lines of *Fe* II.

The *Mg* II lines can be readily excited by chemiluminescence in the formation of H_2, the most abundant molecule.

The spectra of long-period variables display a large number of extraordinary characteristics which set them apart as objects of special interest. Among the outstanding features of the typical emission spectrum may be mentioned: (*a*) strong hydrogen emission (requiring energy of 10 volts) in atmospheres which otherwise show characteristics of very low temperature; (*b*) forbidden lines of ionized iron appearing simultaneously with low-temperature lines of neutral metals; (*c*) other emission lines not observed in other objects, including such anomalies as bright *Fe* 4202 and 4308 (with a common upper state), simultaneously with absorption lines of the same multiplet.

The strength of the emission lines varies periodically with phase, and Joy[1] has divided the lines into two groups—those which follow the light-curve almost exactly, including the hydrogen lines and others, such as ionized iron, requiring high excitation, and, second, low-temperature lines which appear as absorption lines at maximum light and change into emission on the downward phase, reaching maximum intensity some time before minimum light. One important fact that now appears to be established[2] is that the hydrogen

* *Contributions from the Mount Wilson Observatory, Carnegie Institution of Washington*, No. 580.

[1] *Mt. W. Contr.*, No. 311, p. 28; *Ap. J.*, **63**, 308, 1926.

[2] Merrill and Burwell, *Mt. W. Contr.*, No. 399; *Ap. J.*, **71**, 285, 1930. Shajn, *Zs. f. Ap.*, **10**, 73, 1935.

lines have their origin in a layer below that of the *TiO* band absorption and also of *Ca* II and *Fe* I absorption. This is a surprising conclusion, since it is customary to suppose that emission lines arise in truly chromospheric layers; but one is driven to it in order to account for the anomalous intensities in the Balmer series.

Rosseland[3] has shown how a very extensive atmosphere may give rise to emission lines in B-type stars through ionization followed by recombination, but has indicated that this explanation cannot easily be extended to late-type stars since the emission lines here lie to the violet of the observed peak of the energy-curve, and an atom illuminated by dilute temperature radiation is more likely to perform the cycle of one absorption followed by two emissions (in radiation of longer wave-length) than one in the opposite direction. If this process is invoked to explain the Balmer lines in Me stars, there would have to be an abnormal supply of quanta beyond the Lyman limit at 912 A. A second process, involving chemiluminescence, has been suggested by Russell[4] and Wurm.[5] A third mechanism, suggested by Bowen,[6] providing a beautiful explanation of the anomalous appearance of a few *O* III and *N* III lines in planetary nebulae, depends on the close coincidence of a "primary" emission line (produced in a different way) with a resonance line of some other element.

This discussion deals mainly with possible instances of excitation by the last-named process. It should be emphasized that this process is essentially a secondary phenomenon which cannot be used to explain the appearance of the Balmer lines, resonance lines of *Fe* I, or *Mg* 4571, all of which are marked features of Me variables. But it does provide a satisfactory explanation of peculiar phenomena such as *Fe* 4202 and 4308 and *In* 4511, and aids the identification of weaker emission lines. A systematic search for all the most probable cases of such fluorescence in these stars has been made. The absorption spectra, consisting almost entirely of low-temperature neutral lines of the commoner metals, with a few (e.g., *Ca*, *Sr*, *Ba*) represented in the first stage of ionization, indicate an atmosphere of

[3] *Mt. W. Contr.*, No. 309; *Ap. J.*, **63**, 218, 1926.

[4] *Mt. W. Contr.*, No. 490, p. 14; *Ap. J.*, **79**, 330, 1934.

[5] *Zs. f. Ap.*, **10**, 133, 1935.

[6] *Ap. J.*, **81**, 1, 1935.

exceedingly low temperature and pressure. The absence or great weakness of lines of excitation potential greater than 2 or 3 volts shows that normally atoms can occupy states of only the lowest energy. In a normal star the distribution of atoms in different energy levels approximates a Boltzmann distribution and is determined by collisions, the atmosphere being in local thermodynamic equilibrium. But in the late-type giants pressure and temperature are so low that collision excitation can only maintain atoms in the lowest energy levels, and the atmosphere approximates a state of monochromatic, or more strictly polychromatic, radiative equilibrium. This is consistent with the observed departures from a Boltzmann distribution observed by Adams and Russell[7] in α Orionis.

In order that the suggested process of excitation of secondary emission lines may be effective, various conditions must be satisfied: (1) there must be a departure from local thermodynamic equilibrium, otherwise collisions will be more effective in populating the states than selective absorption of primary emission lines; (2) a primary emission line A must lie very close (within 0.2 A unless it is very strong) to another line B whose lower state should not be greater than 2 or 3 volts E.P.; (3) the line A should not lie beyond 2000 A, otherwise its energy is more likely to be used in ionizing neutral atoms than in line excitation; (4) the upper state of the line B must give rise to other lines C, C′, etc., in the visual region. The strength of the fluorescent line C will depend on a large number of factors, including the strengths of the three lines involved (A, B, and C), the degree of coincidence of A and B, and also the number of lines with the same upper state as B; it is favorable to the production of a strong line if the atom has very few permitted transitions by which it can leave this state.

In searching for relevant instances of this process in Me variables it is important to know what lines should be considered as primary lines A. The presence of bright subordinate lines of *Fe* II and *Si* I leads one to expect that the resonance lines of these elements will be prominent features of the spectrum in the region λ 2300–λ 2700. In order to account for the anomalous appearance of *Fe* 4202 and 4308, we postulate bright *Mg* II 2795 and 2802, although there is no

[7] *Mt. W. Contr.*, No. 359; *Ap. J.*, **68**, 9, 1928.

evidence for this in the visual region except that λ 4571 of the neutral atom becomes the strongest line at just the phase when λ 4202 and λ 4308 are most prominent.[8] The strongest subordinate line of *Mg* II in the visual region, λ 4481, requires 10 volts for its excitation, so that its absence is not surprising. In the extreme ultraviolet, the Lyman series of hydrogen, and perhaps the resonance lines of the more abundant light elements such as oxygen and carbon may be bright; such lines, involving energies of the order of 10 volts, may excite lines of ionized elements but would ionize most of the commoner neutral atoms. Consequently the stronger resonance lines of *Mg* II, *Fe* II, and *Si* I have received greatest attention in this search for relevant coincidences.

Results are shown in Table 1. In the third column the boldface wave-length is that of the assumed emission line A; in the same column appears the coincident line B which raises the atom after absorption to the fluorescent state given in the first column. The strongest lines C from this state in the visible region appear in the fifth column, and, in the next, the observed wave-length of the nearest emission line in variables.

The column headed $\Delta\lambda'$ requires some explanation. In Me variables at maximum phase,[9] emission lines are displaced to the violet relative to the absorption spectrum by an amount corresponding to about 20 km/sec. Joy has found that the displacement decreases later in the downward phase to an apparent zero at minimum. When it is remembered that the evidence favors an origin of the emission lines below the absorbing layer, it will be seen that, if the line B belongs to the normal absorbing layer, the degree of coincidence of the lines A and B is measured by their difference in wave-length when λ_A is decreased by a velocity up to 20 km/sec. The tabulated quantity $\Delta\lambda'$ is

$$\Delta\lambda' = \lambda'_A - \lambda_B ,$$

where $\lambda'_A = \lambda_A$ corrected for a shift of 20 km/sec to the violet. Since many of the bright lines appear at a phase when, according

[8] The possibility that λ 4202 and λ 4308 are excited by the ultraviolet *Mg* II line occurred independently to P. W. Merrill. Two preliminary notes have been published jointly (*Pub. A.S.P.*, **48**, 331, 1936; *ibid.*, **49**, 120, 1937).

[9] Merrill, *Mt. W. Contr.*, No. 264; *Ap. J.*, **58**, 215, 1923.

TABLE 1

EXCITATION OF LINES BY *Mg* II, *Fe* II, *Si* AND *H*

COINCIDENT LINES (A AND B)			$\Delta\lambda'$	LINES C, HAVING SAME UPPER STATE AS B	OBSERVED STELLAR EMISSION	NOTES
Multiplet Designation	Int.	λ				
***Mg* II $3^2S_{\frac{1}{2}}-3^2P^\circ_{1\frac{1}{2}}$**	.....	**2795.52**	.....	.....	.....	
Fe $a^5F_3-w^5D^\circ_4$	2	2794.70	+.63	3852.58(6)	3852.62	
				4373.57(2)	.....	(1)
Mn $a^6S_{2\frac{1}{2}}-y^6P^\circ_{3\frac{1}{2}}$	5	2794.82	+.51	5341.1 (20)	.....	(2)
Fe $a^5D_4-z^3G^\circ_4$	3	2795.00	+.33	3521.27(25)	.....	
				3565.40(60)	.....	(3)
				4202.03(30)	4202.03	
				4307.91(35)	4307.94	
				6191.58(20)	.....	
Fe $a^5F_4-y^5G^\circ_3$	2	2795.54	−.21	4037.69(1n)	.....	(4)
***Mg* II $3^2S_{\frac{1}{2}}-3^2P^\circ_{\frac{1}{2}}$**	.....	**2802.70**	.....	.....	.....	
Ti $a^1D_2-v^1P^\circ_1$	15	2802.47	+.04	4372.41(3)	4372.61	(1)
Fe $a^5D_3-z^3G^\circ_3$	2	2803.16	−.65	3558.53(30)	.....	
				4147.67(10)	.....	
				4250.80(25)	.....	
				4325.77(35)	.....	
***Mg* I $3^1S_0-3^1P^\circ_1$**	.....	**2852.13**	.....	.....	.....	
V $a^4F_{3\frac{1}{2}}-u^4D^\circ_{3\frac{1}{2}}$	6	2851.78	+.16	3912.09(c)	.....	(4)
Fe $a^5F_1-y^5G^\circ_2$	8	2851.80	+.14	3305.75(c)	.....	(4)
***Fe* II $a^6D_{4\frac{1}{2}}-z^6F^\circ_{4\frac{1}{2}}$**	7	**2373.73**	.....	.....	.....	
Fe $a^5D_3-x^5P^\circ_3$	6	2373.62	−.05	4030.19(2)	(4030.51)	
				4001.67(5)	4001.82	
				4138.86(c)	4138.62	(4) (5)
Cr $a^5D_3-t^5F^\circ_4$	15	2373.72	−.15	3367.52(20)	.....	
				3858.90(10)	.....	
***Fe* II $a^6D_{4\frac{1}{2}}-z^6F^\circ_{4\frac{1}{2}}$**	10	**2382.04**	.....	.....	.....	
Fe $a^5D_1-x^5P^\circ_2$	1	2381.83	+.05	3949.96(10)	3949.99	
				3977.75(12)	3977.77	
				4009.72(10)	(4010.4)	
***Fe* II $a^4F_{4\frac{1}{2}}-z^6F^\circ_{4\frac{1}{2}}$**	6	**2484.19**	.....	.....	.....	
Fe $a^5D_1-x^5F^\circ_1$	15R	2484.18	−.16	3016.20(12)	.....	
				3031.64(15)	.....	
				4271.63(c)	.....	(4)
***Fe* II $a^6D_{2\frac{1}{2}}-z^6D^\circ_{1\frac{1}{2}}$**	8	**2607.10**	.....	.....	.....	
Fe $a^5F_4-x^5G^\circ_5$	6	2606.82	+.11	4163.65(c)	.....	(4)
***Fe* II $a^4D_{3\frac{1}{2}}-z^4P^\circ_{2\frac{1}{2}}$**	9	**2562.54**	.....	.....	.....	
Fe $a^5F_3-19^\circ_3$	2	2562.22	+.15	4181.76(15)	.....	(6)
***Fe* II $a^4D_{\frac{1}{2}}-z^4D^\circ_{1\frac{1}{2}}$**	4	**2761.81**	.....	.....	.....	(7)
Fe $a^5F_2-w^5D^\circ_2$	18	2761.78	−.15	3753.62(8)	.....	
				3807.54(7)	.....	
				4058.76(3)	.....	

TABLE 1—*Continued*

Coincident Lines (A and B)			Δλ′	Lines C, Having Same Upper State as B	Observed Stellar Emission	Notes
Multiplet Designation	Int.	λ				
***Fe* II a^{4}D$_{1½}$—z^{4}D$^\circ_½$**	7	**2736.97**	.....	.....	.....	
Fe a^{5}F$_2$—55$^\circ_2$	(c)	2736.96	−.17	4229.40(c)	4229.35	(4) (8)
***Si* I 3p^{3}P$_2$—4s^{3}P$^\circ_2$**	15R	**2516.12**	.....	.....	.....	
Fe a^{5}F$_4$—z^{3}H$^\circ_4$	1	2516.25	−.30	3981.78(7)	.....	
				4021.87(12)	.....	(9)
***Si* I 3p^{3}P$_1$—4s^{3}P$^\circ_1$**	8R	**2519.21**	.....	.....	.....	
Ti a^{3}F$_2$—s^{3}D$^\circ_2$	8	2519.07	−.03	3204.87(6)	.....	
				3216.19(3)	.....	
Hδ	.....	**4101.75**	.....	.....	.....	
In 5^{2}P$_{½}$—6^{2}S$^\circ_{½}$	.....	4101.72	−.24	4511.31(8)	4511.41	(10)

NOTES TO TABLE 1

(1) λλ 4372.41, 4373.57 may be blended to give observed λ 4372.61.
(2) Probably masked by band absorption and *Fe* 5341.03.
(3) Observed in *o* Ceti. *Pub. A.S.P.*, **49**, 120, 1937.
(4) C weak.
(5) C blended with Fe^+ 4138.36.
(6) Absorption at this wave-length shows incipient emission on Mount Wilson coudé spectrogram of *o* Ceti.
(7) A weak.
(8) B and C calculated; C, *Fe* b^{3}F$_2$ — 55$^\circ_2$; λ 4229.35 observed by Joy in *o* Ceti.
(9) Line observed by writer at λ 4021.73 on one Mount Wilson plate of *o* Ceti.
(10) *Mt. W. Contr.*, No. 517; *Ap. J.*, **81**, 467, 1935.

to Joy, the shift is considerably less, the correction may have been overestimated; however, if the shift is interpreted as a velocity of expansion integrated over the whole disk, the true relative velocity must be greater.[10]

In assuming the line B to belong to the normal absorbing layer, we are led into a difficulty. Since it is clear that the lines B and C must belong to the same layer, the fluorescent line should on this assumption show a shift corresponding to the absorbing layer. Although the lines λλ 3852, 4372, 4511 do in fact lie slightly to the red of their normal positions (relative to the other bright lines), as they should on this hypothesis, the strongest and best determined

[10] This point was raised by Professor Bowen in verbal discussion.

lines, λ 4202 and λ 4308, are in almost perfect agreement with their normal wave-lengths. The explanation may be that these strong lines take up an outward velocity owing to radiation pressure. A further complication arises when one considers the phenomenon predicted by Weisskopf[11] that an atom absorbing radiation deviating slightly from its normal frequency should emit a doublet, one component having the natural frequency, the other that of the incident radiation. The whole question of shifts of the emission lines appears too complex for a solution at present. It would, however, be an interesting test of Weisskopf's theory and of the mechanism discussed here to examine with high dispersion a line like *In* 4511 for possible duplicity (the predicted separation in this case being about 0.2 A).

One possible case of resonance excitation, although not included in Table 1, is of special interest. The line *Sc* 3933.37 ($a^2D_{1\frac{1}{2}} - y^2F^\circ_{2\frac{1}{2}}$) lies 0.3 A to the violet of the calcium K line, which is a broad absorption line in Me variables. A bright line is observed at λ 3907.53, close to *Sc* 3907.48 ($a^2D_{2\frac{1}{2}} - y^2F^\circ_{2\frac{1}{2}}$), and it is possible that this line is excited by a bright K line[12] which is blotted out by the superposed absorbing layer, just as *Hε* is obscured by *Ca* 3968. The assumption is involved that the upper layer is much more transparent to *Sc* I than *Ca* II radiation. No other suitable lines are blended with either H or K.

Examination of Table 1 shows that on the whole the observations support remarkably well the hypothetical method of excitation. In particular, the attribution of a common origin to the lines λλ 4202, 4308, 3852, and 4372 is consistent with the observed variations of intensity with phase. Moreover, if no bright line is observed near the predicted wave-length, that fact can nearly always be attributed to blending or weakness of one or more of the lines. There is one outstanding exception. If *Mg* II 2795 is broad enough to excite λ 3852 through the line *Fe* 2794.70, 0.63 A to the violet, *Mg* II 2802 should be broad enough to excite λ 4250 and λ 4325 through the line *Fe* 2803.16 lying a similar distance to the red; yet these lines

[11] *Observatory*, **56**, 302, 1933.

[12] Bright fringes to the infrared *Ca* II triplet have been observed by Merrill in R Hydrae. Bright cores to H and K lines are observed in most M dwarfs.

appear as pure absorption. There appear to be two possible explanations. It is probable that, even if there is strong *Mg* II emission at the level of hydrogen emission, considerable self-reversal will be produced by the absorbing layer above. The result will be a contour of absorption bounded on the violet edge by emission. In fact, such a contour is observed at certain phases in many lines, including *Mg* 4571. This condition will intensify the apparent shift to the violet and weaken the bright edge to the red. A second possibility is that the *Mg* II lines have an intrinsic violet shift greater than normal. For the resonance line of a light atom this is not an unreasonable assumption; unexplained differential shifts have been observed in some lines,[13] including *Hα*. The only other unobserved line in Table 1 that might be expected to appear, in spite of a strong neighboring *Fe* line, is *Cr* 3858.9.

Of the remaining unidentified bright lines in Me variables, a number can be attributed to intercombination lines of *Fe* II. Such lines appear to be readily excited in emission in these stars, perhaps owing to lack of self-reversal; noteworthy examples are *Mg* 4571 and *Fe* I multiplets ($a^5D - z^7P^\circ$, $a^5D - z^7F^\circ$). Five such identifications are given[14] in Table 2. All these lines appear to be brightest at maximum phase, in accordance with the normal behavior of *Fe* II lines, and they tend to have wave-lengths corresponding to a slightly smaller velocity, as Joy has found for *Fe* II lines in *o* Ceti. Although all faint lines, they are mostly strong representatives of their multiplets, and other members are frequently masked by blends.

As stated previously, the proposed method of excitation cannot account for the primary emission lines. It is interesting to note that chemiluminescence can be invoked to provide a powerful means of production of bright lines of *Mg* II. According to Russell,[4] H_2 is by far the most abundant molecule in M-type giants and, moreover, its concentration is very sensitive to temperature, varying by a factor of 10 through the range observed in these variables. When two *H* atoms combine to form a molecule, the energy of formation

[13] Joy, *Mt. W. Contr.*, No. 311, p. 22; *Ap. J.*, **63**, 302, 1926.

[14] Wave-lengths are taken from terms given by Dobbie, *Proc. Roy. Soc.*, A, **151**, 703, 1935.

must be taken up by a third body. If the newly formed molecule is in the lowest vibrational state, this energy is 4.45 volts, corresponding to 2770 A. Owing to the complex molecular states, this method of excitation is much coarser than line fluorescence, which depends on a very close degree of coincidence; but the most suitable atoms to absorb this energy are those with strong absorption lines lying to the red of λ 2770, since part may be taken up as kinetic energy. The formation of H_2 (and of *NH*, another abundant molecule with dissociation potential 4.4 volts) is therefore most likely to excite *Mg* II atoms, with consequent emission of λ 2795 and λ 2802. It is interesting to note that *Fe* 4202 and 4308, here attributed to excita-

TABLE 2

Observed λ (Me Stars)		Fe II Identification	
Joy	Merrill	λ	Multiplet
3938.44	3938.32	.30	$a^4P_{2½}-z^6D^\circ_{2½}$
.....	4070.1	.02	$a^2D_{2½}-z^4F^\circ_{2½}$
4119.60	4119.58	.52	$a^2D_{2½}-z^4D^\circ_{2½}$
4122.77	4122.74	.67	$b^4P_{2½}-z^4F^\circ_{2½}$
4461.31	.....	.43	$b^4P_{2½}-z^6P^\circ_{2½}$

tion by *Mg* II, are brightest at just that phase of decreasing light when recombination must be proceeding most rapidly.

In conclusion, we may offer a physical picture of long-period variables, suggested by the present discussion. At minimum we suppose the star surrounded by an atmosphere in which atomic *H* and molecular H_2 predominate. The "veil theory" supposes that molecular clouds absorb radiation until the temperature rises to the point at which they are dissipated. The radiation streams through until the temperature falls below the condensing-point, then the cycle begins again. Since H_2 has no resonance bands in the visible region, it can only indirectly obstruct the passage of radiation by inelastic collisions with excited atoms, thus acquiring vibrational energy. This presumably occurs with resulting increase in temperature, but mainly in the lower layers of greater pressure. (The almost universal instability of cool stars may well be connected with the

fact that unexcited H_2 molecules can readily absorb radiation in the visible region in this way, while H atoms cannot; dissociation of molecules must have a profound effect on the physical conditions.) The molecules will acquire outward momentum in these collisions with atoms which are subject to radiation pressure. The bright lines of hydrogen can be attributed to dissociation of H_2 and possibly H_2^+ in the lower layers, the appearance at maximum being consistent with the phase of dissipation of the clouds. The recombination of H_2 molecules gives rise to bright *Mg* II with secondary excitation of *Fe* 4202 and 4308; *Mg* 4571 and the low-temperature *Fe* multiplets can arise both through chemiluminescence and through atomic recombinations as the temperature falls.

The author's cordial thanks are due to Dr. P. W. Merrill and to Professor A. H. Joy for many helpful discussions on matters relating to long-period variables, and for the loan of many of their plates for inspection; also to Director W. S. Adams for a night's use of the 60-inch telescope for a long exposure on *o* Ceti.

Carnegie Institution of Washington
Mount Wilson Observatory,
Solar Physics Observatory
Cambridge
July 1937

INFRARED STELLAR SURVEYS AND INDEX SEQUENCES

CHARLES HETZLER

ABSTRACT

A discussion of spectral radiation and photometry is followed by the development of the use of the outstanding infrared indices of long-period variables and "infrared stars" as a method for the detection and classification of these objects. The reddest stars in eight fields of 50 sq. deg. have been catalogued and charted.

No infrared indices (visual to 8500 A) have been found greater than about 9 or 10 mag., which seems to be a critical limit, since a considerable fraction of the sky—about 3000 sq. deg.—has been covered to the eighth magnitude (for Ao stars). New red variables are among the stars listed, most of which are probably giants. No proper motions have been noted for the brighter ones by superposition of the plates. Four intrinsically faint (visually) proper-motion stars, Wolf 359, M_v 16.5; o^2 Eridani C, M_v 12.3; Barnard's star, M_v 13.7; and CC 1382, M_v 11.8, have been found to have infrared indices of 5, 2.8, 3.0 and 2.5 mag., respectively.

With one possible exception, no infrared Algol stars have been found on a number of survey plates examined for this purpose. Attention is called to certain other stars which may be suspected of duplicity, there being possible infrared companions.

INTRODUCTION

The author has two distinct, yet related, infrared stellar surveys in progress: (1) a study of the infrared curves of representative long-period variables has been carried on for four years (a report was made at the end of two years of work,[1] and a second is contemplated in the near future); (2) an infrared survey with effective wavelength 8500 A has been made of considerable portions of the Milky Way, the main purpose being the detection of "infrared stars," i.e., stars whose blue and infrared magnitudes differ more than 5 mag. This survey was tentatively started with the 24-inch reflector but was continued with the 10-inch Bruce telescope in order to obtain larger fields. The present paper deals particularly with this second survey, but some remarks on spectral radiation and photometry applicable to both surveys are included.

SPECTRAL RADIATION AND PHOTOMETRY

A convenient relationship of the general form[2]

$$T = \frac{a}{I_{(\lambda_1-\lambda_2)} + b}$$

[1] *Ap. J.*, **83**, 372, 1936. [2] Russell, Dugan, and Stewart, *Astronomy*, **2**, 733, 1927.

between the temperature, T, and the color index, I, between any two wave-lengths, λ_1 and λ_2, can be readily deduced assuming black-body radiation, provided the temperatures are not very high or the wave-lengths very long. Such a formula is useful for many purposes, but for a clear picture of the relation between temperature and energy at various wave-lengths, Table 1, and its plot with color index as ordinate, is believed to be particularly instructive. In the table relative energies are given in magnitudes, the zero point being the energy at 10,000° and 5600 A (close to the visual region of an Ao star), and bodies of this temperature have been assumed to have zero index between any two wave-lengths whatever. The wave-lengths represented are those near which I have worked by using various plate and filter combinations. In Plate XVIII is shown a series of diffraction images for the determination of these effective wave-lengths, produced by an objective grating. The grating wires were 0.0395 inches in diameter, separated by spaces of equal size. With the 24-inch reflector this gives a separation of 2 mm between the two first-order images at 8500 A. Most of the wave-length regions are sharply defined and are nearly identical for widely different stellar types, but for the M and Q infrared plates no filter cutting sharply at sufficiently long wave-lengths has so far been procurable, with the resulting spread and difference in wave-lengths for different stars. With a long-focus refractor this difficulty can be largely offset by a proper focus,[1] but for a reflector either a more suitable filter or a more nearly monochromatic plate is desirable for most kinds of photometric work. The M and Q plates have been used only at the maxima and minima of a few variables, to determine the magnitude ranges, which are independent of the comparison stars as long as the same ones are always used. The Bruce survey has been at 8500 A, and the sharp focus helps to make the effective wave-length about the same for all spectral types.

In Table 1, column 10 gives the ordinary color index; column 10 plus column 11 is the "red index," being about 1.5 times the color index—in general agreement with the observations.[3] Column 12 gives the *infrared index*, the difference between the yellow and infrared magnitudes. Column 12 added to column 10 more than doubles

[3] *Ap. J.*, **82**, 80, 1935.

PLATE XVIII

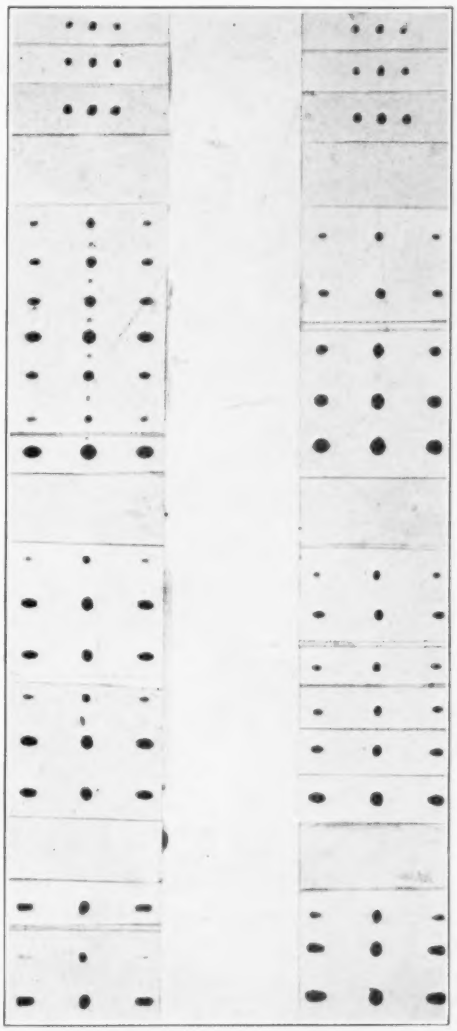

EFFECTIVE WAVE-LENGTHS WITH VARIOUS PLATE AND FILTER COMBINATIONS FOR RED AND BLUE STARS

Twenty-four-inch reflector plus grating of 0.079-inch space; enlarged about 7×. The effective wave-lengths are longer for the variables at minimum by about 25 A. For the "ultra" and P plates the effective wave-lengths are longer by 50 to 100 A for infrared stars than for blue; for the M and Q plates the difference is about 300 A.

TABLE 1

RELATIVE ENERGY OF A BLACK BODY AT DIFFERENT TEMPERATURES AND WAVE-LENGTHS, IN MAGNITUDES

APPROXIMATE SPECTRAL TYPE	TEMP. (DEGREES)	RELATIVE ENERGY						INDICES					ENERGY RATIOS		
		U.V. 3600 A	Blue 4400 A	Yellow 5600 A	Red 6400 A	Infrared		U.V. to Blue	Blue to Yellow	Yellow to			Blue to 8500 A	Yellow to 8500 A	Red to 8500 A
						8500 A	9300 A			Red	8500 A	9300 A			
O.....	25,000	− 3.7	− 3.0	− 2.1	− 1.6	− 0.5	0.1	0.6	−0.2	−0.2	− 0.4	− 0.8	2.5	1.6	1.1
B.....	20,000	− 3.2	− 2.5	− 1.7	− 1.2	− 0.2	0.2	0.6	−0.1	−0.2	− 0.3	− 0.5	2.3	1.5	1.0
A.....	10,000	− 0.8	− 0.7	0.0	0.3	1.2	1.4	−0.0	0.0	0.0	0.0	0.0	1.9	1.2	0.9
K.....	5,000	3.5	3.0	2.8	2.9	3.2	3.3	−0.6	0.9	0.2	0.8	0.9	0.2	0.4	0.3
M.....	3,000	8.9	7.8	6.6	6.1	5.6	5.6	−1.2	1.9	0.8	2.2	2.4	− 2.2	− 1.0	−0.5
N.....	2,000	15.5	13.8	11.2	10.2	8.7	8.4	−1.8	3.3	1.3	3.7	4.2	− 5.1	− 2.5	−1.5
I.....	1,600	20.4	18.1	14.7	13.3	11.0	10.6	−2.4	4.1	1.7	4.9	5.5	− 7.1	− 3.7	−2.3
—.....	1,000	35.0	31.4	25.0	22.3	17.6	16.7	−3.7	7.1	3.0	8.6	9.7	−13.8	− 7.4	−4.7
—.....	800	44.6	40.1	32.1	28.4	22.1	20.7	−4.6	8.7	4.0	11.2	12.8	−18.0	−10.0	−6.3

the base line of the color index. The ultraviolet index, column 9, and the far-infrared index, column 13, extend the base line still farther. It may be remarked that the ultraviolet indices, determined by me in a previous paper,[3] agree closely with those of the table for both a B2 and an Ma star. The ratios of the last three columns of the table are useful in determining exposure times when the relative speeds of plates are known for any typical star. The exposure times on blue sensitive and on panchromatic plates are roughly equal to those in the infrared (both for P and for M plates) for stars of infrared indices of 6 and 8 mag. For low-temperature stars of still greater indices the advantage of the infrared emulsions builds up very rapidly, both in theory and in practice. With any telescope it is now possible to photograph additional stars on infrared emulsions faster than on any other emulsion. The two principal reasons for this, aside from the plate speed, are: (1) there exists a number of at least fairly infrared stars; (2) infrared photography is almost unlimited as to length of exposure, due to greatly lessened sky brightness. A comparison of columns 7 and 8, or of columns 12 and 13, indicates that low-temperature bodies are conspicuously brighter at 9300 A than at 8500 A relative to stars earlier than M. For some of the red variables this was verified empirically, particularly at their minima (W And, R Cas, R Vul, and others), though conceivably this might be interpreted as being partly caused by differential absorption in the stellar atmospheres. The coolest stars might readily be picked out by using twin cameras, one at 8500 A and the other at 9100 A, since the exposure times with the P and M emulsions are nearly the same for the cooler stars. The method actually used by me, however, was adapted to the apparatus at hand and has some advantages, as described below.

A SURVEY OF INFRARED STARS

Infrared indices and the detection of very red stars.—Observationally, the infrared index (the magnitude at 5600 A minus the magnitude at 8500 A), assumed to be zero for Ao stars, is about 1.5 mag. for type K, 3 mag. for type M, and as high as 8 mag. for a few late M- and S-type variable stars at minimum.[1] The infrared intensity of some of these stars is so outstanding that often the variable is the only star showing on an infrared plate covering several square de-

PLATE XIX

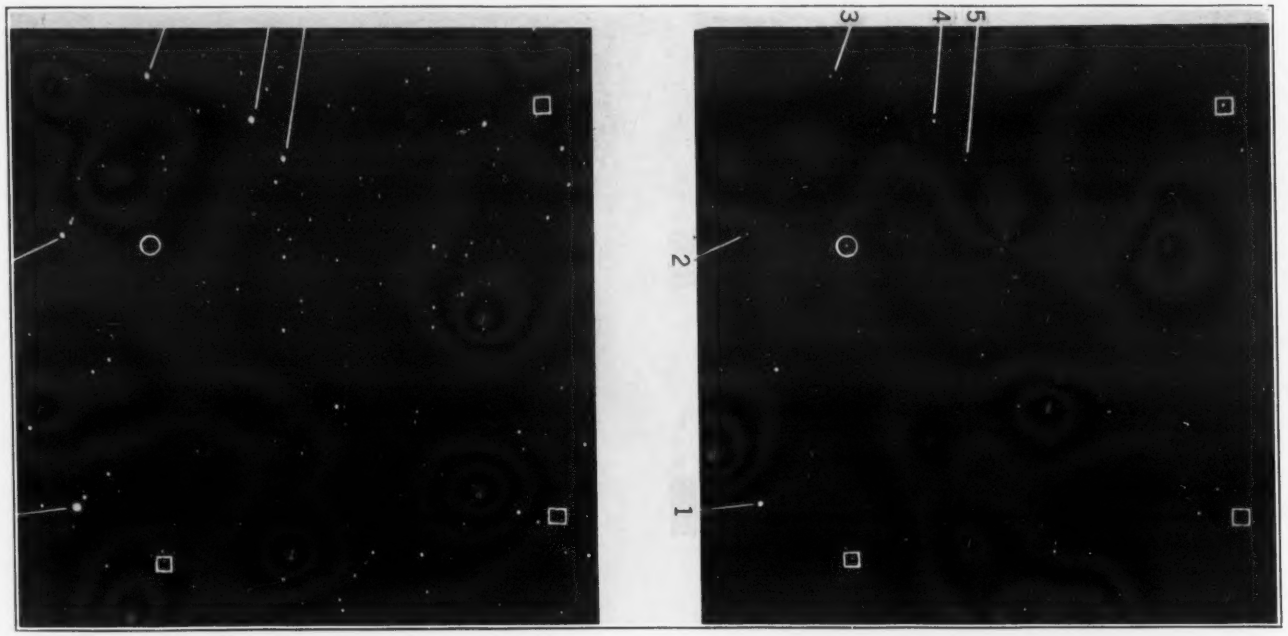

ENLARGED (ABOUT THREE TIMES) INFRARED AND BLUE (*left*) PHOTOGRAPHS OF THE SAME REGION IN CEPHEUS WITH THE 24″ REFLECTOR

The encircled "infrared star" (see Fig. 1, Field I, Chart 1) does not show on the blue plate, while those in squares have only weak photographic counterparts. Stars of varying degrees of infraredness and blueness are seen (see key, p. 513, Table 2*a*).

grees. The inference was natural that here was a method for the discovery of new red variables and generally of stars that are too red to be recorded on ordinary plates. Among known but unclassified variables, those of long period could be separated from the other variables; the ones of largest infrared index could be selected, and a critical limit could be defined. A few faint dwarf stars may be found, in addition. The method should also uncover peculiar reddened stars, as well as red companions to bluer stars, these being conspicuously stronger in the infrared than would be expected from the spectral type. For example, infrared Algol stars may be found showing early-type spectra, and certain peculiar variables may prove to have a red variable as one component.

TABLE 2*a*

KEY TO PLATE XIX

No.	HD	Ptm. Mag.	Sp.	No.	HD	Ptm. Mag.	Sp.
1.....	208501	6.01	B9	4.....	209146	7.26	Fo
2.....	208948	9.0	A3	5.....	209089	8.7	Bo
3.....	209217	8.1	A2				

Trial surveys with the 24-inch reflector, showing infrared images to the tenth magnitude for Ao stars, have revealed occasional strong images where none is seen near the limit of the blue-sensitive plates and where only faint images are seen on panchromatic plates. Such stars are very faint visually and are estimated to have visual to infrared indices of at least 9 mag., the photographic to infrared index being unknown for the fainter ones. The very red stars are easily detected by blinking (see Pl. XIX of which the key is given in Table 2*a*), since only bright or fairly red stars show at all on the infrared plates.

It was decided to use the Bruce 10-inch telescope to survey a considerable region of the sky for the brighter infrared stars. With an infrared gelatine filter near the focal plane, the Bruce telescope has a fine infrared focus over a field of 25 square degrees and reaches magnitude 8 or 9 for Ao stars in three or four hours. A field of 60 sq. deg. is usable, but the remoter portions reach less faint magni-

tudes, since the field is curved. For comparison, fast panchromatic plates of the same fields have been taken within a few days, using a red focus without filter. The panchromatic plates show more red stars than do the blue plates of even longer exposure; and there are already available blue plates taken by Barnard and Ross for most of the fields so far surveyed. The more striking objects are stronger on the infrared plates than on the panchromatic plates, on which there is occasionally no corresponding image or only a very weak one. Before some of the more outstanding stars are listed, a discussion of the infrared behavior of classified stars is given.

TYPICAL STELLAR BEHAVIOR IN THE INFRARED

Plate XX is an enlargement, of about 2.5 times, of a portion of a pair of Bruce survey plates. The key to this plate is found in Table 2*b*. The infrared images (readily distinguished by being somewhat elongated on this particular plate) have been placed just above the corresponding panchromatic images (of which many have strong out-of-focus blue halos). The plate was chosen as a good illustration of a B star possibly reddened by interstellar scattering, but it serves for other stars as well. There happen to be two stars of the same HD visual magnitude which also look nearly the same on the panchromatic plates and are the same in the infrared; one is of type B_3, the other of Type G_5 (Pl. XX, 1 and 2). The B_3 star is HD 4841, whose color excess, as determined by Stebbins and Huffer,[4] is $+0^m.28$. The Harvard photographic magnitudes are 7.33 (B_3) and 7.71 (G_5). It is of interest to compare these with a B_5 star of visual magnitude 7.40 (Pl. XX, No. 19) and an F_5 star of visual magnitude 7.70 (No. 16), although Plate XX is too far from the axis for the best comparison. Attention is called to the increasing infrared strength of the K, Ma, Mb, and the long-period variable stars like TY Cas; TY Cas, although faint in the infrared, has practically no corresponding red image. BL Cas, a known but unclassified variable, is seen by its infrared intensity to be of the red-variable type.

For convenience, we shall designate as "infrared stars" those having indices of 5 or more magnitudes from blue to infrared, or about

[4] *Pub. Washburn Obs.*, **15**, 224, 1934.

PLATE XX

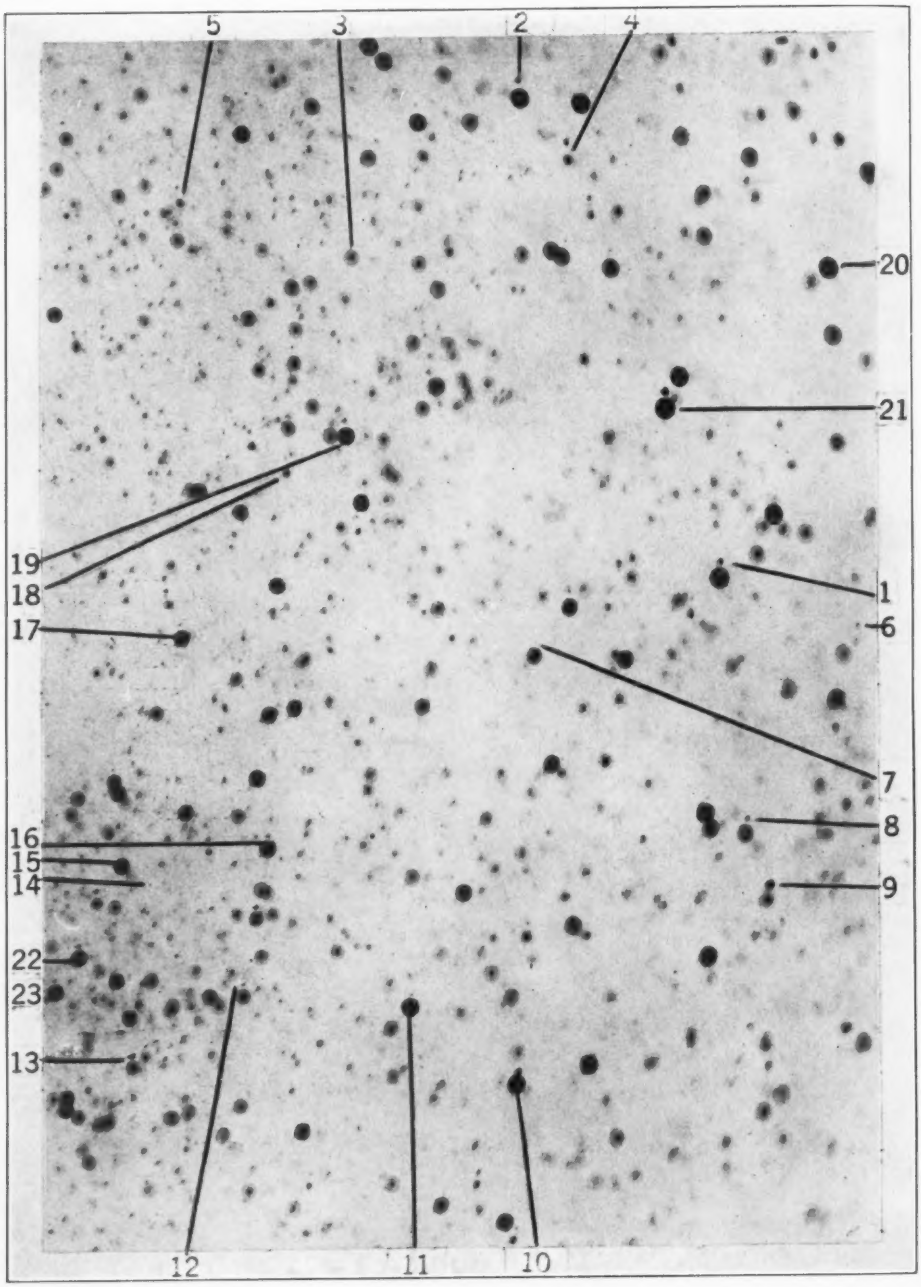

ENLARGED PORTION OF SUPERPOSED (SLIGHTLY DISPLACED) INFRARED AND PANCHROMATIC PLATES

(See key, p. 515, Table 2*b*)

half that from visual to infrared. In general, these will be of types M, N, R, and S. Of these, the M and S stars behave similarly, being strikingly strong in the infrared, moderately so in the red, and having conspicuous out-of-focus blue halos for the brighter stars (Pl. XX). The R and N stars are outstandingly strong in the red, have no blue halos whatever (they are relatively very weak on the blue plates), and are only weak or moderately strong in the infrared. Plate XX has no classified R or N stars, but shows their characteristic behavior. There seem to be stars somewhat intermediate in be-

TABLE 2*b*

KEY TO PLATE XX

No.	HD	Ptm. Mag.	Sp.	No.	HD	Ptm. Mag.	Sp.
1	4841	7.06	B3	13	3223	8.8	Ma
2	4523	7.06	G5	14	TY Cas	14±	.....
3	4004	10.2	Ob	15	3249	8.5	Ao
4	.....	.....	N?	16	3637	7.70	F5
5	.....	.....	N?	17	3465	8.1	Ko
6	BL Cas	13±	.....	18	.....	.....	N?
7	4334	8.5	Ko	19	3940	7.40	B5
8	4811	8.0	K2	20	5244	7.54	A3
9	4842	9.9	Mb	21	{4775 4776}	5.45	A2+F2
10	4179	6.84	Ko				
11	3949	7.8	Ao	22	3123	7.36	Fo
12	3529	8.8	Ma	23	3067	7.51	F5

havior having both fairly large color indices and infrared indices. Whether there are stars of both extreme color indices and extreme infrared indices is a matter under investigation. Among stars of earlier type, those of types A, G, and K seem to be most consistently true to type. Some of the F stars are weaker, and many of the B and O stars are stronger in the infrared than might be expected.

Table 3 shows how various stars, particularly those of type B, behave as to infrared index, in a region whose center is $\alpha = 3^h35^m$, $\delta = +32^\circ$ (1855), which is often cited as conspicuous for interstellar reddening. The table shows, according to spectral type, infrared indices derived in the following provisional way: measured HD magnitudes were used, and the infrared magnitudes were then adjusted to obtain zero index for Ao stars. In the mean, the indices should be

TABLE 3*

INFRARED INDICES IN THE REGION CENTERED AT $\alpha = 3^h35^m$; $\delta = +32°$

HD	Ptm. Mag.	Index	HD	Ptm. Mag.	Index	HD	Ptm. Mag.	Index
	B2			A2			F8	
22951	5.04	+0.4	25999	7.40	+0.1	20904	7.60	0.0
	B3		23193	5.57	+0.5	21847	7.32	0.3
25833	6.61	−0.4	22194	9.07	+0.2	23730	7.12	0.8
25799	6.87	−0.1	23848	5.10	+0.1			
21483	7.06	+0.4				Mean		+0.4
21856	5.80	+0.2	Mean		+0.2			
23478	6.51	−0.3					Go	
23625	6.36	+0.1		A3		21269	6.74	1.1
2419	7.49	−0.5	24167	6.22	−0.1	23626	6.23	0.4
24640	5.48	−0.1		A5				
24131	5.73	0.0	22317	6.63	+0.1	Mean		+0.7
			22224	7.62	+0.2			
Mean		−0.1	24809	6.39	−0.4		G5	
						21904	7.47	1.8
	B9		Mean		0.0	21450	7.32	1.5
24012	7.57	−0.6				22159	8.52	0.7
	A0			F0		22814	7.76	1.4
22766	6.86	+0.1	22124	6.62	+0.4			
21611	7.51	−0.3	23922	6.67	0.3	Mean		1.3
21834	7.96	+0.2						
22280	7.76	+0.2	Mean		0.4		K0	
21402	5.60	+0.2				25373	7.67	0.9
20995	5.64	−0.4		F2		21110	7.49	1.8
22327	7.42	0.0	21913	7.58	+0.2	20905	7.46	1.0
23204	8.32	0.0	20933	7.90	−0.2	21403	7.66	0.6
						20812	7.55	1.0
Mean		0.0	Mean		0.0	21730	7.79	1.8
						22306	6.98	2.0
				F5		21864	7.92	0.8
			22734	8.67	+0.6	24228	6.70	0.8
			22692	6.85	+0.7			
			22418	7.01	+0.5	Mean		1.2
			Mean		+0.6		K5	
						23962	7.36	2.2

1855		MAG. 8500 A	ESTIMATED INDEX	REMARKS
α	δ			
3^h19^m2	33°03′.6	6.0	6.0	No known variable
44.6	36 07.0	6.4	5.7	No known variable
27.5	31 26.0	7.1	5.3	No known variable
		5.0	5.2	AF Per Ma
		6.3	4.7	R Per M2e
		4.8	4.5	UZ Per M4
		7.5	4.5	AZ Per

* The stars HD 24398 (2.91, B1), HD 23180 (3.94 B1), and HD 24912 (4.05, oe5) are too bright for good magnitudes on this plate, but probably all have positive indices.

fairly good; at least we have a preliminary indication of what can be done in a statistical way without a redetermination of magnitudes and spectra. The extreme cases might be worth a special study. At the bottom of the table appear the positions and the approximate infrared indices of the three most infrared stars (possibly variables) in this field of 60 sq. deg., followed by the indices of the known variables. There are a few other stars almost as infrared and still others with indices grading into those of the upper part of the table. For the variables the infrared magnitudes apply only for the time of the plate.

INFRARED INDEX SEQUENCES

The main purpose of the survey has been the detection of stars of extreme coolness. About 3000 sq. deg. have now been covered, mostly in the Milky Way. Extremely red objects are not numerous, but many of the plates contain one or several stars which are outstanding for their strength in the infrared. Some of the unclassified variables and almost all of the known long-period variables are among the striking objects, and many uncatalogued objects have been found, in addition. To make a biological analogy, it is unlikely that any of the new objects are a new species; but they are merely individuals with more pronounced characteristics than are usually found. While the method is very reliable for their detection, no indices greater than 9 or possibly 10 mag. have been found, which may correspond to some critical point of stellar evolution. Several of the new infrared stars have decreased in brightness since their discovery (see charts I, 1, and II, 1). If the indices increase toward minimum, as do those of all variables so far investigated,[1] they may become the largest known.

No proper motions large enough to be noted by manual superposition of Barnard's plates with my infrared plates have been seen. However, the scale is somewhat different, owing to the longer infrared focus. Further, the fainter stars do not appear on the blue plates. The possibility that occasional dwarf stars may be found among the infrared stars is indicated by the infrared behavior of Wolf 359—the intrinsically faintest star, visually, for which the absolute magnitude, M_v, is 16.5. The apparent photographic magnitude is 15, the apparent visual magnitude is 13.5, and the apparent infrared mag-

TABLE 4

INFRARED INDEX SEQUENCES

CHART NO.	1855 α	1855 δ	MAG. 8500 A	ESTIMATED INDEX	REMARKS
	Field I centered at $\alpha = 21^h47^m$; $\delta = +56°$				
1....	$21^h53^m.1$	56° 2′.5	8.0	$10^m.0$	Variable; gets fainter
2....	46.5	3.2	9.0	8.5	
3....	54.9	40.2	6.4	8.0	Variable; gets fainter
4....	51.6	58 6.7	9.0	7.0	
5....	22 1.1	5.3	7.5	6.6	
6....	21 43.8	56 42.5	8.0	6.3	
7....	28.2	53 40.9	5.5	6.1	
8....	22 6.4	56 20.0	6.0	6.1	
9....	21 47.6	55 17.7	5.5	6.0	
10....	33.4	57 4.9	6.2	6.0	
11....	22 3.1	55 49.0	6.3	6.0	
12....	21 44.1	51 45.2	6.2	5.7	
13....	21 16.3	55 43.5	6.4	5.7	
14....	52.7	52 11.3	6.8	5.6	
15....	40.4	58 11.2	5.5	5.6	
16....	47.3	56 5.9	8.4	5.5	
17....	50.0	43.5	9.8	5.3	
18....	47.8	55 50.7	10.0	5.2	
19....	52.5	58 25.1	9.3	5.2	
20....	22 0.5	52 55.2	7.6	5.2	
21....	21 59.4	52 12.9	8.0	5.0	
22....	49.4	56 3.5.	9.7	5.0	Variable
23....	12.0	56.43.8	7.0	4.7	
24....	22 16.5	54 33.6	6.5	4.5	
BD...	+54°2511	.....	2	5	$7^m.16$ Mb. Too bright for mag.
	54 2517	.....	5	5	
	53 2684	.....	2	7	RU Cyg. M8e
	54 2603	.....	5	5	9.5, Mb
	56 2617	.....	5−	0.6	Oe5
	58 2316	.....	2	3	μ Cep. M_2
	57 2374	.....	6−	1+	6.98, BoP
	55 2737	.....	4	3	7.06, Ma. RW Cep
	58 2402	.....	5	.....	5.19, Od
			7.5	5	SU Lac
			6.5	6.8	AB Cep
			7.5	5.5	WZ Lac
	51 3117	.....	5.5	4.5	
			7.0	.....	DQ Cyg influenced by BD 54°2672.
			7	5.5±	BQ Cyg. Near edge
	53 2736	.....	6	3	Weak ptg. image. Var. or N-type
	51 3188	.....	5	5	

TABLE 4—*Continued*

Chart No.	1855 α	1855 δ	Mag. 8500 A	Estimated Index	Remarks
	Field II centered at $\alpha = 4^h55^m$; $\delta = +55°6$				
1....	$4^h48^m.8$	55°57′.3	4.0	$9^m.0$	Probably variable
2....	54.2	53 37.7	6.5	5.2	
3....	54.0	56 25.6	6.6	5.1	
4....	48.2	58 0.6	7.2	5.1	Weak ptg. image. Probably variable
5....	41.6	12.3	7.5	5.0	
6....	5 1.7	53 44.7	7.8	5.0	
7....	5 5.0	46.1	8.0	4.8	
			4	4	RV Cam. Mb
		.....	2	5	R Aur
BD...	+55°934	.....	6.5	3.0	
	Field III centered at $\alpha = 21^h52^m$; $\delta = +62°.5$				
1....	$22^h15^m.3$	61°26′.3	6.3	$8^m.8$	Probably variable
2....	21 38.7	5.8	7.4	6.0	
3....	53.9	63 8.4	7.2	5.5	
	.....	.....	6.0	7.0	TT Cep
BD...	+62°2030	.....	4.0	5.0	Blue halo; red faint
	60 2267	.....	7.0	3.3	N-type
			4.5	4.0	SW Cep. Mc
	61 2246	.....	4.5	0.7	Oe5
	2169	.....	4.0	0.9	B2ep, $4^m.87$
	60 2217	.....	4	3	Mb, $6^m.80$
	62 2028	.....	2	3	Mb, 5.46. Too bright for mag.
			2	3	VV Cep M2. Too bright for mag.
	63 1770	.....	6.4	3.0	
	64 1583	.....	5.0	3.3	
	1596	.....	4.5	3.0	
	1541	.....	6.0	3.3	
	63 1740	.....	5.0	3.4	
	62 1924	.....	5.1	4.0	
	64 1527	.....	5.1	0.1	B3p
	64 1664	.....	4.9	0.8	Bo
	66 1405	.....	5.5	−0.1	B5
	59 2395	.....	5.2	0.3	Bo
	62 2079	.....	4	3+	Mb, $7^m.18$. Too bright for mag.

TABLE 4—*Continued*

Chart No.	1855 α	1855 δ	Mag. 8500 A	Estimated Index	Remarks
	Field IV centered at $\alpha = 19^h23^m$; $\delta = +24°20'$				
1....	$19^h29^m.5$	22° 1′.5	6.7	$8^m.5$	Variable or weak ptg. image
2....	9.8	42.1	6.4	8.0	
3....	26.1	23 20.3	4.8	7.8	
4....	19.6	21 12.3	7.8	6.7	
5....	18.5	11.5	7.6	6.5	
6....	17.0	26 52.8	7.3	6.2	
7....	17.2	42.6	7.1	5.9	
8....	37.4	22 23.4	6.3	5.5	
9....	37.9	23 49.8	7.7	4.8	
10....	37.0	11.3	7.0	5.5	
BD...	+22°3360	.....	4	3	Mb
	21 3737	.....	6.0	3.2	Variable or weak ptg. image
	22 3659	.....	5.1	4.2	
	3792	.....	5.7	2.8	North of BD position
	3648	.....	5.3	0.1	Bo
	Field V centered at $\alpha = 1^h30^m$; $\delta = +56°.5$				
1....	$1^h17^m.6$	54°23′.9	6.5	$7^m.5$	
2....	51.0	57 54.6	6.5	6.8	
3....	24.2	0.9	6.2	5.0±	Variable or weak ptg. image
4....	13.8	6.1	8.0	6.1	A spiral? Ptg. image diffuse
5....	32.4	55 46.7	8.0	6.1	
6....	37.7	57 24.5	8.5	6.0	
7....	38.5	55 34.5	8.8	5.7	
8....	32.0	56 12.4	8.8	5.7	
9....	27.7	36.2	9.0	5.6	
10....	21.9	29.1	9.0	5.3	
11....	24.4	55 54.7	8.5	4.7	
12....	39.8	28.7	8.3	4.5	
13....	30.2	58 58.5	7.8	4.5	
14....	34.1	4.5	6.1	4.9	
15....	54.9	56 48.5	8.8	5.5	
16....	53.2	35.9	8.5	5.6	
17....	36.0	54 58.3	7.5	4.5	
18....	15.9	58 4.4	7.0	3.5	
19....	34.6	55 36.8	8.3	4.2	
			4.4	4.2	TT Per. M_5
			8.8	2.7	AX Per
BD...	+53°413	.....	5.4	3.8	Mb
			5.1	5.4	U Per. M6e
			4.5	3.5±	AA Cas, Mb

TABLE 4—*Continued*

Chart No.	1855 α	1855 δ	Mag. 8500 A	Estimated Index	Remarks
	Field V—*Continued*				
BD..	57°237	.....	3.8±	3m	Mb
			6.7	4.3	BQ Cas
			8.7	5.8	BT Cas
			7.7	5.3	TY Per
			6	2	T Per
			8.5	2.5	X Cas. N1e
			5	3	XX Per. Ma
	Field VI centered at $\alpha = 12^h5^m$; $\delta = +87°$				
1....	21h20m7	87°43′.2	7.0	7m0	Variable
2....	9 52.0	86 44.6	9.0	4.0	
BD...	+85°122	.....	7.0	2.5	
	256	.....	6.5	2.8	
	86 175	.....	6.7	2.8	
			5.5	3.5	R Cam
	Field VII centered at $\alpha = 6^h48^m$; $\delta = -15°$				
1....	6h49m2	−16°40′.6	5.5	7m5	
1....	48.9	37.0	8.1	6.4	
2....	48.5	13 58.6	5.9	6.8	
3....	47.8	14 49.2	6.8	6.3	
4....	7 3.7	16 1.8	6.0	5.0	
5....	6 40.5	29.6	8.5	5.2	
6....	44.9	42.1	8.1	6.4	
7....	43.9	41.3	8.1	6.2	
8....	36.7	15 48.0	6.0	5.3	
9....	44.8	16 4.8	7.0	3.5	Var. or weak ptg. image; strong red
10....	46.1	12 0.5	7.0	3.5	Var. or weak ptg. image; strong red
11....	55.9	15 27.8	5.7	6.0	
12....	53.2	58.3	8.6	5.6	
13....	44.0	14 11.9	8.0	5.3	
14....	50.1	15 17.1	7.0	6.1	
15....	47.3	13 1.9	7.0	6.0	
16....	53.4	15 44.2	7.0	5.8	
BD...	+16°1586	.....	6.6	2.0	Ptg. mag. 8.68. Red companion?
			8.5	5.5	Y CMa
			5.0	6.0	RV CMa
			2	5	W CMa, Na. Too bright for mag.

TABLE 4—*Continued*

Chart No.	1855 α	1855 δ	Mag. 8500 A	Estimated Index	Remarks
	Field VII—*Continued*				
BD..	11°1797	.....	5.7	3^m2	Probably N-type
	14 1776	.....	4.5±	4	Mb. Near edge and too bright
	15 1662	.....	5.3	3.8	Ma
	16 1802	.....	6.3	−0.3	B3, 6.03
	11 1790	.....	5.1	0.2	B3, 5.28
	10 1862	.....	6.6	−0.2	B3, 6.38
	1848	.....	6.6	0.4	Bo, 7.01. Near edge
	11 1747	.....	6.2	0.4	B3, 6.57
	15 1629	.....	8.5	−0.2	B5, 6.35
	1681	.....	7.3	−0.3	B5, 7.03
	Field VIII centered at $\alpha = 6^h23^m$; $\delta = +17°$				
1....	6^h19^m3	20°37′6	6.2	6^m5	SX Gem. Catalogued as Ao, Algol type. Red Companion?
2....	15.9	18 43.3	6.4	6.5	
3....	16.0	14 17.7	6.8	6.5	
4..	22.4	13 45.3	6.8	6.5	
5....	18.0	18 46.4	6.0	6.0	
6....	19.2	19 3.5	7.7	5.8	
7....	8.8	15 10.0	8.0	6.1	
8....	33.8	16 26.0	7.3	5.7	
9....	22.8	18 20.5	6.8	5.5	
10....	21.9	15 3.6	6.0	5.7	
11....	41.7	16 51.4	6.8	5.4	
12....	4.9	18 34.4	5.5	5.0	
13....	28.5	15 0.2	6.8	5.5	
14....	19.1	16 12.2	6.8	5.5	
15....	20.7	20 32.1	7.0	5.0	
BD...	+14°1296	.....	6.9	0.2	Oe5, 7^m09
			5.5	6.3	AQ Gem
			5.7	5.8	DD Ori
	16 1070	.....	5.5	5.0?	May be 2″ south of BD star
			6.8	5.0	AT Gem
			7.1	6.4	AS Gem
			6.8	5.3	AZ Gem. W UMa-type
			4.0	1.6	BL Ori. Nb
			5.0	4	AX Gem
			9.3	5.2	AP Gem ?
			8.2	3.3	RT Gem
			8.1	5.7	UU Gem
	14 1350	.....	4.8	4.6	
	15 1236	.....	5.2	3.8	Blue halo strong; red weak
	16 1194	.....	5.2	3.8	Red strong; no blue halo

nitude is 8.5. o^2 Eridani C has an infrared index of about 2.8 mag. Two others among the nearer stars, CC 1069 (Barnard's star), $M_v = 13.7$, and CC 1382, $H_v = 11.8$, have been found to have infrared indices of 3.0 and 2.5, respectively. There may be dwarfs which are still more infrared than those cited, but most of the infrared stars which can be detected by our survey will be giants.

Charts and catalogues.—Rather than list only the most infrared stars, it has been decided, at least for the present paper, to deal with a limited number of fields more completely by listing all the red stars down to a certain index and limiting magnitude in the form of infrared index sequences. Finder charts have been prepared for all stars not previously known to be catalogued, and these are reproduced in Figures 1–4. The method of preparing the charts is new and perhaps to be recommended. A region of 20 minutes square around each star is enlarged about twelve times on photographic paper. (In this case negatives by Barnard or Ross were used as having the greatest number of field stars.) Holes of sizes corresponding to the approximate magnitudes of the stars are then punched through the star positions, the contact prints from the punched charts giving quite realistic and useful fields. On the charts the BD stars are indicated by short, straight lines, the infrared stars by arcs. The magnitudes of the infrared stars are visual, estimated on the panchromatic plates and occasionally by direct observation. For the field stars the relative magnitudes are probably fairly good, but they are photographic rather than visual. The charts will probably be useful both visually and photographically, but they are meant strictly for identification, not for magnitude purposes. Since many of the infrared stars are variable, the magnitudes hold only for the time of observation.

For each Bruce field (about 60 sq. deg. are useful) there is a catalogue listing the stars approximately in the order of infrared index. These catalogues are found in Table 4. The positions are given for the epoch of the BD, reduced from the photographic enlargements with a ruler. The infrared magnitudes are estimated from the Ao stars near the same part of the plate and are accurate within a few tenths of a magnitude for the time of observation. Known red variables and other stars of special interest have been listed following the

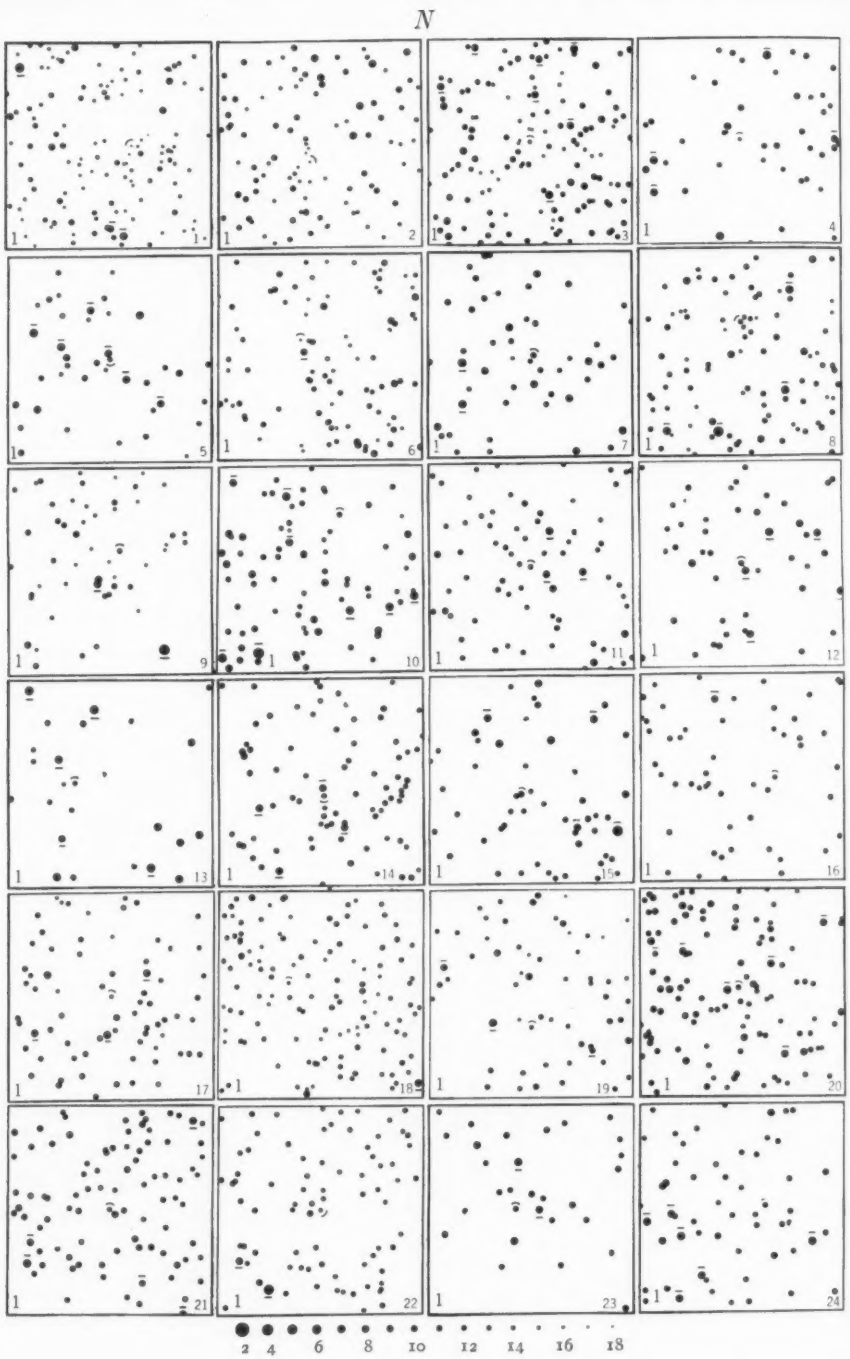

FIG. 1.—Field I, Charts 1–24 (see Table 4)

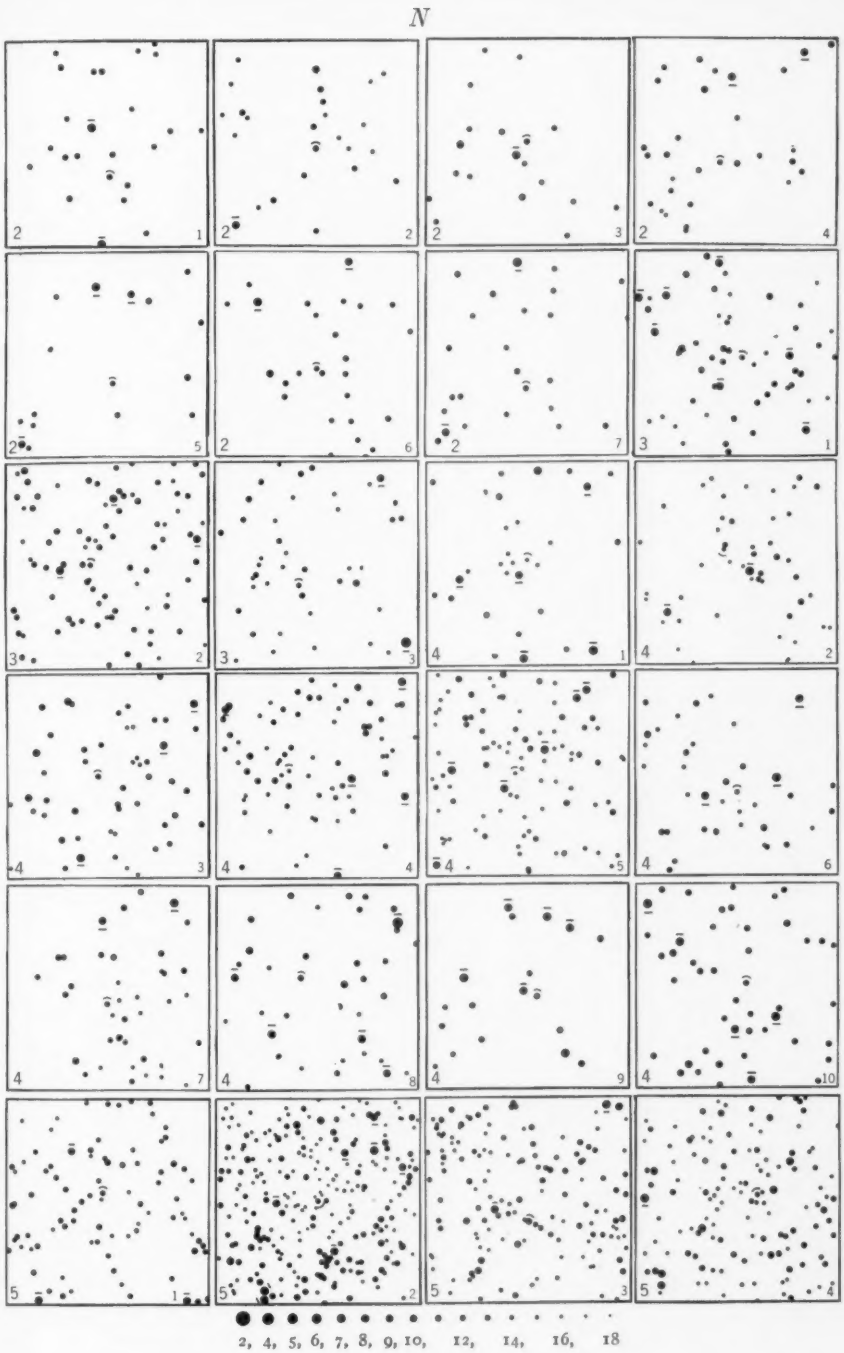

FIG. 2.—Fields II–V (see Table 4)

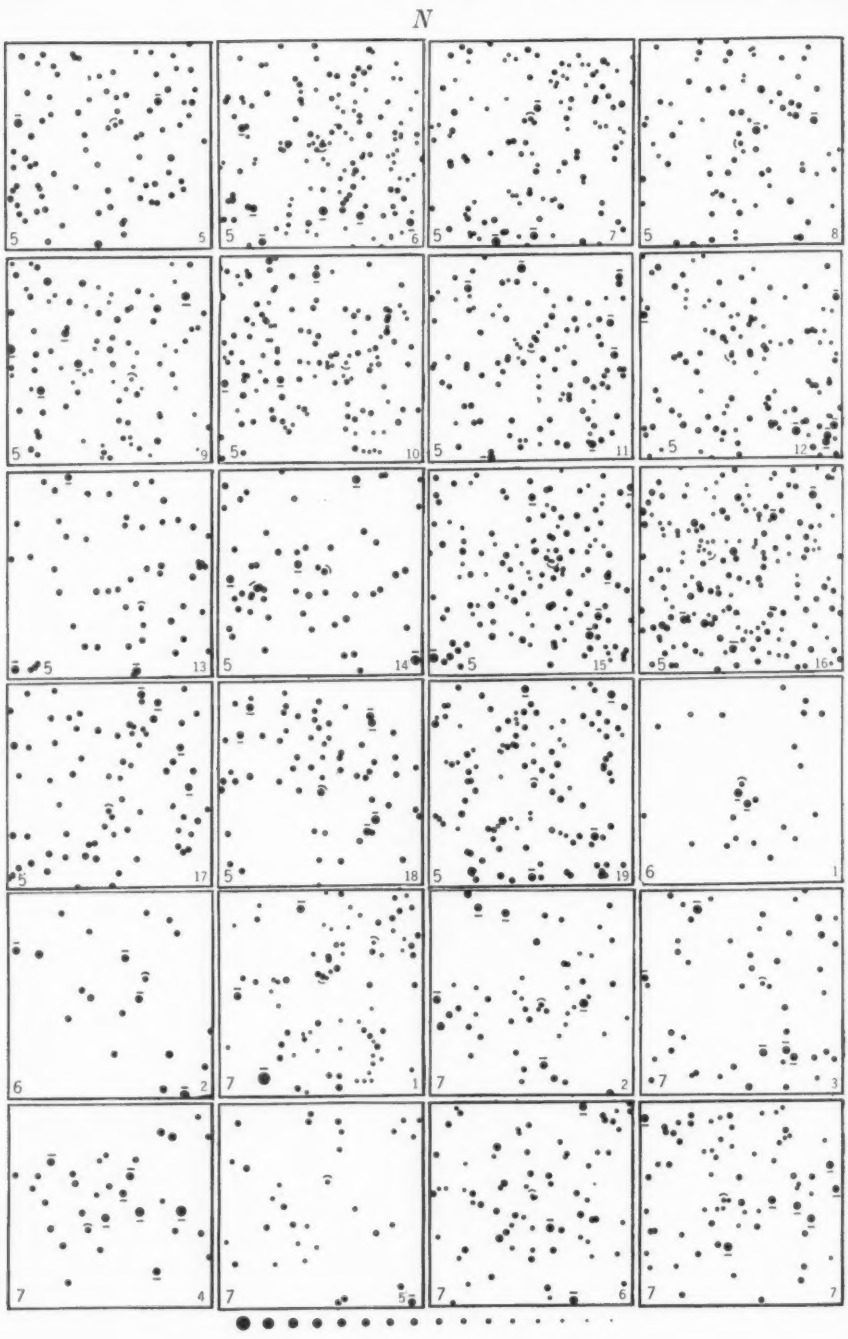

FIG. 3.—Fields V–VII (see Table 4)

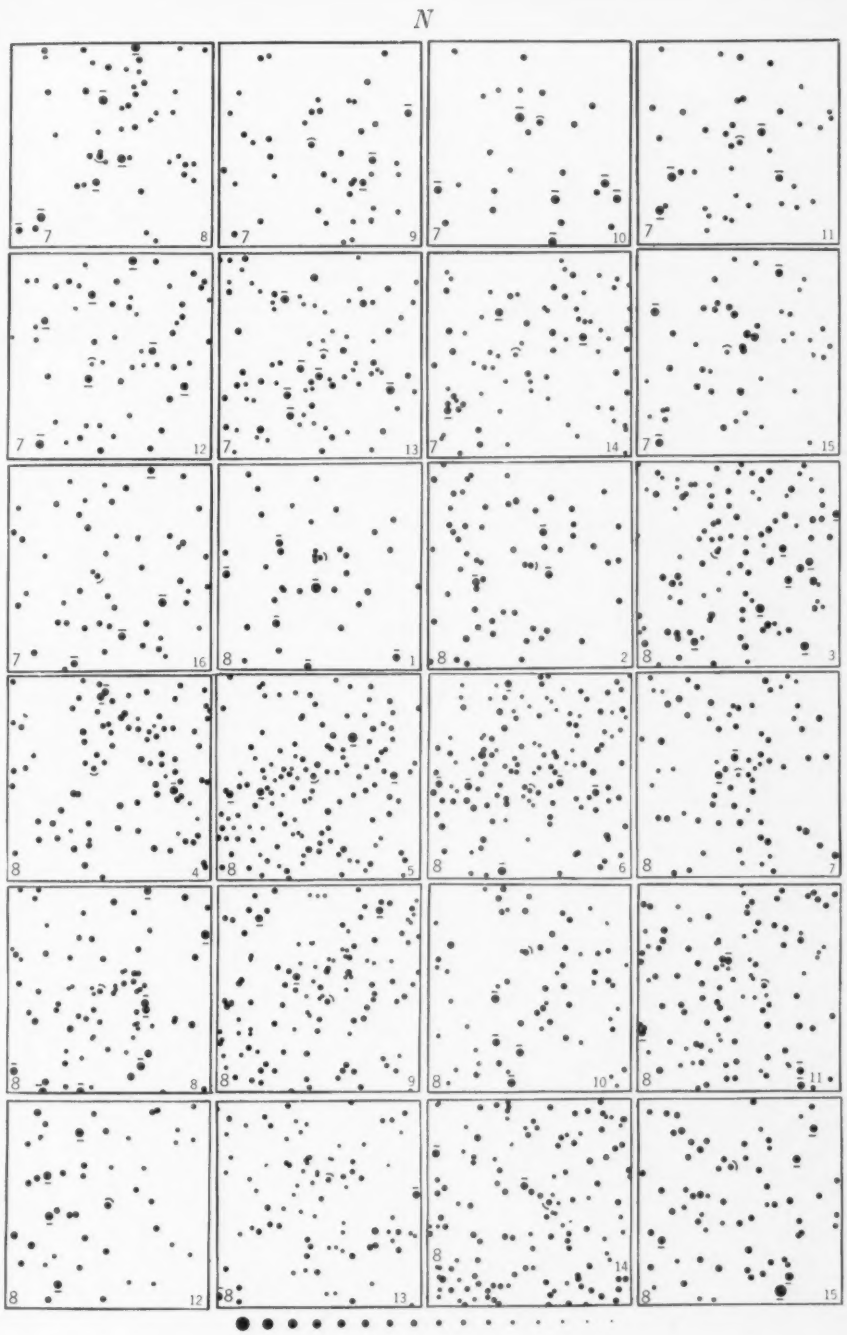

FIG. 4.—Fields VII–VIII (see Table 4)

chart sequences, although these are not necessarily less infrared. The infrared stars were selected on the basis of relative panchromatic to infrared intensity, but occasional stars which are very weak photographically (presumably N stars or variables, since the blue plates were taken at different times) have also been charted or noted, although no attempt was made to do this systematically. The fields included in this study were chosen because they contain some of the brighter infrared stars thus far found and are typical survey fields. It is planned to treat in a similar manner a number of other fields that have already been photographed; at least the more striking stars will be listed. It is felt that a comparison of infrared sequences in various parts of the sky, as well as of bright and faint stars in the same fields, will yield valuable information, particularly for statistical purposes. The behavior of the O and B stars at this wavelength seems to be particularly noteworthy; in at least some cases there may be red companions. A large number of Algol stars have been examined, but no unexpected infrared color was found, with the exception of SX Gem (Field VIII), which probably has been misclassified but which may have a red companion. BD = 16°1586 also increases exceptionally from red to infrared intensity and may have a companion. Some of the stars noted as relatively strong in the infrared, weak in the red, but with strong blue halos, may also reasonably be suspected of duplicity. Unusual absorptions or duplicity seem the only alternatives in all these cases.

YERKES OBSERVATORY
WILLIAMS BAY, WISCONSIN
August 1937

COLOR INDICES OF REFLECTION NEBULAE

O. C. COLLINS

ABSTRACT

Color indices for 18 reflection nebulae have been determined. Two methods were used, both of which employ corrections for the removal of the superimposed sky brightness from the nebular image and comparison of the nebula with the surrounding sky. In the first method a mean color index of +0.5 mag. is adopted for the sky. In the second, which gives results with much less scatter, the surface brightness of sky and nebula in blue and in red light is calculated by the use of extrafocal images of the stars which illuminate the nebulae. Corrections are made for differences in length of focal and extrafocal exposures. Time effects in sensitometry are discussed.

All results are reduced to the Mount Wilson system, and use is made of the known color excesses of the illuminating stars.

The sky brightness is found to vary with time and with altitude, particularly on the red exposures.

The nebulae are found to be, in general, bluer than their illuminating stars. The difference of color ranges from −0.5 mag. to 0.0 mag., the mean being −0.3 mag. There is an indication that the color excesses of the nebulae are correlated with the color excesses of the stars. The observed facts are consistent with the hypothesis that the star's light is made uniformly bluer by reflection, by about 0.5 mag., and that passage through the nebula superimposes a change of color toward the red in proportion to the color excess shown by the star.

Several recent investigations have shown that the colors of the reflection nebulae are not as blue as would be expected from Rayleigh's law. Struve and Story[1] consider the selective absorption in nebulae to be produced by particles "somewhat too large to produce true Rayleigh scattering but small enough to give an appreciable amount of space reddening." For the nebula in the Pleiades the spectrum has been found by Struve, Elvey, and Keenan[2] to be slightly stronger in the violet than for the illuminating star (Maia). In NGC 7023, Keenan[3] has found by photometric comparison of the brighter parts of the nebula with the star that the nebula is, for the most part, slightly redder than the star, with, in one portion, a red excess of the order of 0.3 mag. Struve, Elvey, and Roach,[4] using a Schmidt camera in tests for Rayleigh scattering, found a large red nebula extending about one degree north from Antares. By photometric comparison with the sky, for which a color index of +0.5 mag. was adopted, this nebula was found to have a color index cor-

[1] *Ap. J.*, **84**, 203, 1936.

[2] *Ibid.*, **77**, 274, 1933.

[3] *Ibid.*, **84**, 600, 1936.

[4] *Ibid.*, p. 219.

responding to the spectral class of the star. The mean color index of nebulae associated with five B-type stars was also found to correspond to the spectral class of those stars.

These results all give general confirmation to the reflection theory of nebular illumination and suggest that for the C nebulae (which have a continuous spectrum) the light comes to us but little changed in color by whatever form of scattering it has undergone.

It should not be overlooked, however, that the stars associated with nebulae are known to show colors which are not normal for their spectral classes. Seares and Hubble[5] found such stars, for the most part, strongly reddened. The color excesses observed for these stars may be taken as indicative of the change in the stars' light due to passage through the nebula.[6] That portion of the star's light which comes to us by reflection would then be expected to suffer not only the change of color occurring in the reflection process but also a change similar to that noted for the star itself, and greater in amount on account of the longer light path traveled through the nebula.

The purpose of the present paper is: (1) to determine more precisely the color differences between the nebulae and the associated stars for those nebulae which give continuous spectra; (2) to ascertain, by a study of numerous cases, whether this color difference is approximately the same for the various objects; (3) to obtain the color indices of the nebulae from these color differences by the use of the known color excesses of the stars; (4) to find the relation of the color index of the nebula to the color index of the star and to the normal color index for a star of the same spectral type; (5) to determine the surface brightnesses of these nebulae; and (6) to obtain incidental information on the brightness of the night sky.

THE PROGRAM

Table 8 gives the designations for fifteen nebulae, selected from Hubble's list[7] as having continuous spectra, and for four other objects which are undoubtedly of the same type.

[5] *Ibid.*, **52**, 8, 1920.

[6] A contrary conclusion was reached by Shajn, *Zs. f. Ap.*, **8**, 168, 1934.

[7] *Ap. J.*, **56**, 404, 1922.

THE TELESCOPE

Photographic observations were made at the Newtonian focus of the 24-inch reflector of the Yerkes Observatory. Precautions were taken that no stray illumination could reach the plate during exposure at the telescope.[8] Both the large and the small mirror are aluminized.

THE FILTER

A Schott GG 11 glass filter, which cuts off at 5000 A, was used in front of the red-sensitive plate. This replaced a glass filter which cuts off near 5200 A and which was used on the IC 4601 and B 214 fields only. With the blue-sensitive plate no filter was used.

THE PLATES

For the red exposures Eastman 1-C Special plates[9] were adopted after preliminary use of Eastman 1-G and Wratten and Wainwright Hypersensitive Panchromatic plates on the two fields already mentioned. With the filter used, the effective wave-length on the 1-G plate was approximately 5500 A and on the 1-C plates 6000 A. Eastman 1-O, which is sensitive to slightly beyond 5000 A, was used for the blue plate, and the effective wave-length was about 4000 A. The IC 4601 and the B 214 fields were taken on Guilleminot plates, with effective wave-length around 4400 A. All plates were backed.

THE OBSERVATIONS

The exposures needed for these faint nebulae were of such length that the sky background could not be disregarded. The general illumination of the sky necessarily overlies the image of the nebula, so that it has to be measured and removed, as is explained hereafter.

[8] A red-sensitive plate exposed at the Newtonian focus when the dome was closed was found to be darkened unequally by the guiding eyepiece illumination that shone on the surface of the eyepiece lens and traveled to the large mirror by reflection in the flat mirror. When this was corrected, a plate was exposed similarly for two hours without any darkening.

[9] An especially fast emulsion was obtained through the courtesy of Dr. C. J. Staud, of the Eastman Kodak Company. It is understood that selection for speed may make these plates vary in other characteristics from batch to batch. Those used were all of one emulsion, No. 56020. The value of p determined from six separate plates used with the yellow filter (see Table 4) differs from that adopted by Keenan (*op. cit.*, p. 601), who used a ciné-red filter.

The exposures were therefore made long enough to bring the sky background to a convenient density (0.5 specular density).

Two methods were used for obtaining the color indices of the nebulae. The first method (I) relies on a comparison of the nebula with the sky background and the adoption of a mean color index of +0.5 mag. for the latter. This method has been applied to all objects, and the results are shown in Table 8. The second method (II) also is dependent upon comparison of the nebula with the sky background, but on each plate separately the magnitude of the latter per square degree is calculated by use of an extrafocal image of the illuminating star. The use of these extrafocal images necessitates certain corrections, which will be explained in due course. This method was used for about one-half of the objects and leads to results which show less scatter. These, too, are shown in Table 8.

For the purpose of making the comparison as direct as possible between the color of the nebula and the color of the star, the extrafocal exposures were made on a part of the plate not previously exposed. These exposures were made too brief to record the nebula or the sky background, but long enough to produce within the annular ring of the star's image a density comparable with that of the sky background in the longer exposure. The star was on the optical axis in both exposures, except in the first two fields already referred to, where the use of the Ross correcting lens insured uniform images up to at least 15′ off the axis. The exposures were timed to the nearest second, and the ratio (r) of the focal to the extrafocal exposure was the same for each plate of a pair.

Exposures.—The blue plates were exposed from thirty minutes to one hour, and the corresponding red plates from two to three times the blue exposure. The extrafocal exposures ranged from three seconds to fifteen minutes, ($r = 900$ to $r = 8$). They were made at a constant distance outside the focus (100 scale units—[approx. 4.5 mm]) and produced images slightly more than 1 mm in diameter. For nine fields both plates of a pair were taken on the same night in immediate succession. The short extrafocal exposures were made within a few minutes of each other between the long focal exposures. No observations were made when the polar aurora was visible.

Material obtained.—Pairs of plates were obtained for fifteen fields. For eight of these pairs satisfactory extrafocal images were obtained on each plate. In many of the remaining fields the star was too faint for this method.

SENSITOMETRY

All plates were provided with a density-intensity calibration by exposure in a tube sensitometer. For the red plates the light was passed through the same filter as that used at the telescope. The sensitometer exposures were made on a portion of the plate not previously exposed. The standard exposure times were two minutes on the blue plate and four minutes on the red. In order to test the effect of changes of exposure time, additional sensitometer exposures were made for various multiples of the standard exposures, up to the full length of the telescope exposure. On account of the latitude of the plates it was necessary to reduce the intensity of the illumination in the sensitometer for the longer exposures, and this was done by geometric means.

METHOD OF MEASUREMENT

The photometer.—The plates were measured with the thermoelectric photometer recently described by Ross.[10] The magnitude differences were obtained by interpolation in the curve of galvanometer deflections given by the sensitometer exposures. The smallest aperture of the instrument was used; and the diameter of the beam was 0.24 mm, corresponding to 21 seconds of arc on the plate. In measuring the plates, three or more well-defined points in the sky around the nebula were selected for their good agreement, and the mean deflection given by them was adopted as the value for the sky. In the image of the nebula one or more points were selected for their uniformity over the cross-section of the beam. The extrafocal images of the stars were measured at four points, and the mean was adopted. These extrafocal images, having the shadow of the flat mirror in their center, had been made just large enough to permit the use of the smallest aperture of the photometer within the annular area of the image. The measures of sky and nebula and extrafocal

[10] *Ap. J.*, **84**, 241, 1936.

image were made at the same time against two sets of sensitometer exposures.

TABLE 1

COMPARISON OF MEASURES OF Δm AGAINST LONG AND SHORT SENSITOMETER EXPOSURES

BLUE PLATES		RED PLATES	
2 min.	45 min.	5 sec.	75 min.
−0.34	−0.37	−0.19	−0.12
2 min.	60 min.	2 min.	30 min.
−0.65	−0.61	−0.18	−0.19

TABLE 2

COMPARISON OF MEASURES AT CORRESPONDING POINTS ON PAIRS OF PLATES OF THE SAME FIELD (NEAR MEROPE) TAKEN ON DIFFERENT NIGHTS

POINTS	FIRST PAIR OF PLATES		SECOND PAIR OF PLATES	
	Blue	Red	Blue	Red
	Δm	Δm	Δm	Δm
1	−0.45	−0.14	−0.49	−0.16
2	−0.28	−0.08	−0.37	−0.12

CORRESPONDING MEASURES AFTER APPLICATION OF CORRECTION FOR REMOVAL OF SUPERIMPOSED SKY BRIGHTNESS

POINTS	FIRST PAIR OF PLATES			SECOND PAIR OF PLATES		
	Blue	Red	Blue-Red	Blue	Red	Blue-Red
	Δm corr.	Δm corr.		Δm corr.	Δm corr.	
1	0.72	2.15	−1.43	0.61	2.00	−1.39
2	1.33	2.79	−1.46	0.98	2.33	−1.35

Agreement of measures.—No systematic change in the magnitude differences was found, whether the longer or the shorter sensitometer exposure was used. A comparison of such measures is shown

in Table 1. Measurement of single plates of the same field, repeated on different nights, showed agreement (see Table 2).

Areas of extrafocal images.—The extrafocal images are large and were taken at a standard distance from the focus. The diameters of the images were measured; and the probable error in the resulting computed area is, expressed in magnitudes, ± 0.01 for a single image.

REDUCTION OF MEASUREMENTS

Correction for sky brightness.—The impression of the sky brightness on the plate necessarily overlies the image of the nebula. In order to measure the intensity of the light from the nebula, it is essential to know the relative intensity of the sky brightness and to subtract it.[11] Thus, for each measured Δm, a corrected value is obtained as follows:

$$\frac{I_{\text{sky}} + I_{\text{neb}}}{I_{\text{sky}}} = 10^{0.4\Delta m}. \tag{1}$$

$$\frac{I_{\text{neb}}}{I_{\text{sky}}} = 10^{0.4\Delta m} - 1 = 10^{0.4\Delta m_{\text{corr}}}. \tag{2}$$

The difference between these corrected values of Δm for two effective wave-lengths measures the color of the nebula alone relative to the sky background in the scale of these plates. For the Δm between the sky background and the extrafocal image of the star, this correction is not used, because these exposures are not superimposed and the exposure for the star was too short to record the sky background.

Correction for ratio of focal and extrafocal exposure.—It is important to correct for the length of these exposures; although the ratio of focal to extrafocal exposure is the same on each plate of a pair, this ratio has a different effect on the two types of emulsion. Figure 1 shows the interpolation curves of galvanometer deflection against magnitude difference obtained from sensitometer exposures of 6 minutes and 60 minutes, which corresponded precisely to the exposures on the same plate at the telescope. This change of the exposure time by a factor of 10, made without altering the intensity

[11] Struve, Elvey, and Roach, *op. cit.*, p. 224.

of illumination in the sensitometer, is seen to correspond for this plate to a shift of the curve by 2.19 mag., parallel to the axis of Δm.

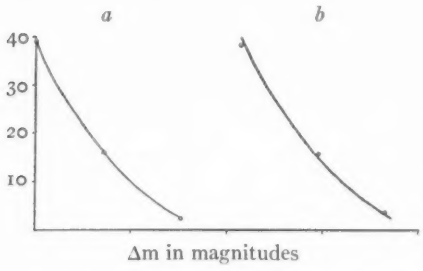

FIG. 1.—(*a*) 60-minute exposure; (*b*) 6-minute exposure.

Where the ratio of focal to extrafocal exposure time was greater than in the example given, the latitude of the plate made it impossible to obtain both of these curves without a change in the intensity of illumination in the sensitometer. This change of illumination was made geometrically, in order not to affect the color of the lamp; but it was done without accurate calibration. It was therefore necessary to compute the shift corresponding to the full change of exposure time by means of exposures of intermediate length.

The fact that, throughout the full range of exposure times employed, these curves showed no systematic difference in slope, justified the use of the Schwarzschild formula,

$$I_1 t_1^p = I_2 t_2^p , \tag{3}$$

where I is the intensity, t is the length of the exposure, and p is a constant. It follows that

$$p = \frac{\log \frac{I_1}{I_2}}{\log \frac{t_2}{t_1}} = \frac{0.4(m_2 - m_1)}{\log \frac{t_2}{t_1}} \tag{4}$$

and

$$m_2 - m_1 = 2.5\, p \log \frac{t_2}{t_1} . \tag{5}$$

Here $m_2 - m_1$ is the shift of the curve in magnitudes corresponding to a change of exposure time from t_1 to t_2. For each type of plate used, values of p have been determined according to equation (4). The change for each time ratio was found from equation (5) by use

of the adopted value of p, and has been applied as a correction to the Δm measured between sky points and the extrafocal image on the plate.

Table 3 shows the values of p for the different plates, and Table 4 shows the probable errors determined from separate plates.

TABLE 3

ADOPTED VALUES OF p

Plate	p	P.E.
Eastman 1-G	0.84	±0.02
W. W. Hyper. Panchrom. (ammoniated)	.63	.02
1-C Special	.90	.01
Guilleminot	.80	.02
Eastman 1-O	0.86	±0.005

TABLE 4

1-O			1-C SPECIAL		
p	Δ	Δ^2	p	Δ	Δ^2
0.84	−2	4	0.86	−4	16
.85	−1	1	.87	−3	9
.86	0	0	.89	−1	1
.86	0	0	.91	1	1
.87	1	1	.93	3	9
0.88	2	4	0.94	4	16
0.86		0.0010	0.90		0.0052

$$\text{P.E.} = \pm 0.6745\sqrt{\frac{0.0010}{5\times 6}} = \pm 0.004 \qquad \text{P.E.} = \pm 0.6745\sqrt{\frac{0.0052}{5\times 6}} = \pm 0.009$$

Confirmation of the values of p was obtained by exposing a plate at the telescope and closing the slide of the plateholder in steps of about 0.5 cm at measured intervals of time. This gave on the plate a series of strips graduated in density. The mean density taken over four points in the sky background in each strip was converted into magnitudes. The ratio of two exposure times and the corresponding Δm were used in equation (4) to obtain the values of p.

The 1-O plate gave $p = 0.87$; and 1-C Special, $p = 0.94$. These values fall within the limits of those found with the sensitometer,

although the measures on the plates necessarily referred to slightly different areas of the sky background.

In measuring the plates in this way the selected sky points serve as an intermediary in comparing the star with the nebula after the removal of the sky brightness.

CORRECTION FOR EXTINCTION

The Δm between the adopted sky and the nebula with superimposed sky brightness removed, and between the sky and the extrafocal image of the star, have been corrected to air-mass unity by use of the formula[12]

$$\text{Ext.} = m_z - m_0 = \frac{\log q}{0.4}\,[F(z) - 1]\,, \tag{6}$$

where $F(z)$ is the air mass traversed according to Bemporad's tables[13] and q is the transmission coefficient for unit air mass. The values of q adopted for the different effective wave-lengths are given in Table 5. These values were taken from those given for Washington.[14]

TABLE 5

Effective Wave-Length	q
6000 A	0.76
4000	.50
5500	.74
4400	0.62

The zenith distance at mid-exposure was used for each exposure, and the correction was applied to the magnitude of the nebula relative to the sky after the superimposed sky brightness was removed according to equation (2). The correction was also applied to the magnitude of the extrafocal images relative to the sky. Since both these magnitudes were measured at the same time against precisely the same sky points, their difference gives the surface brightness of the nebula relative to the brightness in the extrafocal image of the star.

[12] *Handbuch d. Astrophysik*, 1, Part II, 232.

[13] *Ibid.*, p. 268, Table XII*a*.

[14] *Handbuch d. Astrophysik*, 1, Part II, 199.

REDUCTION TO THE MOUNT WILSON SCALE

Since use will be made of Hubble's data, reduction is made to the Mount Wilson scale. For the combination Eastman 1-O and East-

TABLE 6

MAGNITUDES AND COLOR INDICES ON MOUNT WILSON SCALE FOR STARS IN NGC 1647 AS GIVEN BY SEARES

Stars	Pg	Pv	Color (Mount Wilson)
Red stars:			
No. 62	13.74	12.33	1.41
No. 153	13.62	12.30	1.32
White-yellow stars:			
No. 115	12.24	11.83	0.41
No. 169	13.32	12.95	0.37
No. 96	13.84	13.59	0.25

VISUAL COMPARISON OF RED STARS WITH WHITE-YELLOW STARS ON 1-O AND 1-C SPECIAL PLATES BY ARGELANDER STEPS

BLUE PLATE	RED PLATE
(96) 1 (62) 1 (169)	(115) 0 (62)
∴ No. 62 = 13.58 mag.	∴ No. 62 = 11.83 mag.
(96) 1 (153) 1 (169)	(169) 1 (153) 10 (115)
∴ No. 153 = 13.58 mag.	∴ No. 153 = 11.94 mag.

COMPARISON OF THE SCALE OF THESE PLATES WITH THE MOUNT WILSON SCALE

Stars	C (Mount Wilson)	C (Observed)
No. 62	1.41	1.75
No. 153	1.32	1.64
Mean of white-yellow stars	0.34	0.00

$$\text{From No. 62; correction factor} = \frac{1.41 - 0.34}{1.75} = 0.61$$

$$\text{From No. 153; correction factor} = \frac{1.32 - 0.34}{1.64} = 0.60$$

man 1-C Special, the reduction factor was determined from two pairs of plates of NGC 1647 taken slightly out of focus. Colors in this

cluster have been determined by Seares.[15] There are no blue stars in this cluster; but since the relation of color to spectral type is approximately linear, the correction factor is adequately determined by comparing very red stars with slightly yellow stars. The comparison was made visually by the step method of Argelander, and Table 6 shows the details for one of the two pairs of plates. The resulting correction factor 0.6 is applied to the corrected measures from these plates to bring them to the Mount Wilson scale. For the other plate pairs the correction factors adopted are shown in Table 7, which gives also the effective wave-lengths of the various plates used in pairs and the magnitude differences predicted by Rayleigh's law. The correction factors adopted reduce these differences to very close to unity in all cases.

TABLE 7

Field	Plate	Effective Wave-Lengths	Corr. Factor to Mount Wilson Scale	$2.5 \log \left(\frac{\lambda_2}{\lambda_1}\right)^4$	Product
All, except as below..	1-O 1-C Sp.	4000 6000	0.6	1.76	1.06
IC 5146.....	1-O W. W. Hyper. Panchrom.	4000 6000	0.6	1.76	1.06
IC 4601.....	Guilleminot W. W. Hyper. Panchrom.	4400 6000	0.75	1.35	1.01
B 214.....	Guilleminot 1-G.....	4400 5500	1.0	0.97	0.97

SURFACE BRIGHTNESS

For the objects selected from Hubble's catalogue of galactic nebulae we have the magnitude of the star, its spectral type, and the color excess on the Mount Wilson scale. Addition of the color excess to the normal color index for the spectral class[16] gives the color index of the star on the Mount Wilson system. By dividing by the appropriate correcting factor, this color index is brought to the scale of the plates here used, and the corresponding photo-red magnitudes are computed.

[15] *Ap. J.*, **42**, 120, 1915.

[16] *Ibid.*, **52**, 11, 1920.

For each extrafocal image separately we have the light corresponding to a certain stellar magnitude spread over the measured area of the image. From this we obtain the intensity in the extrafocal image in magnitudes per square millimeter. By use of the known scale of the plate (87″.4 per mm) the surface brightness in the nebula which would correspond exactly to this intensity in the extrafocal image is calculated in magnitudes per square second of arc.

The magnitude difference between equal small areas in the extrafocal image and in the nebula has been measured and corrected, as already explained; and the addition of this quantity gives the actual surface brightness of the nebula. The difference of these surface brightnesses, as obtained from a pair of plates, is the color index of the nebula on the scale of the plates used. Multiplication by the correcting factor reduces this quantity to the Mount Wilson system. For the sake of uniformity the surface brightnesses have been tabulated (Table 8) on the Mount Wilson scale for both colors. This has been done by applying the color indices on this scale to the photographic magnitudes per square second of arc.

SURFACE BRIGHTNESS OF THE NIGHT SKY

For the sky we cannot similarly obtain a proper estimate of the color index because the blue and the red plates were not taken simultaneously at the same altitude. The work of Lord Rayleigh and other observers[17] has shown that, owing to fluctuation of the permanent aurora, the red intensity of the sky brightness varies not only from night to night but even from hour to hour. The calculated intensities of sky brightness in the two colors have therefore not been combined but have been plotted separately against zenith distance at mid-exposure (Figs. 2 and 3). The mean for the blue plates is 3.68 mag. per square degree and the mean for the red plates is 2.97 mag. These results, which refer to many different nights over a period of several months, merely serve to emphasize the variability of the night sky in red intensity and the smaller variability in the blue. The blue intensity shows a definite increase toward the horizon in spite of the scatter in the times at which the observations were made.

[17] Déjardin, *Rev. Mod. Phys.*, **8**, 14, 1936.

IC 4601 AND BD−19°4357

Δm (Neb.−Sky)

Average of Points	Blue	Red
1, 2, 3, 4, and 9	+1.11	+2.30
5, 6, 7, and 8	1.04	2.11
10 and 11	1.98	3.24
12–19	+2.60	+3.40

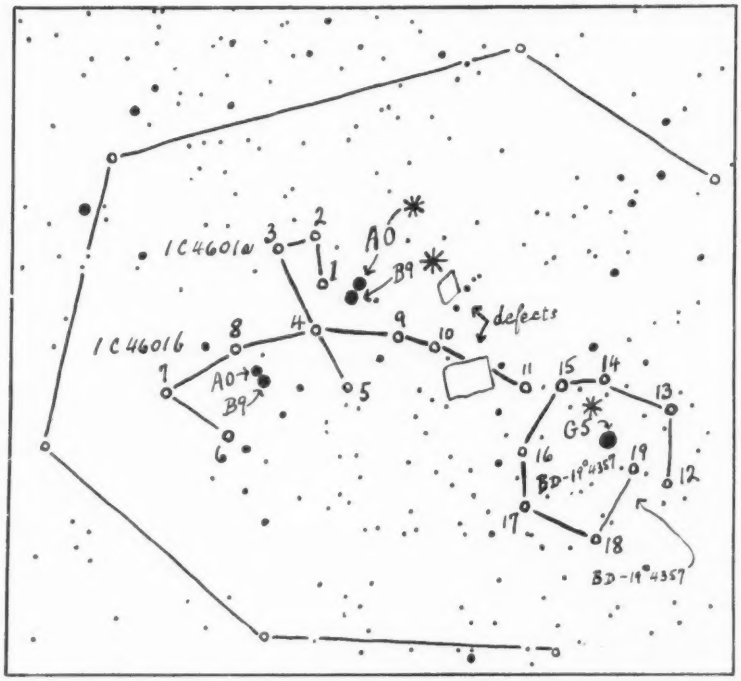

Scale: 1 mm = 27″

PLATE XXI

IC 4601 AND BD −19°4357

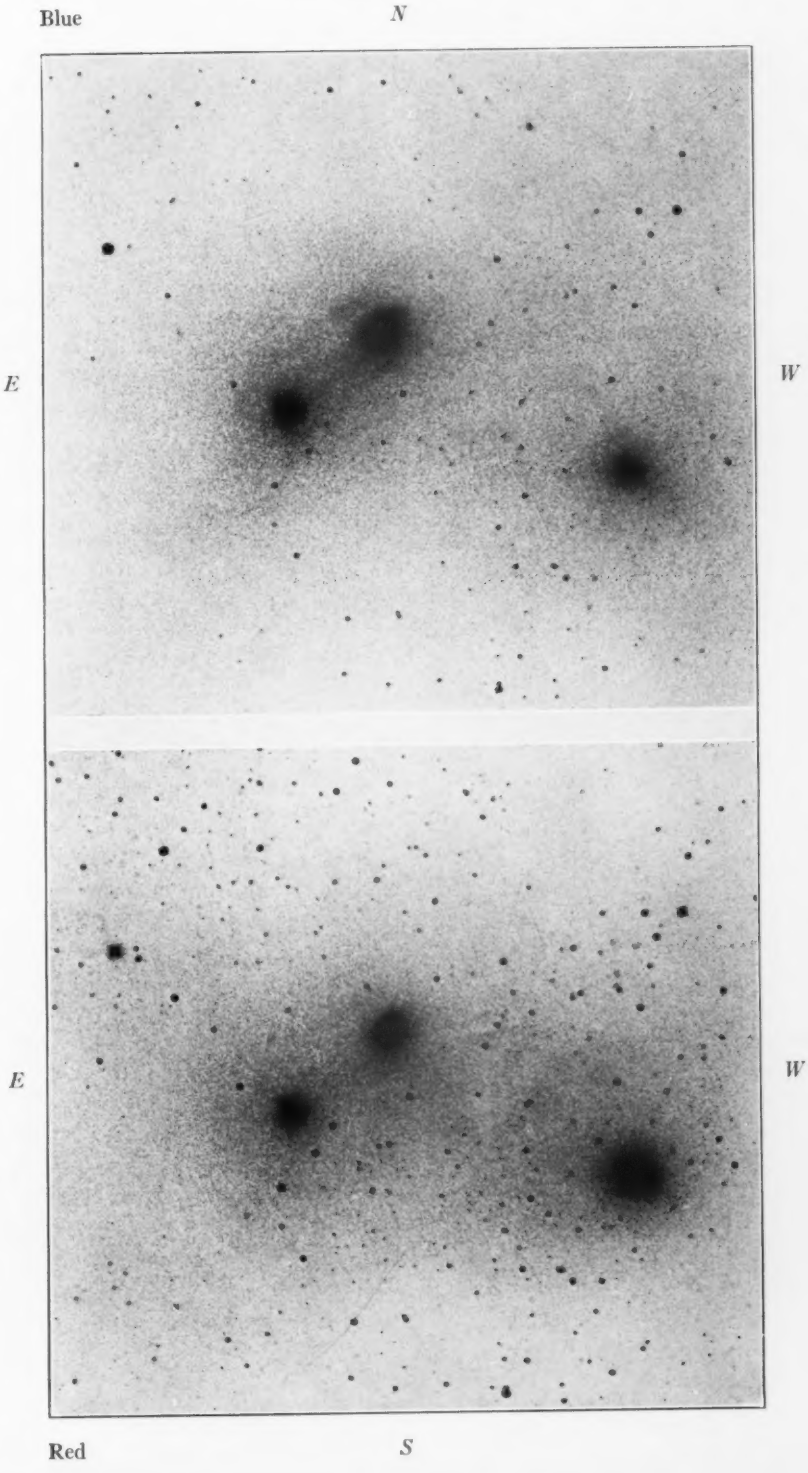

PLATE XXII

B 214

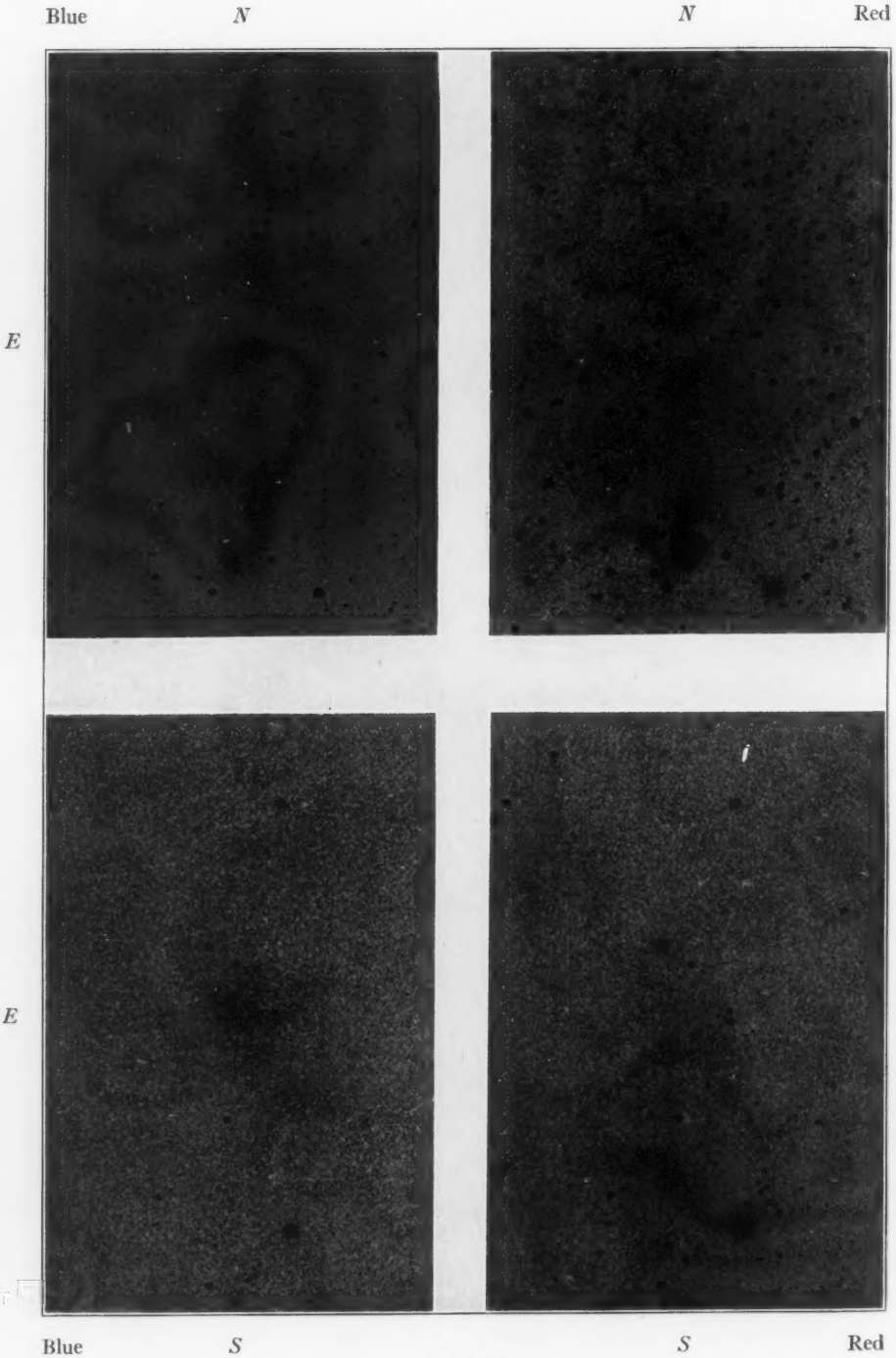

IC 359?

B 10

B 214

Scale: 1 mm = 21″

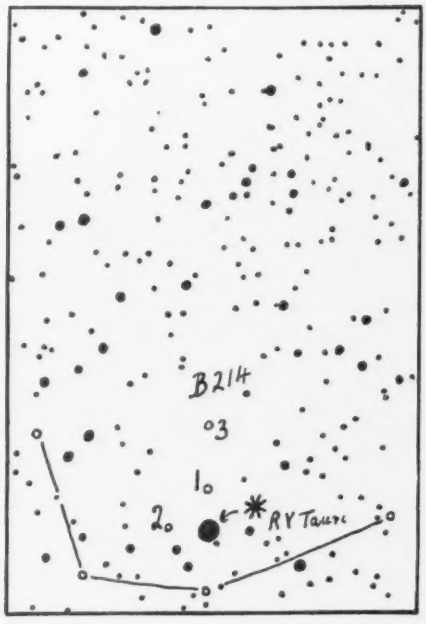

Δm (Neb.−Sky)

	Blue	Red
1	+1.30	+1.23
2	(2.73)	2.29
3	(+3.51)	(+2.97)

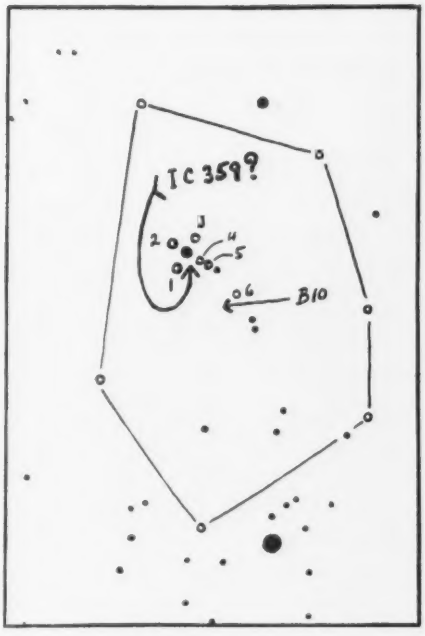

Δm (Neb.−Sky)

	Blue	Red
1	(+5.06)	+2.53
2	(5.06)	2.42
3	(5.06)	(3.31)
4	(5.06)	2.42
5	(3.09)	(3.55)
6	+2.22	(+3.31)

Scale: 1 mm = 23″

IC 359?

B 10

NGC 1333

Scale: 1 mm = 23″

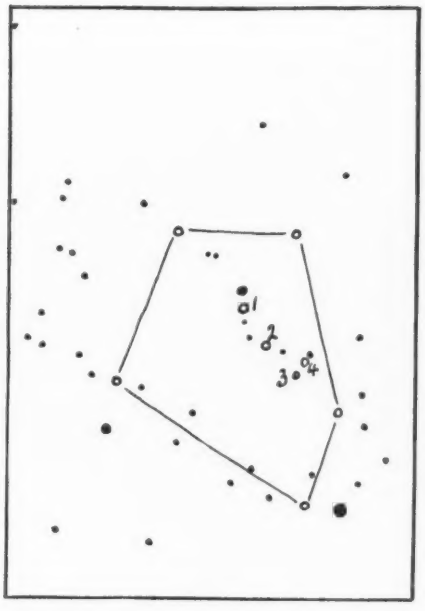

Δm (Neb.−Sky)

	Blue	Red
1	+0.59	+1.60
2	0.98	1.42
3	1.98	(2.59)
4	(+2.59)	[+2.23]

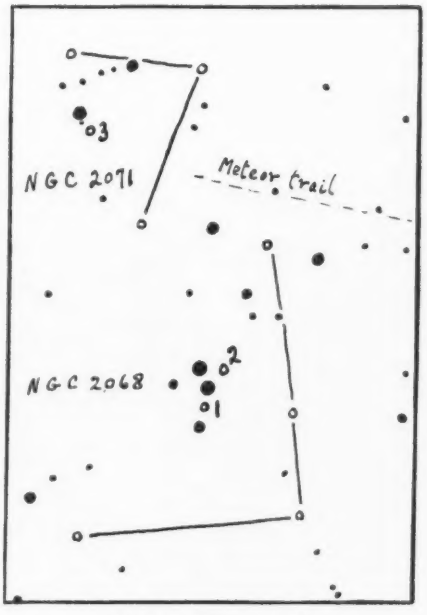

Δm (Neb.−Sky)

	Blue	Red
1	−1.33	+0.37
2	−1.69	+0.13
3	−0.27	+1.26

Scale: 1 mm = 23″

NGC 2071
NGC 2068

PLATE XXIII

NGC 1333

Blue *N* *N* Red

E *W*

E *W*

Blue *S* *S* Red

NGC 2071

NGC 2068

PLATE XXIV

NEAR MEROPE

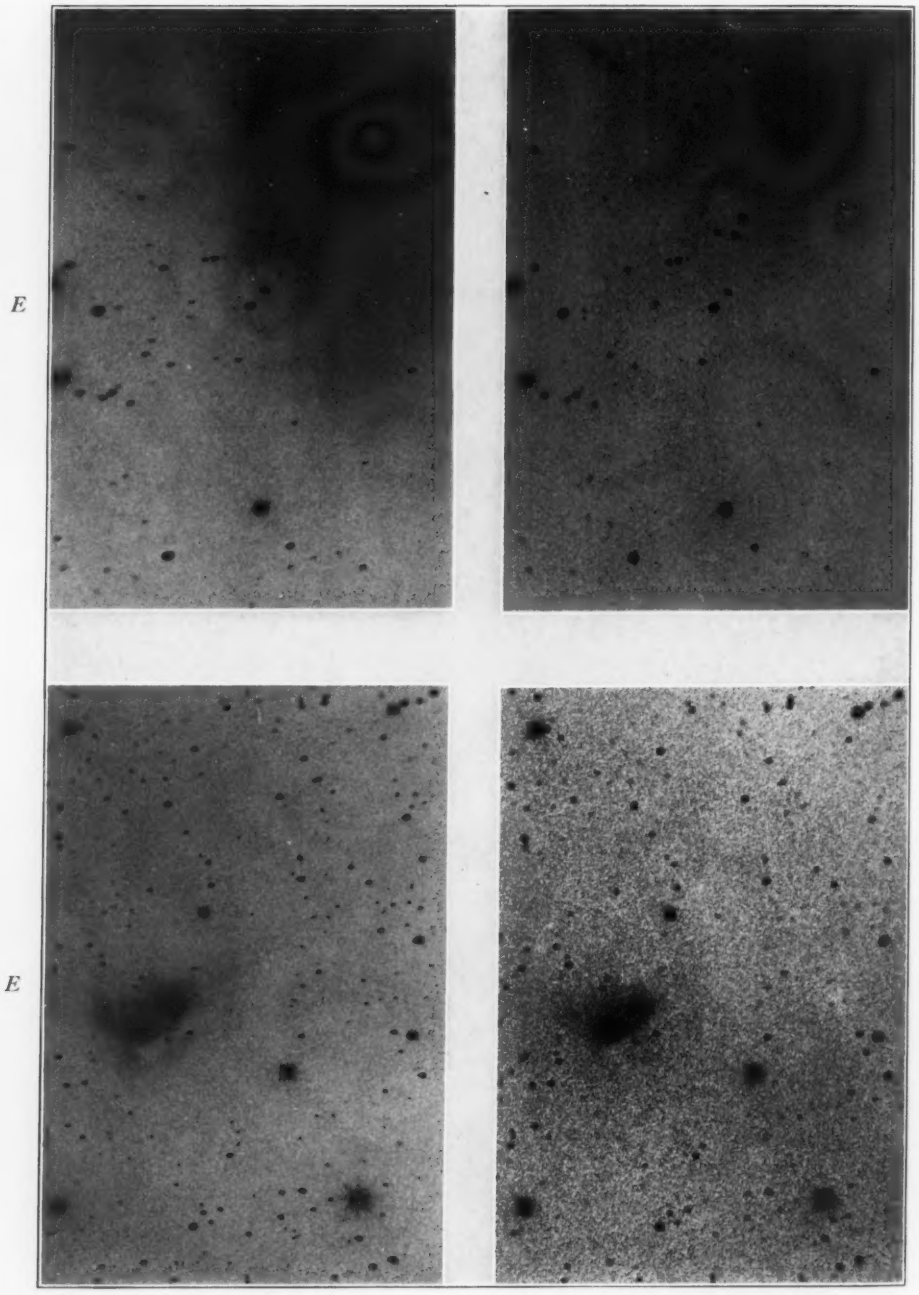

NGC 1788

NEAR MEROPE

Scale: 1 mm = 23″

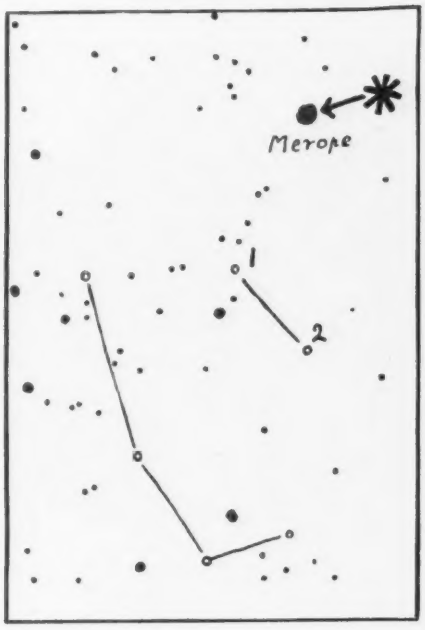

Δm (Neb.−Sky)

	Blue	Red
1	−0.01	+1.88
2	+0.36	+2.21

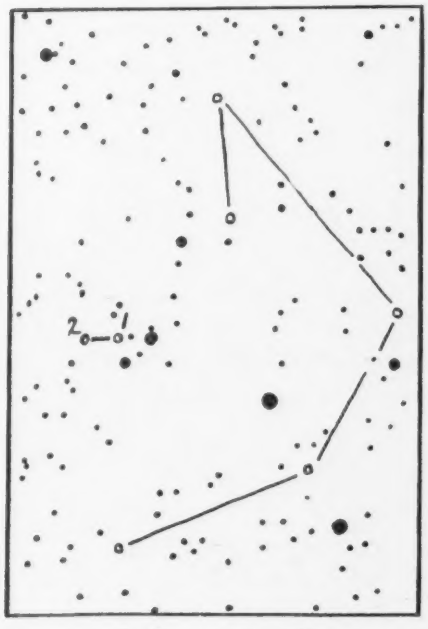

Δm (Neb.−Sky)

	Blue	Red
1	−0.28	+1.03
2	+0.57	+1.24

Scale: 1 mm = 23″

NGC 1788

IC 348

Scale: 1 mm = 23″

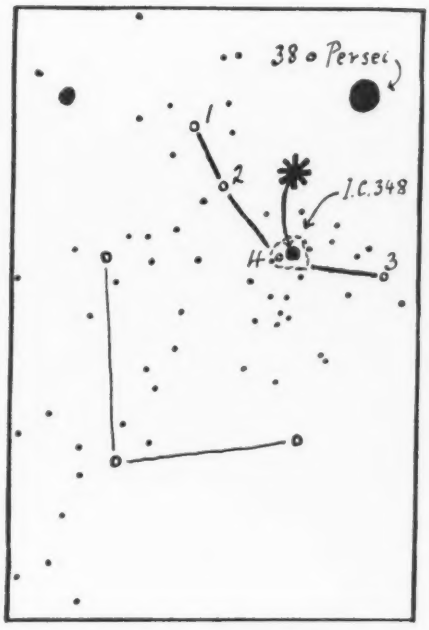

Δm (Neb.−Sky)

	Blue	Red
1	+0.45	(+2.91)
2	+ .97	(3.53)
3	+ .83	(3.08)
4	−0.63	+0.28

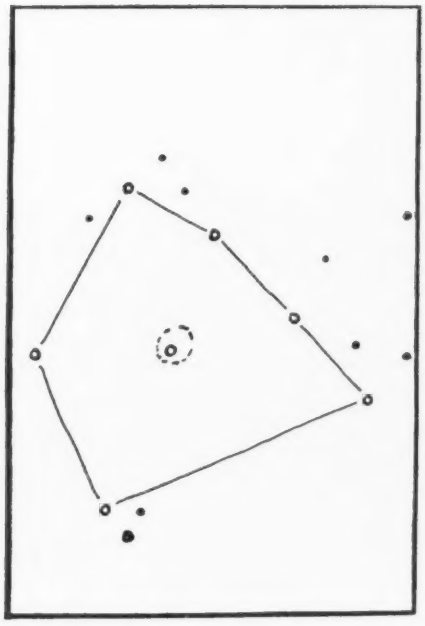

Δm (Neb.−Sky)

	Blue	Red
1	+2.49	+1.77

Scale: 1 mm = 23″

B 14

PLATE XXV

IC 348

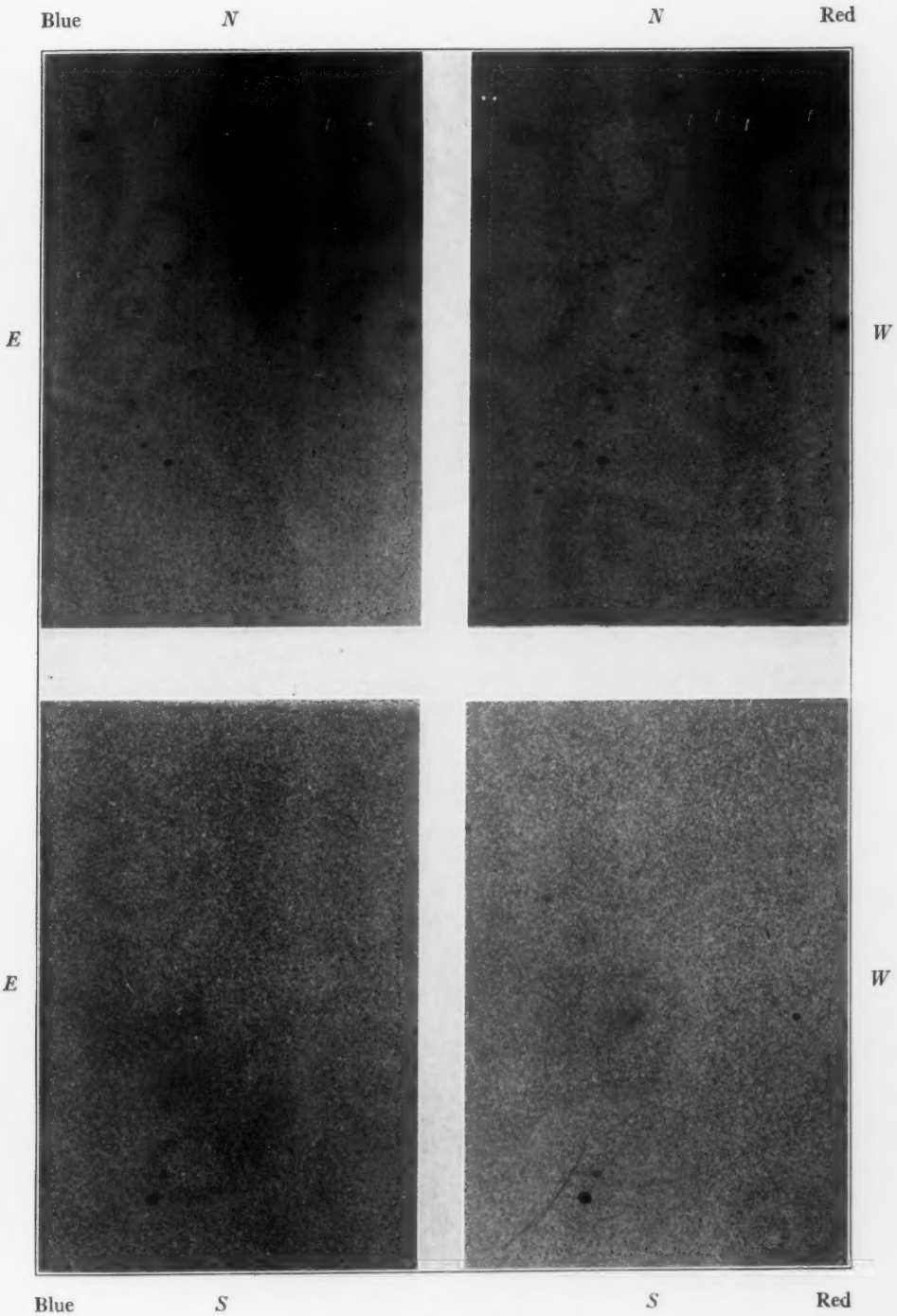

B 14

PLATE XXVI

NGC 2023
IC 435

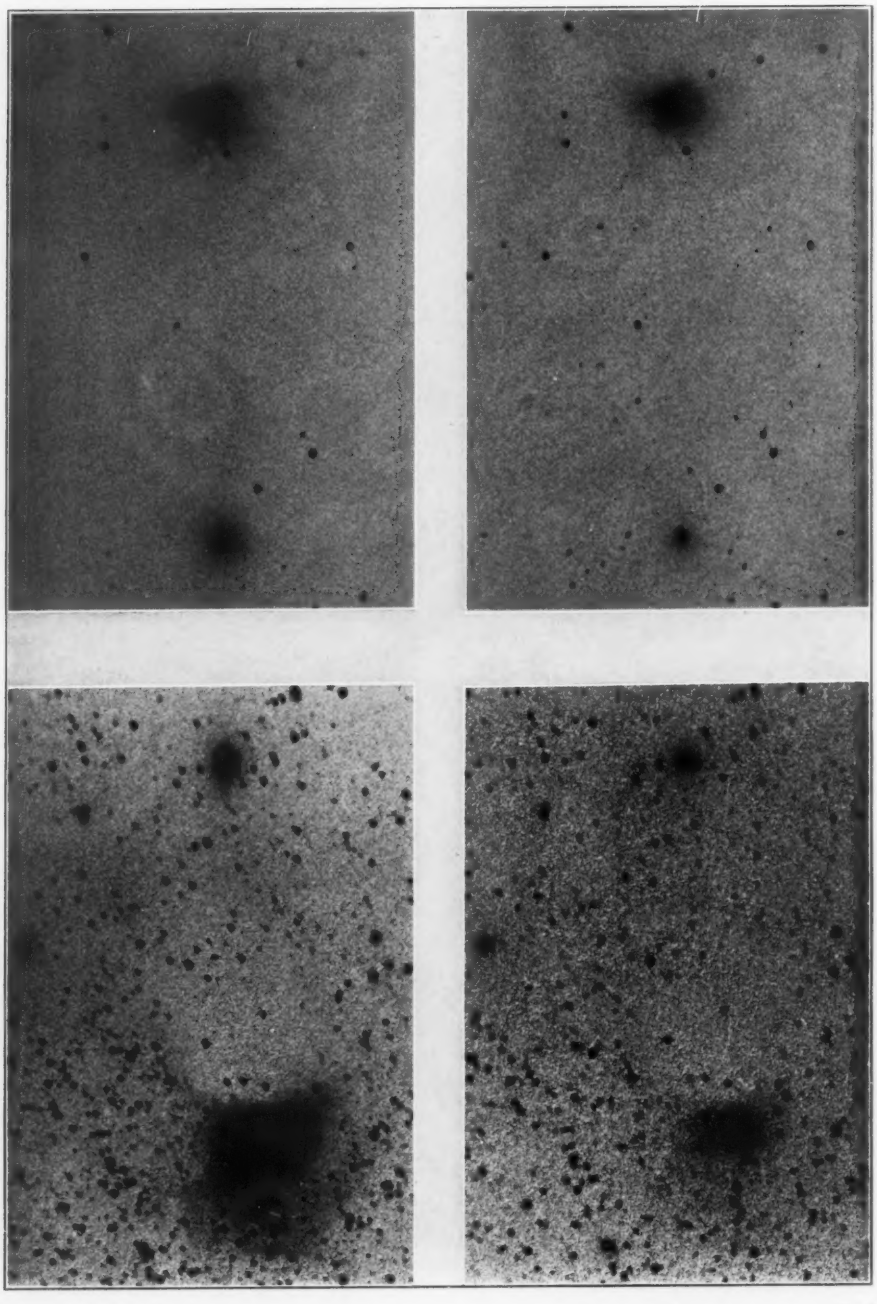

BD −12°1771

NGC 2023

IC 435

Scale: 1 mm = 23″

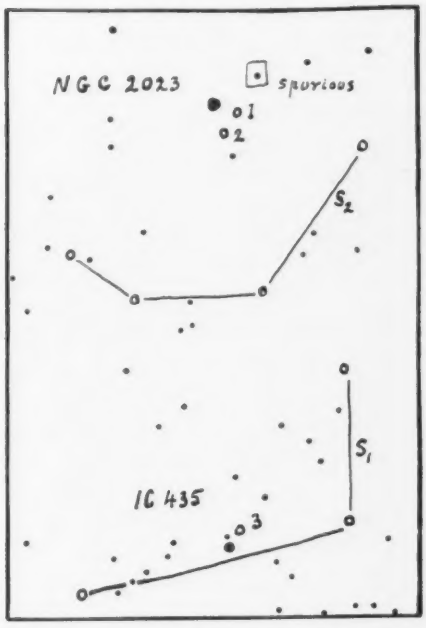

Δm (Neb.−Sky)

	Blue	Red
1	−0.80	+0.01
2	− .75	0.47
3	+0.20	+2.19

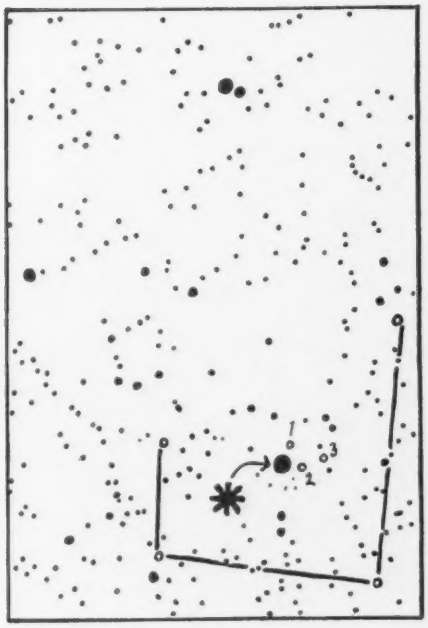

Δm (Neb.−Sky)

	Blue	Red
1	−0.92	+0.94
2	−1.14	0.76
3	+0.23	(+2.89)

Scale: 1 mm = 23″

BD−12°1771

IC 5146

Scale: 1 mm = 23″

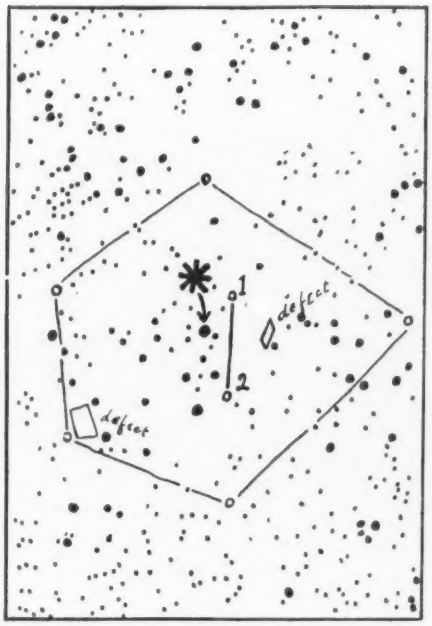

Δm (Neb.−Sky)

	Blue	Red
1	+0.70	+1.24
2	+0.46	+1.33

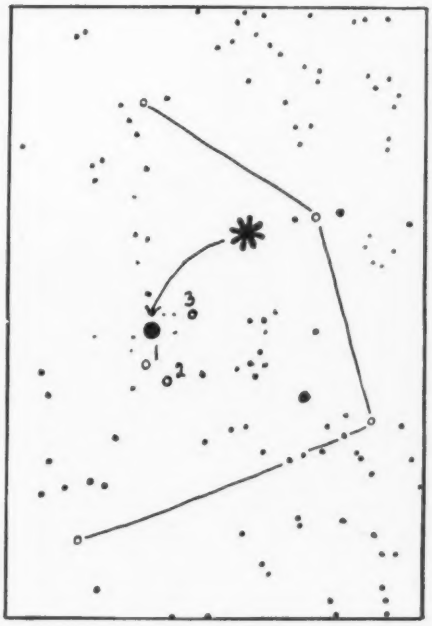

Δm (Neb.−Sky)

	Blue	Red
1	−1.49	−0.10
2	+0.28	+1.69
3	−0.48	+1.07

Scale: 1 mm = 23″

NGC 7023

PLATE XXVII

IC 5146

Blue *N* *N* Red

E *W*

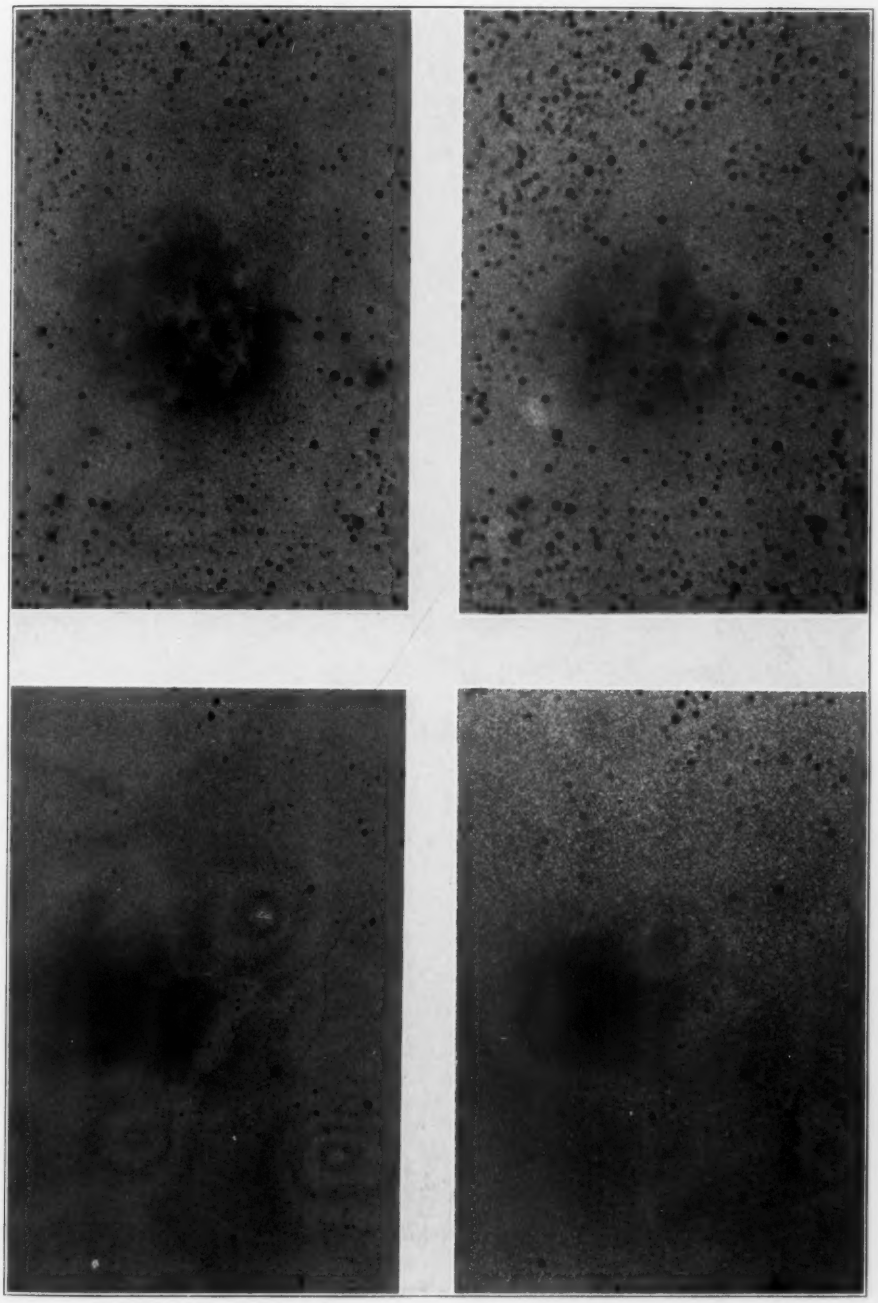

E *W*

Blue *S* *S* Red

NGC 7023

PLATE XXVIII

NGC 6914

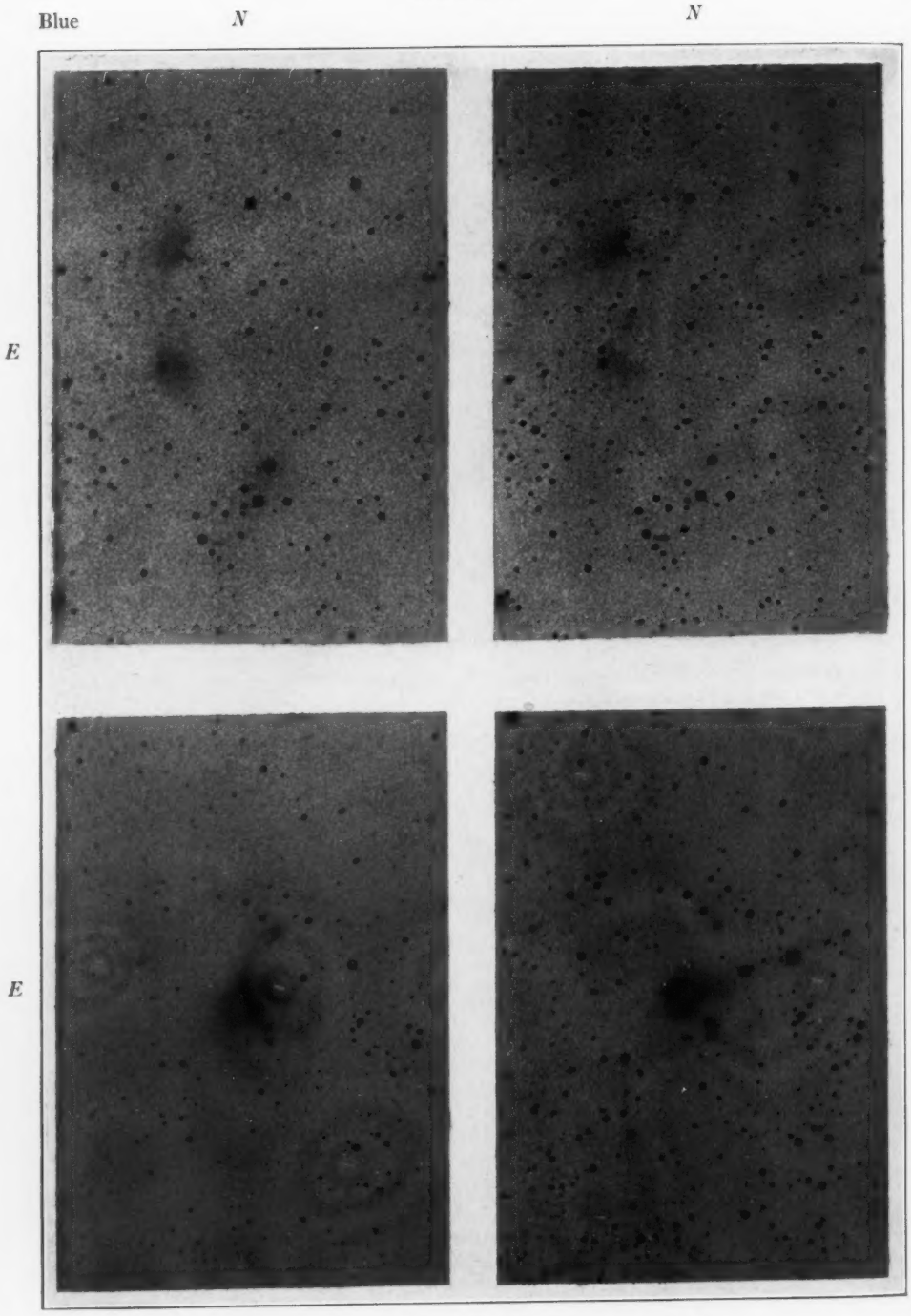

NGC 7129

NGC 6914

Scale: 1 mm = 23″

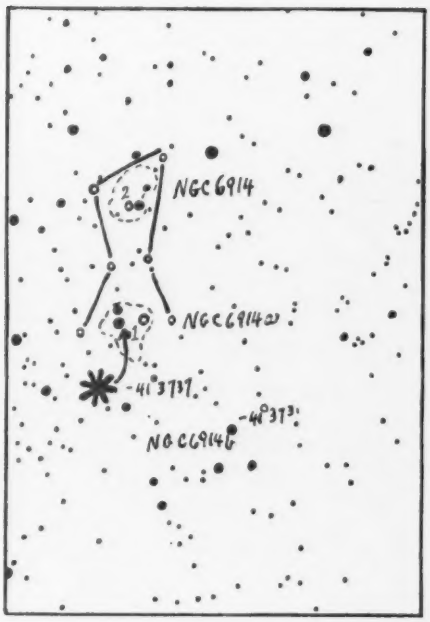

Δm (Neb.−Sky)

	Blue	Red
1	+1.02	+2.35
2	+0.86	+1.34

NGC 7129

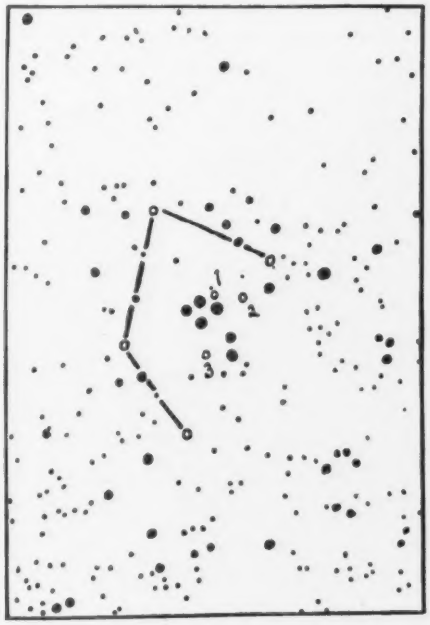

Scale: 1 mm = 23″

Δm (Neb.−Sky)

	Blue	Red
1	−0.90	−0.26
2	+0.94	+1.26
3	+1.22	+1.13

This variability of the color of the sky background must be taken into account in forming judgment from visual inspection of the plates.

DISCUSSION OF THE INDIVIDUAL FIELDS

For each field reproductions are given of a pair of negatives on a scale which is about four times that of the original plates. These were made from prints selected for equal density of sky background. The charts accompanying the reproductions give the positions at which measures of Δm were made in the images of the nebulae, and the comparison is in each case with the intensity at the points adopted as representing the mean sky background. To aid the eye,

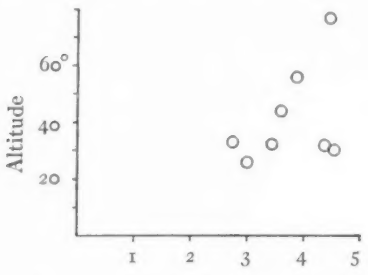

FIG. 2.—Magnitude per square degree of night sky in blue light.

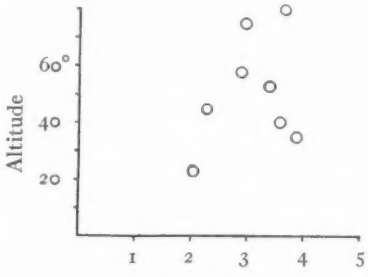

FIG. 3.—Magnitude per square degree of night sky in red light.

these points have been joined by straight lines. An asterisk on the chart indicates the star of which the extrafocal image was measured on a separate short exposure on the same plate.

Beside each chart is given the difference in magnitude, on the scale of the plates, between the nebula at the numbered points and the sky background, as defined by the mean of the unnumbered points on the chart. This magnitude difference has been corrected so as to remove the superimposed sky background from the nebula and to give, relative to the sky, the brightness of the nebula alone as seen through unit air mass. A positive sign indicates that the nebula is fainter than the sky; and a negative sign, that it is brighter.

Parentheses inclose certain results, concerning the precision of which special comment is made later. Square brackets inclose results which refer to areas of exceptional color in the nebulae. Results in both these classes are disregarded in forming the mean values for the color indices, which appear in Table 8.

IC 4601 and BD−19°4357 (Pl. XXI).—These plates were taken through the Ross correcting lens, with the result that the extrafocal images were measurable at 15′ off the optical axis. The stars in IC 4601 b were not measurable because of the overlapping of the two large extrafocal images.

This field has been shown on a smaller scale and briefly discussed by Struve, Elvey, and Roach.[18] These objects are less than 30′ apart

TABLE 8

Object	Spec. of Nebula	m_{pg}	Spec. of Star	C.E.	C.I.	Sky per Square Degree		Nebula per Square Second of Arc		Color Index of Nebula	
						m_{pg}	m_{pv}	m_{pg}	m_{pv}	II	I
IC 4601 a	C	7.1	B9, Aop	+0.20	+0.20	3.04	2.09	21.93	21.87	+0.06	−0.39
IC 4601 b	C	7.1	B8, Ao	0.32	+0.30	.....	.....	.....	.....	.....	− .30
BD−19°4357	.....	7.2	Ko	0.00	+1.20	2.94	2.10	23.32	23.08	+0.24	− .10
B 214	.....	v	F8?	.....	+0.93	4.56	3.59	23.64	22.60	+1.04	+ .57
IC 359?	C	13.5	K8d	0.00	.....	.....	.....	.....	.....	.....	.....
B 10	.....	.....	.....	.....	.....	.....	.....	.....	.....	.....	− .15
NGC 1333	C	10.9	B9p	0.30	+0.27	.....	.....	.....	.....	.....	+ .07
NGC 2071	C	10.8	B9	0.80	+0.77	.....	.....	.....	.....	.....	− .42
NGC 2068	C	10.8	B5	1.00	+0.80	.....	.....	.....	.....	.....	− .52
Near Merope	C	4.0	B5	0.00	−0.13	2.75	2.26	20.89	21.51	−0.62	− .62
NGC 1788	C	10.2	B8	0.22	+0.15	.....	.....	.....	.....	.....	− .44
IC 348	C	9.0	B6, A1	0.80	+0.65	3.88	2.89	21.40	20.78	+0.62	+ .13
B 14	.....	.....	.....	.....	.....	.....	.....	.....	.....	.....	+ .93
NGC 2023	C	7.9	B2	0.30	0.00	.....	.....	.....	.....	.....	− .10
IC 435	C	8.2	B3	0.20	−0.05	.....	.....	.....	.....	.....	− .69
BD−12°1771	C	8.1	B1	0.20	−0.15	4.36	3.88	21.22	21.86	−0.64	− .63
IC 5146	c	10.4	B1	0.97	+0.62	4.48	3.64	22.82	22.16	+0.66	+ .08
NGC 7023	C	7.4	B2p	0.55	+0.25	3.65	2.87	21.71	21.78	−0.07	− .34
NGC 6914 a	C	8.9	B3	0.00	−0.25	3.46	3.38	22.26	22.98	−0.72	− .30
NGC 7129	C	10.5	B3	+0.60	+0.35	.....	.....	.....	.....	.....	+0.24

and are evidently involved in the same nebulosity, the color of which at different points is dependent on the color of the illuminating star. The nebula surrounding the early-type stars is bluer than the stars by 0.14 mag. Around the late-type star the measures indicate that the nebula is less red than the star by nearly 1 mag. This is the amount which would be required by Rayleigh scattering, but the color difference is likely to be overestimated in this case because of the faintness of this part of the nebula.

The star BD−19°4357 is given in the *Draper Catalogue* as Ko (HD 146834). Its color index, as determined by comparison with the early-type stars on these plates, agrees with this classification, which

[18] *Op. cit.*, p. 223.

is therefore adopted in place of G5, as given by Seares and Hubble.[19] Its color excess, accordingly, is taken as zero instead of the negative value (−0.2 spectral classes) which they assign.

The structure of the nebula is of interest and is seen to be the same in both colors. The defects indicated on the chart refer to the red plate.

B 214 (*Pl. XXII*).)These plates were taken through the Ross correcting lens. The star which illuminates the southern end of Barnard's dark object B 214 is RY Tauri, a variable of R Coronae Borealis type. This star was not used for comparison with the nebula, but the surface brightness was measured by means of an Ao star (HD 27404) which lies outside the limits of the reproduction. The extrafocal images of RY Tauri were measured, and by comparison with the Ao star its color index is +0.93 mag.

A star of high color index is noted within the dark area on the red plate. Comparison with plates taken by Barnard failed to reveal any proper motion in this object over a period of fifteen years.

IC 359? (*Pl. XXII*).—This object is described by Hubble[20] as follows: "A nebulous star north following the nebula at $\alpha = 4^h14^m$, $\delta = 28°5'$ (1920), described by Barnard in *Ap. J.*, **25**, 223, 1907, and which may be IC 359."

Visual inspection of the plates shows the faint nebulosity around the star (K8) to be redder than the sky. The nebular image on the blue plate gives a measured Δm of only −0.01 mag. when compared with the sky. For values of Δm so near zero the formula for the removal of superimposed sky brightness leads to an increase in the uncertainty by a factor of about 100. The nebula is undoubtedly red, but a reliable measure was not obtained.

Barnard's dark area B 10, which appears on these plates, has been discussed recently by Struve.[21]

These plates and all that follow were taken without use of the Ross correcting lens.

NGC 1333 (*Pl. XXIII*).—In this field a point (No. 4) is noted as being redder than the remainder of the nebula by at least half a magnitude. On the blue plate a distinct gap is seen in the nebular

[19] *Op. cit.*, p. 14. [20] *Op. cit.*, p. 406. [21] *Ap. J.*, **85**, 211, 1937.

filament at this point, and on the red plate a stellar image appears within 20″.

Nebula near Merope (*Pl. XXIV*).—These plates show the nebula near Merope to be bluer than Merope by 0.49 mag. Struve, Elvey, and Keenan[22] compared the spectrum of the nebula near Maia with the spectrum of Maia and found the nebula bluer than the star by 0.3 ± 0.2 mag.

IC 348 (*Pl. XXV*).—This object is less than 8′ distant from 38 *o* Persei (B1), the scattered light from which is superimposed on the nebula in addition to the ordinary sky background. Measures were made at points 1, 2, and 3 in addition to that at point 4 in IC 348. Correction for sky background was made as usual. The mean of the residual intensities at points 1, 2, and 3 on each plate was adopted as a measure of the intensity due to *o* Persei at point 4. The intensity at point 4 in IC 348 was correspondingly reduced for each plate, and the color difference between the nebula and the sky was calculated in magnitudes.

B 14 (*Pl. XXV*).—This object has been discussed recently by Struve.[23] No illuminating star brighter than photographic magnitude 17 is found.

IC 5146 (*Pl. XXVII*).—The spectrum of this nebula is classified by Hubble as c (presumed to be continuous), and the spectral class of the illuminating star as B1. A photograph by M. de Kerolyr[24] taken with the 80-cm reflector at Fourcalquier and having a total exposure time of 12^h30^m shows the nebula extending as a faint cloud to the east. The defects indicated on the chart refer to the red plate. No real differences of structure are noted.

NGC 7023 (*Pl. XXVII*).—At the points indicated on the chart this nebula is bluer than the illuminating star by 0.3 mag. Keenan,[25] who observed this object with the Perkins reflector, has given reproductions on a larger scale, showing in more detail the inner structure of the nebula, in which he found color differences ranging from −0.23 mag. to +0.26 mag., relative to the star, and a stronger red excess in certain parts.

[22] *Op. cit.*, p. 279.

[23] *Op. cit.*, p. 211.

[24] *M.N.*, **96**, 122, 1935.

[25] *Op. cit.*, p. 600.

NGC 7129 (*Pl. XXVIII*).—On the red plate of this field there is seen (at point No. 3) a small patch of nebulosity about 20″ in diameter. This area is 0.3 mag. redder than the rest of the nebula. The observation is confirmed by a second pair of plates taken on a different night.

DISCUSSION OF RESULTS FROM ALL OBJECTS

In Table 8 the first six columns contain data for each nebula observed and for its illuminating star, all of which is adopted from the Mount Wilson work, with the exception already noted with respect to BD $-19°4357$.

The next five columns contain, for certain nebulae, the average results obtained in the present investigation by using extrafocal images of the illuminating stars in conjunction with the Mount Wilson data (Method II).

In the last column are the color indices of the nebulae as obtained by adopting a mean value of +0.50 mag. for the color index of the sky. From the figures given beside the charts for each of the measured points the colors of the nebulae at these points relative to the sky background have been obtained, and these have been reduced to the Mount Wilson system by the use of the correcting factors. To the average of these quantities for each nebula has been added the adopted color index of the sky (Method I).

Comparison of Methods I and II.—Lack of uniformity in the color of the sky background renders results obtained by the first method less reliable.

Agreement of results from the two methods occurs where the effective color index of the sky, as given by the pair of plates concerned, happens to approximate the adopted value of 0.50 mag.

The mean color index of all objects, obtained by the first method, is −0.16 mag.

The mean color index obtained by the second method, for those objects to which it was applied, is +0.06 mag. The mean color index of these last objects alone, obtained by the first method, is −0.18 mag. This is sufficiently close to the mean for all objects taken by this method to make it appear that the selection of objects for the

second method was made without dependence on color. In the mean the color indices given by the first method are lower than those given by the second method, by 0.24 mag. This amount is dependent on the value adopted for the color index of the sky.

An effective color index for the sky.—The difference of the means of the sky background intensities in the two colors for the fields where the second method was employed is +0.71 mag. This cannot be taken as a mean value for the color index of the sky, for reasons already given. It may, however, be adopted as a mean effective color index of the sky for the pairs of plates here used, since all pairs were taken in the same manner.

Modification of Method I.—If the value +0.71 mag. is used in place of the adopted value +0.5 mag. in the first method, the mean then obtained from the color indices of all objects is +0.05 mag., which agrees closely with +0.06 mag. given by the second method. The corresponding mean color index for those objects alone to which the second method was applied is +0.03 mag. Method I, thus modified, agrees well in the mean with Method II; but the latter is preferred for accuracy of individual determinations. The individual values according to this modified Method I may be obtained by adding +0.21 mag. to the values in the last column of Table 8.

Probable error of color indices.—The departures of these new figures from those given by Method II have been used for calculating their probable error on the fictitious assumption that the results given by Method II are exact. The true probable error for the modified Method I is greater than the value ±0.22 mag. thus found, and may be obtained by combining this quantity with the probable error due to Method II.

In Method II the accuracy of the figures for the intensity of the sky and for the intensity of the nebula is dependent on the adopted magnitudes of the stars used for the comparisons, on the spectral classes assigned, and on the color excesses found, as well as on the precision of the present comparisons of nebula and star. The color indices of the nebulae, however, are independent of the adopted magnitudes of the stars and depend only on the color indices of the stars and on the present observations.

The precision of measurement of these plates is shown in Table 9, where there are given, in parallel columns, the Δm of the nebular images over the sky background for two focal exposures of the NGC 1333 field, made separately on a single plate on consecutive nights over precisely the same range of hour angle. This plate was calibrated in the usual way, and the two exposures were measured together against the same set of sensitometer exposures.

Where extrafocal images were obtained, they were on the same plate with the focal exposure and were measured against the same sensitometer exposures. The comparison in each color was thus con-

TABLE 9

MEASURES FROM SEPARATE FOCAL EXPOSURES ON A SINGLE PLATE SHOWING PRECISION OF MEASURING

Point	Exposure *a*	Exposure *b*
	Δm	Δm
1	−0.39	−0.38
2	.26	.30
3	.12	.11
4	.08	.07
5	−0.13	−0.11

tained on a single plate and was independent of the plate in the other color, provided no variability of star or nebula was to be considered. It was, however, considered desirable to take the two plates on the same night whenever possible; and in doing this, the red plate was in each case taken at the higher altitude in order to give it the advantage of the lesser air mass.

The correction for the removal of the superimposed sky brightness increases the uncertainty from the original measures in a ratio which is greater for the measures nearer to zero. For Δm <0.10 mag., the uncertainty is increased by a factor greater than 10, and the results from such measures have therefore been set in parentheses to indicate their lower precision. For the values of Δm most commonly encountered, the uncertainty was increased by a factor between 1 and 4 (see Table 2).

The correction for the ratio (r) of focal to extrafocal exposure depends on the probable error of the determination of p for each plate and on the value of r, and may in the most extreme case ($r = 900$) amount to 0.09 mag. The application of a correction factor less than unity in bringing the results to the Mount Wilson scale has had the effect of reducing their uncertainty. In plotting the graphs in Figures 4 and 5 the points corresponding to each observation have been indicated by circles of which the radius corresponds to 0.10

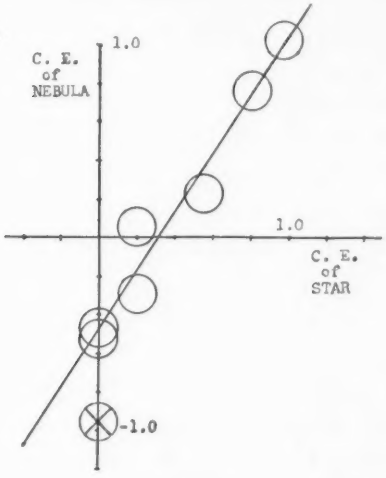

FIG. 4

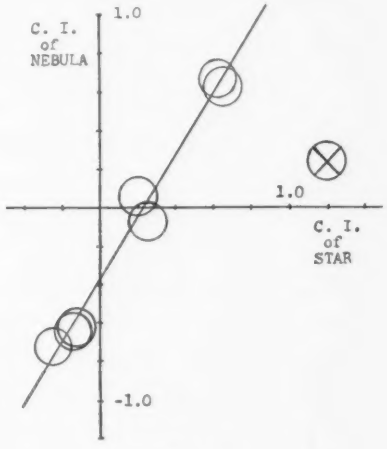

FIG. 5

mag. This value has been adopted as an estimate of the mean probable error in the results obtained by the use of extrafocal images (Method II).

Mean color difference, nebula minus star.—For the illuminating stars the mean of the color indices has the value +0.35 mag. The mean difference of color between the observed nebulae and their illuminating stars is therefore −0.3 mag., the negative sign indicating that the nebulae are, in the mean, bluer than the stars. These color differences trend from −0.50 mag. to zero with increasing color excess of the star (see Fig. 4).

Color excess of nebula.—We shall adopt the term "color excess of the nebula" to indicate the difference between the color of a nebula

and the color of a normal star of the same spectral type as the star which illuminates that nebula.

Discussion of graphs.—The color excess of each nebula[26] has been plotted in Figure 4 against the color excess of its illuminating star. Greater physical significance might be expected to attach to these quantities than to the actual color indices, which are measured from an arbitrary zero-point (Ao) not necessarily near the color of the star concerned. The observations are seen to be gathered about a straight line which does not pass through the origin and is inclined more steeply than 45°. The 45° straight line through the origin is not drawn, but it is on this line that the observations should fall if the observed colors of the nebula and the star were the same. The distance by which the observation falls vertically below (or above) this line corresponds to the difference of color between nebula and star as observed, the mean of which difference is −0.27 mag.[27] The minus sign indicates that the nebulae are bluer than the stars.

The trend of the observations at an angle greater than 45° indicates that with increasing color excess of the star there is less difference in color between nebula and star.

A similar graph was made of the same data before correction for zenith distance had been applied. The same trend was apparent in that graph, and the line of best fit had about the same slope as in Figure 4. The effect of correction to air mass unity was, of course, different for different points; but the effect in the graph was merely to lower the straight line by about 0.1 mag. The reason for this systematic effect lies in the fact that all the pairs of plates were taken with the blue plate at the lower altitude.

In Figure 5 the same observational material is presented as a plot of the color indices of the nebulae against the color indices of the stars. The straight line of best fit is seen to be placed similarly to

[26] B 214 illuminated by the variable RY Tauri is here omitted from the discussion.

[27] The uncertain color excess of the nebula near the Ko star has been omitted. If it were included, the mean value of the difference would be −0.40. The Ko observation is marked by a cross in the circle. With this observation omitted, a least-squares solution for the straight line gives

$$(y - 0.11) = 1.52\,(x - 0.39)\,.$$

that in the previous graph and to have nearly the same slope.[28] This is a necessary result of the relations of the quantities concerned. To convert the color excess graph into a color index graph we add to each color excess of a star or nebula the same quantity, namely, the color index of the normal star having the same spectral type as the star involved in the nebula. This addition of the same quantity to each co-ordinate of a point shifts that point along a 45° line, but by a different distance for each point according to the spectral type of star.

If the collineation of the points on the one graph were precise, then the points on the other graph would necessarily lie on a family of parallel straight lines on which they would be sorted out according to spectral type.

A comparison of the two graphs suggests that the color-excess relation is the fundamental one. Most of the stars are too nearly of similar spectral type to make the separation clear, except in the case of the K star, which is well separated from the others on the color-index diagram. This is the star BD $-19°4357$ (Pl. XXI), in discussing which it was suggested that the difference of color between nebula and star might be overestimated somewhat on account of the faintness of the object. It will be seen that a diminution of this difference from -0.97 by as much as 0.4 mag. would not adversely affect the collineation on the color-excess diagram.

The inclination of the line of the observations to the 45° line is probably real and is due to the progressive diminution of the color difference between nebula and star with increasing color excess of the star. This color difference between nebula and star would be changed by the adoption of a different correcting factor in bringing these results to the Mount Wilson scale. This change would be in the same proportion for all those observations to which it applied, and would have the effect of altering the inclination of the line to the 45° line. No such change, however, could bring these lines into coincidence, and a change of as much as 10 per cent in the correcting factor

[28] For this line, with the Ko observation omitted as before, a least-squares solution gives

$$(y + 0.10) = 1.58\,(x - 0.17).$$

would alter the slope very slightly. The fact that various pairs of plates have different correcting factors applied to them diminishes the probability of error from this cause.

The conclusion is that for stars of high color excess there is little difference of color between stars and nebula, but that for stars of color excess near zero the nebulae associated with them are bluer than the stars, as observed, by an amount which is at least 0.5 mag. and, in the case of the single K star, may be as much as 0.97 mag. This last quantity, if not overestimated, would come close to the difference required by the Rayleigh law of scattering.

The results from the modified Method I are not shown on these graphs. When plotted as circles of 0.25 mag. radius on the color-excess diagram, they cluster about the straight line already obtained, and only three[29] of the fifteen circles fail to intersect this line. On the color-index graph four of the circles[30] fail to intersect this line. The agreement is as good as can be expected from this material, which depends on the conformity of the color index of the sky to a mean value.

It is tempting to explain the gradual increase of the color excesses of the nebulae from −0.5 mag. to 0.0 mag. as a result of selective reddening within the nebulae. Let us assume that at least a part of the large color excesses of some of the illuminating stars are produced within the nebulae.[6] Since the light path for the star's light reflected by the nebular particles is larger than that coming to us directly from the star, the effect of reddening should be somewhat greater for the nebula than for the star. Hence, it is possible that the true selective effect produced by the nebula is measured by the color excess of −0.5 (or about one-half of the Rayleigh value) found for those nebulae which are associated with the bluest stars. The diminution of the difference in color between the nebula and the star is, then, due to the combination of two effects: the constant selective color excess of −0.5 mag., and the progressive reddening which depends upon the optical thickness within the nebula.

It is difficult, with the material at hand, to test this hypothesis

[29] These are NGC 2071, NGC 2068, and NGC 6914 a.

[30] These are NGC 2071, NGC 2068, NGC 6914 a, and NGC 2023.

quantitatively. Shajn's results[6] seem to be unfavorable to it. It would be of interest to determine whether reflection nebulae tend to get redder as the angular distance from the illuminating star increases. However, the amount of this reddening depends upon the shape and the density distribution of the nebula, and it is at present difficult to predict the amount.

This work was done while on leave of absence from the University of Nebraska.

To the members of the staff of the Yerkes Observatory I am indebted for very many helpful conferences. In particular to Dr. Otto Struve I wish to express my thanks for the suggestion of this problem and my appreciation of his inspiring counsel during its progress.

YERKES OBSERVATORY
August 1937

THE VARIATION OF THE LIGHT FROM THE NIGHT SKY AND ITS EFFECT ON THE PHOTOGRAPHY OF FAINT NEBULAE

C. T. ELVEY AND PAUL RUDNICK

ABSTRACT

Observations have been made with a photoelectric photometer using a potassium photoelectric cell, and they show irregular variations, through the night, in the intensity of the light from the sky in the region of the North Pole. Also, there are variations from night to night which are quite large.

Computations have been made of the limiting magnitude of nebulae which could be observed, taking into consideration the variation of the sky brightness with respect to zenith distance, the zodiacal light, and the Milky Way.

It is concluded that the limiting magnitude of a nebula is a function of the position with respect to the zenith, the zodiacal light, and the Milky Way, and also with respect to time. For precise photometry of faint nebulae it is necessary to determine the brightness of the sky background by calibration with stars in the field at the time the photograph is being made.

During the spring of 1937 numerous photographs of faint nebulae were made at the McDonald Observatory with a Schmidt camera of aperture ratio 2.0, for the purpose of determining the colors of the nebulae. In order to obtain these, it was necessary to take photographs in two colors at different times. Since it was not possible to obtain the exposures simultaneously, any changes, then, in the intensity of the sky background would introduce errors in the results. In order to have a control on such errors, observations were made with the photoelectric photometer, described by Elvey and Roach,[1] for the constancy of the light from a given region of the night sky, in this case the North Pole.

There have been numerous observations of the light from the night sky, and much of this work has been summarized by G. Déjardin.[2] The observations indicate diurnal, annual, and long-period changes in the light from the night sky. This, of course, refers primarily to the light originating in the atmosphere of the earth and called the "permanent aurora." There are some discrepancies among the observations of the diurnal variation, in that some observers find a maximum of light early in the night while others find the light reaching its maximum intensity about 2 o'clock.

[1] *Ap. J.*, **85**, 213, 1937.

[2] *Rev. mod. phys.*, **8**, 1, 1936.

We have taken observations on several nights during April and May, 1937, when there was no moon in the sky, and we do not find any regularity for the variation of the intensity of the light (blue)

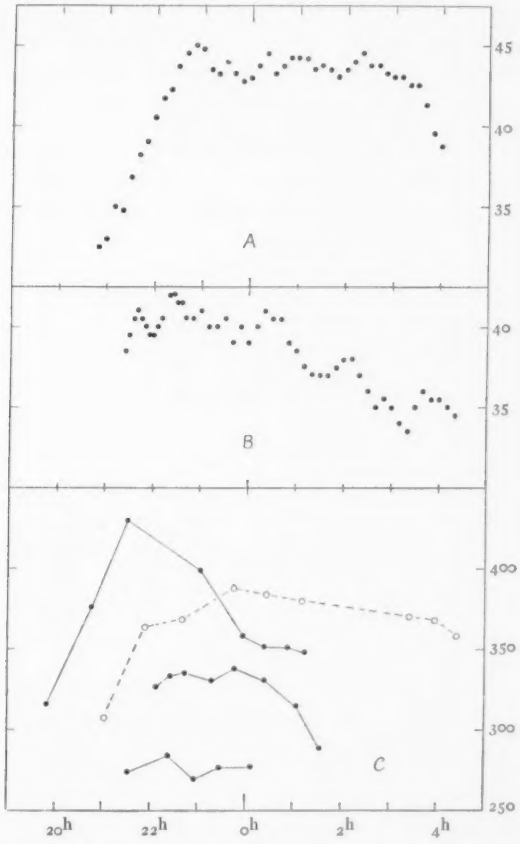

FIG. 1.—Variations of the light from the night sky in the region of the North Pole. The intensities in *A* and *B* are arbitrary units. In *C* the intensities are numbers of tenth-magnitude stars per square degree.

from the night sky. On one night there was a rather abrupt increase in the light after twilight, and then the intensity remained rather constant with small fluctuations during the remainder of the night, as is shown in Figure 1*a*. At other times we found variations through the night much like those shown in Figure 1*b*.

Although we did not find a regular diurnal variation in the in-

tensity of the light from the night sky, this must not be taken as a contradiction of the observations of Lord Rayleigh and others,[3] who have found diurnal effects, since we have observed with a potassium photoelectric cell which is sensitive to the region from 5000 A toward the violet. Our apparatus contains a rather large condensing lens of ordinary glass, which cuts off the ultraviolet. The radiations effective for the region observed are primarily those originating from the molecule of nitrogen, while the observations made by others, referred to above, are mainly in the region of the spectrum containing the green auroral line which has an entirely different

TABLE 1

VARIATION IN SKY BRIGHTNESS AT THE NORTH POLE

Date	Maximum Departure from the Mean for the Night	Date	Maximum Departure from the Mean for the Night
1937 Apr. 5	± 6%	1937 Apr. 30	± 5%
6	16	May 1	3
9	9	2	9
10	8	7	12
11	9	13	4
12	7	14	8
15	5		

origin, being a radiation from the metastable state of the oxygen atom. There is no a priori reason for believing that the two radiations should behave in the same manner.[4]

Our observations made during the months of April and May were not calibrated with stars, but comparisons were made with an artificial-light source to check the constancy of the photometer. The range of variation of the observed intensity may be seen by referring to Table 1, in which the maximum departures from the mean of the night are shown as percentages. Since the variation of intensity may go through the entire range within a short time, a factor is intro-

[3] The paper by Déjardin gives many references.

[4] Recent observations by Ceriajev, Khvostikov, and Panschin (*J. d. phys. et rad.*, **7**, 149, 1936) show that the green and red radiations from the night sky have marked variations with maxima near 1 o'clock, while the light from the blue region is more or less constant.

duced which must be taken into account in the photometry of nebulae.

In Figure 1*c* we show some observations made by Elvey and Roach with the same instrument and calibrated by means of observations of standard stars. The data are plotted on about the same scale as the others in order that approximate comparisons can be made. Only a few observations were obtained each night, but it is evident that there are rather large variations in intensity of the light from the night sky over short intervals of time.

TABLE 2

INTENSITY OF AURORAL *plus* SCATTERED LIGHT AT THE ALTITUDE OF THE NORTH POLE

Date	Intensity in No. of Tenth-Magnitude Stars per Square Degree	Date	Intensity in No. of Tenth-Magnitude Stars per Square Degree
1934 Nov. 8	144	1935 Feb. 27	104
9	165	Mar. 4	228
27	139	Apr. 3	200
Dec. 1	152	4	176
4	72	5	183
10	145	May 5	269
11	145	6	207
		June 6	214
1935 Jan. 8	148	July 9	195
25	145	10	173
27	114	Oct. 2	268
Feb. 26	114		

The variations from night to night in the intensity of the light from the night sky are even larger than the variations during the night. Since our observations were not calibrated, we will not discuss them but will refer to those made by Elvey and Roach[5] in their studies of the light from the night sky. The mean data for each night are given in Table 2 for the auroral plus scattered light. It is seen that there are large fluctuations in the intensity of the light, and also the annual variation, which has been noted by others, is evident. The maximum occurs in the summer months and the

[5] The data used here were not published in the paper referred to in n. 1.

minimum in the winter. The mean of the observations from November, 1934, to March, 1935, is 140, the unit being the number of tenth-magnitude stars per square degree, while the months of April–October, 1935, show a mean intensity of 210 in the same unit.

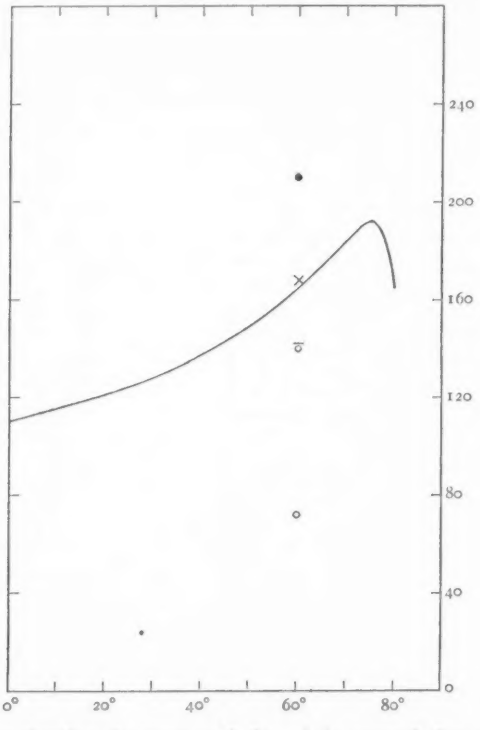

FIG. 2.—A curve showing the mean variation of the auroral plus scattered light of the night sky with zenith distance. The highest and lowest observed values at the zenith distance of the Pole are shown, as well as the mean of all observations (*cross*), and the means for the summer (*dot and bar*) and the winter months (*circle and bar*). The ordinates are intensities expressed in numbers of tenth-magnitude stars per square degree.

The distribution of the auroral plus scattered light with respect to the zenith distance is shown in Figure 2, which is plotted from the mean of all observations taken in 1934–1935. The variations from night to night are shown again in the figure by plotting the highest and the lowest intensities observed at the altitude of the Pole. Also, the mean intensities for the summer and the winter observations are shown.

The faintest nebulosity which can be photographed will depend upon the smallest difference that the photographic process can detect between the combined light of the sky background plus the nebula and the sky background itself. This, of course, is a function of many variables. For purposes of illustration we will assume that the photographic technique will enable us to detect a 5 per cent difference between the nebula plus sky and the sky background.

The data for the mean amount of auroral plus scattered light are given in Figure 2. By adding to this the sum of the zodiacal light and the unresolved stars, an average value for which is 100 in units of number of tenth-magnitude stars per square degree, and with appropriate corrections for extinction for the zodiacal light, we obtain an average brightness of the sky background for regions of the sky not too close to the ecliptic or the Milky Way. At a zenith distance of 60°, the foregoing is equivalent to 4.0 mag. per square degree.

Under the assumption that we have made—namely, that a 5 per cent increase in the brightness of the sky background would be detectable—we can readily compute the brightness of a nebula which would be just visible. We have made the computations for various zenith distances, applying the appropriate extinction corrections, and the results are shown in Figure 3*a* by the continuous curve. Similar curves are shown for 25 and 50 per cent increases and decreases in the intensity of the auroral plus scattered light, keeping the same intensity of the zodiacal light.

Since the zodiacal light changes greatly for different parts of the sky, we have computed values for the limiting brightness of a nebula which would be distinguishable for intensities of the zodiacal light up to 600 units. These are shown as functions of zenith distance in Figure 3*b*. However, the larger values of the zodiacal light would not be observed near the zenith.

If the observations are made in the Milky Way, the galactic light[1] and the light from the unresolved stars would be an additional factor which may equal or exceed the average amount of zodiacal light.

For illustration let us consider an example. The maximum variation of the observed auroral plus scattered light is greater than ± 50 per cent; but, assuming these figures and referring to Figure 3*a* we can determine easily the limiting magnitude of a nebula observed

under these conditions, say at the North Pole, the zenith distance being 60° for the McDonald Observatory. We find for the brighter sky the limiting brightness which can be detected is 6.50 mag. per square degree, while for the fainter sky it is 7.35 mag. This, of course, is near the extremes that have been observed in the season from November, 1934, to October, 1935, but we see that it is possible for the limiting brightness to differ by 0.85 mag.

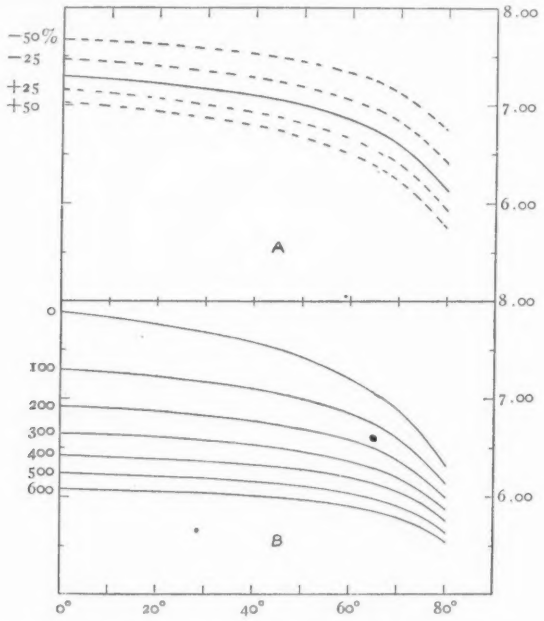

FIG. 3.—Curves showing the limiting brightness of a nebula which can be photographed under conditions described in the text.

Considering a variation over the sky due to the increased intensity of the zodiacal or galactic light, we may take the region of the Pleiades as compared with the Pole for an example. In the most favorable position the Pleiades would, at the McDonald Observatory, cross the meridian near the zenith. For the minimum of zodiacal light at that region the elongation would have to be from 130° to 150°. The data by Elvey and Roach give a mean value equal to 135–140 stars of the tenth magnitude per square degree for this region. Referring to Figure 3*b*, we find that the limiting brightness

of a nebula is about 7.15 mag. per square degree. The average brightness of the zodiacal light at the Pole is 70 stars of the tenth magnitude per square degree, and using these data we find from Figure *3b* that the limiting brightness of a nebula is about 6.95 mag. per square degree. Next, let us consider the unfavorable case when the Pleiades are in the zodiacal cone, say, at the altitude of the Pole and shortly after dark, thus giving that position an elongation of 60°–70°. The intensity of the zodiacal light at this elongation is equivalent to 350 stars of the tenth magnitude per square degree. The limiting brightness in this case is found from the curves to be about 6.30 mag. per square degree. If we make comparisons with the Pole, we find that the limiting brightness is 0.20 mag. fainter than at the Pole when the Pleiades are on the meridian, and in the latter limiting brightness due to the changing amount of zodiacal light is 0.85 mag.

We may conclude that the limiting magnitude of nebulosity obtained in a given exposure is a function of the position in the sky with respect to the zenith, the zodiacal light, and the Milky Way and also with respect to time. In precise photometry of faint nebulae the calibrating exposure must be made simultaneously with that of the nebula and must use stars of the same field.

McDonald Observatory
Fort Davis, Texas
August 26, 1937

THE INTERPRETATION OF ϵ AURIGAE

G. P. KUIPER, O. STRUVE, AND B. STRÖMGREN

ABSTRACT

The light-curve of this eclipsing binary is rediscussed with the help of the spectrographic elements determined at the Yerkes Observatory. The ratio of the radii and the mass ratio are determined with the assumption that the visible component falls upon the empirical mass-luminosity-curve. The orbital inclination is found to be about 70°. The spectrum is formed by the smaller, F2 star. The larger component has a temperature of about 1200°–1400° and gives no appreciable light in the region covered by the spectroscopic observations.

The spectroscopic and photometric observations during the eclipse show that the infrared star is semitransparent and that its nonselective opacity for visual and photographic light is concentrated in an outer shell. It is suggested that this effect is produced by photo-electric ionization from the F2 star.

The spectral lines of the F2 star are visible throughout the total phase of the eclipse. In addition, there are lines produced in the ionized shell of the infrared star. The latter are displaced by the rotation of this component, and the displacements and intensities are in accord with the hypothesis. The close proximity, before mid-eclipse, of the rotationally displaced lines of the infrared star to the normal lines of the F2 star results in a relatively small increase of the equivalent breadth. After mid-eclipse, when the two lines are better separated, the increase in the equivalent breadth is more pronounced. The equatorial velocity of rotation of the infrared star is approximately 50 km/sec.

The problem of the formation of an absorbing layer in the atmosphere of the infrared component by the radiation of the other component is investigated. Relations giving the extent of the region of the infrared star ionized by the outside radiation are derived. The optical thickness of the ionized region in visual and photographic light is calculated as a function of the maximum density along the ray traversing the atmosphere. An approximately constant optical thickness is found for a range of maximum density sufficiently wide to account for the observed constant minimum. A considerable excess of the amount of ionizing radiation over that calculated from Planck's law is required in order to give an optical thickness equal to that observed. The opacity of the non-ionized region of the infrared component between the ionized region considered and the observer is calculated. The effect of this opacity is found to be sufficiently small, provided the relative hydrogen content of the atmosphere of the infrared component is below a certain limit. Some aspects of the problem of line absorption in the atmosphere of the cool companion are considered. The results obtained are summarized, and the possible importance of a source of opacity other than the electron scattering and photo-electric transition opacity is briefly discussed.

INTRODUCTION

As is well known, the combination of the photometric and the spectroscopic data on ϵ Aurigae seems to lead to contradictions unparalleled in the study of other eclipsing systems. A beautiful constant minimum is found from the visual observations by Schmidt, reduced by Ludendorff,[1] or from the photoelectric observations[2] published by Huffer and by Miss Güssow. The light-curve suggests

[1] *A.N.*, **192**, 389, 1912.

[2] *Ap. J.*, **76**, 1, 1932; Veröff. Berlin-Babelsberg, **11**, No. 3, 193[illegible].

that the system is an eclipsing binary with a period of about twenty-seven years. This interpretation is in agreement with the spectroscopic orbit published by Ludendorff[3] and with an orbit just derived at the Yerkes Observatory, which includes recent observations. The epoch of the eclipse agrees approximately with the predicted time based upon the spectroscopic orbit. Hence, there can be no doubt about the binary nature of ε Aurigae.

But there is a wide discrepancy between the ratio of the surface brightnesses of the components derived from the light-curve and that derived from the spectral types. Since the depth of the constant minimum is about 0.8 mag., it would follow that the components are about equally bright. The ratio of the radii, k, depends, of course, upon the assumed inclination of the orbit. For $i = 90°$, Shapley, from the Schmidt-Ludendorff observations, found[4] $k = 0.35$; and Huffer, from his photoelectric observations, found $k = 0.318$. Since $k^2 = 0.1$, and the total brightnesses of the stars are equal, the ratio of the surface brightnesses is about 0.1. If the inclination is smaller than 90°, this ratio as Shapley has shown, decreases and becomes 0.01 for $i = 76°$. These results lead to four apparent contradictions:

1. The extreme ratio of the surface brightnesses suggests a large difference between the spectral types, but in reality the spectral type during the constant minimum is nearly identical with that observed outside of the eclipse.

2. The conclusion that the two components are equally bright cannot be reconciled with the fact that only one of the F-type spectra is seen at maximum light, even at phases where doubling of the lines must be expected.[5]

3. The F-type spectrum measured at maximum shows small fluctuations in radial velocity superimposed over the regular orbital velocity, and these fluctuations persist during the constant minimum.[5] Also, the light variations found by Huffer and Stebbins are present during the minimum. Although not impossible, it is very improbable that two stars, having quite different radii and probably very different densities, have such similar fluctuations both in brightness and velocity.

[3] *Sitz. Acad. Berlin*, p. 49, 1924. [4] *A.N.*, **194**, 229, 1913.

[5] Struve and Elvey, *Ap. J.*, **71**, 136, 1930; *Pub. Yerkes Obs.*, **7**, Part II, 1932.

4. The asymmetry of the lines, which should probably be attributed to a rotational effect produced by the atmosphere of the occulting star, extends into the constant part of the minimum,[5] where the total eclipse should, geometrically, remove all light from the eclipsed star.

These four inconsistencies may be removed by supposing, as has been done in the past, that the occulting star is semitransparent. But this model introduces new difficulties. As Struve and Elvey have pointed out,[5] the mass of the secondary is considerable, and a large opacity should be expected. Furthermore, even if the density gradient inside the star were zero, and hence if the star were homogeneous, the minimum could not be constant. Also, it is not clear why the spectrum during the constant minimum should be so similar to that outside of the minimum; many additional lines would be expected to be present.

In Section I, by Mr. Kuiper, it is shown, first, that the inclination of the orbit cannot be close to 90° but must be about 65°–70°; second, that this inclination results in a grazing eclipse, not a nearly central one; third, that only a *shell* of absorbing material surrounding the eclipsing star will be able to produce the observed type of minimum; and fourthly, that the physical conditions in the system are such that in the upper layers of the eclipsing star a shell of highly ionized material will be formed which is identical to the absorbing shell required by the light-curve.

In Section II, by Mr. Struve, the spectral features are discussed in the light of the new hypothesis.

In Section III, by Mr. Strömgren, the astrophysical aspects of the conditions existing in the atmosphere of the eclipsing star are developed.

I

Since the orbit of ϵ Aurigae is eccentric, the spectroscopic elements must be used in the photometric solution. We have adopted the following values, derived in Section II.

$P = 9890$ days $= 27.08$ years (Güssow)	$K_1 = 15.7$ km/sec
$e = 0.33$	$T = 1924.2$
$\omega = 350°$	$a_1 \sin i = 2{,}014{,}000{,}000$ km
$V = -2.5$ km/sec	$f(m) = 3.34\odot$

These elements are quite similar to those previously derived by Ludendorff. They relate to the cF2 component.

The value of k, the ratio of the radii, is smaller than 0.3, the value obtained for $i = 90°$. As will be seen later, k is probably smaller than 0.1. On account of the small value of k and the fact that fluctuations of small amplitude are superimposed on the general light-curve, it is impossible to obtain both i and k from the observed light-curve. We shall make solutions for different values of the inclination and then limit the range of probable inclinations from the results obtained.

The method used is believed to be considerably simpler than that used in the study of a similar system, ζ Aurigae.[6] This method is an adaptation of the Innes–van den Bos method of computation commonly used for orbits of visual binaries. The procedure is briefly described here.

The rectangular co-ordinates in the tangential plane of the eclipsing star with respect to the eclipsed star are[7]

$$x = AX + FY\,; \qquad y = BX + GY\,.$$

For a spectroscopic binary we may put conventionally $\Omega = 0°$. Taking the semimajor axis of the relative orbit, a, as unit, we have

$$A = +\cos\omega\,, \qquad B = +\sin\omega\cos i = -F\cos i\,,$$
$$F = -\sin\omega\,, \qquad G = +\cos\omega\cos i = +A\cos i\,.$$

If $i = 90°$, $B = G = 0$, and $y = 0$; the motion is then along the x-axis. From the value of ω (belonging to the eclipsing star) an estimate may be made of the range of values of the mean anomaly, M, that will apply to the neighborhood of the minimum. For a few representative values of M we compute the values of X and Y with the aid of the *Union Observatory Tables* of X and Y, and the resulting x-values are found. The problem is now to find two x-values, x_D and x_d, such that the time intervals between $-x_D$ and $+x_D$, and $-x_d$ and $+x_d$, are equal to D and d days, respectively. (D is the duration of

[6] Guthnick, Schneller, and Hachenberg, *Abh. Preuss. Akad. d. Wiss., Phys. Math. Kl.*, 1935.

[7] *Union Obs. Circ.*, No. 68, 1926; *B.A.N.*, **3**, 149, 1926.

the eclipse; and d, of totality.) This is most readily done if D and d are first converted into degrees of mean anomaly. From

$$R_1 + R_2 = x_D \qquad \text{and} \qquad R_1 - R_2 = x_d$$

the radii are found, expressed in terms of a, and hence in kilometers.

If the inclination is different from 90°, the projected distance between the centers of the stars is no longer x but $\Delta = \sqrt{x^2 + y^2}$. In this case Δ_D and Δ_d are found, similarly to x_D and x_d above.

In finding solutions for different values of the inclination it will be seen that the x-co-ordinates remain unchanged and that the y-co-ordinates are proportional to cos i. The whole operation is reduced to a few multiplications and interpolations. Since ω in the spectrographic orbit is somewhat uncertain, the computation has been carried out for two extreme values, $\omega = 340°$ and $\omega = 0°$.

Table 1 gives the solutions for five different values of the orbital inclination, based upon the spectroscopic elements quoted and upon Huffer's constants of the minimum, $D = 754$ days and $d = 360$ days. The first four columns contain, respectively: (1) the assumed inclination; (2) the radius of the eclipsed F2 star, expressed in terms of a; (3) the radius of the eclipsing star in terms of a (the letter "I" is used to designate an infrared star); and (4) the maximum value of the dip of the center of the F star under the occulting limb of the I star as seen from the earth, expressed in a as unit.

Since $a_1 \sin i$ is known from the spectroscopic orbit, for each line of Table 1 the quantity $a_1 = [m_2/(m_1 + m_2)]a$ is known. Hence the radii of the two stars are known except for the factor $m_2/(m_1 + m_2)$. By adopting a value for this factor, the radii are fixed, and also the masses, because of the known mass function. For the F2 star we know the approximate effective temperature, $\log T_e = 3.80$, which, in connection with the radius, fixes the luminosity. We may now obtain an approximate value of the mass ratio by the condition that the F2 star shall lie on the empirical mass-luminosity relation. This relation is derived in a paper to be published soon. It appears that for each value of the inclination the mass ratio is fixed between rather narrow limits. The reason is that a change in the mass ratio affects the masses strongly but the lu-

minosity only slightly. Hence, only a small range of mass ratios is compatible with the mass-luminosity relation, and in particular the luminosity should be well determined. The only exception is the solution for $i = 90°$, which leads to such a high luminosity that the nearly horizontal part of the mass-luminosity relation is reached. In this case the mass ratio is uncertain; but the luminosity should still be fairly accurate, at least for $\omega = 340°$.

TABLE 1

i (1)	R_F (2)	R_I (3)	Dip (4)	$\frac{m_F}{m_I}$ (5)	log R_F (6)	log R_I (7)	log m_F (8)	log m_I (9)	M_{pv}(F) (10)	T_e(I) (11)
	$\omega = 340°$									
90°	0.0572	0.1646	0.1646	3±	2.82	3.28	2.20	1.73	−9.9	2400
75	.0283	.3080	.0492	1.65	2.35	3.39	1.63	1.42	7.5	1450
70	.0221	.3776	.0366	1.40	2.21	3.45	1.51	1.37	6.8	1270
65	.0176	.4474	.0282	1.15	2.08	3.49	1.38	1.32	6.2	1120
60	0.0136	0.5143	0.0223	0.97	1.95	3.53	1.29	1.30	−5.5	1040
	$\omega = 0°$									
90	0.0657	0.1855	0.1855	*	.....	.....	.....	.....	.....	.....
75	.0382	.2958	.0655	2.4±	2.59	3.48	2.01	1.63	−8.7	1730
70	.0303	.3535	.0506	1.7	2.40	3.47	1.70	1.48	7.8	1460
65	.0243	.4127	.0405	1.4	2.27	3.50	1.56	1.41	7.1	1270
60	0.0194	0.4699	0.0322	1.15	2.15	3.53	1.44	1.38	−6.5	1190

* No solution of the mass ratio can be found which will bring the star on the average mass-luminosity relation.

The other columns of Table 1 contain: (5) the value of the mass ratio, found as described above; (6 and 7) the logarithms of the resulting radii (with the sun as unit); (8 and 9) the logarithms of the resulting masses (with the sun as unit); (10) the absolute photovisual magnitude of the F star, which happens to be equal to the absolute bolometric magnitude, since the bolometric correction is zero; (11) the computed effective temperature for the I star, based on the assumption that this star also falls on the mass-luminosity-curve (in this case the luminosity is found from the mass, and the luminosity and the radius define the effective temperature; even if

this assumption is not strictly correct, the temperature found should be approximately correct, since errors in the luminosity are reduced by at least a factor of 4 in the temperature.)

The next step is to select from the solutions of Table 1 the most probable solution. The higher inclinations ($i > 70°$) lead to excessive absolute magnitudes for the F2 star. Since the color index of ϵ Aurigae is 0.4 mag., and stars of absolute photographic magnitude brighter than -6.5 are extremely rare in extragalactic systems,[8] we may conclude that very probably the inclination is not greater than 70°.

It is not only possible to give an upper limit for i, but a lower limit may also be found. A solution for $i = 30°$ (not included in Table 1) shows that for this inclination no eclipse takes place at all, even if the I star is as large as $R_I = (1 - e)a$, or $0.67a$, that is, extends up to the periastron distance of the F star, which, of course, is dynamically impossible. For $i = 45°$, a grazing eclipse is present if $R_I = 0.67a$ (for $\omega = 340°$). But since only a considerably smaller radius will lead to a tidally stable system, the inclination must be considerably larger than 45°. Even $i = 60°$ seems to be excluded by the stability argument. For this inclination the masses of the components are roughly equal, and by reason of symmetry for any stellar model the condition that the large star be stable even at periastron requires that $R_1 < \frac{1}{2}(1 - e)a = 0.335a$.

Table 1 shows that this condition is not fulfilled. Inclinations higher than 72° or 73° make R_I smaller than this limit, but for these inclinations a different mass ratio is obtained which decreases the limit below $0.33a$.

Considering together the evidence of the two restrictions on the inclination, we believe that a value near 65° or 70° is the most probable. It is true that this value leads to an instability of the outermost layers of the I star at periastron. But the density of these layers is probably small enough to render the loss in mass insignificant, in spite of the fact that these layers have sufficient density to cause the eclipse. A more detailed discussion of this point will be given later.

[8] Hubble, *Ap. J.*, **84**, 164–165, 1936.

From the computations underlying Table 1 it follows that for $i = 70°$ the mean anomaly at the time of mid-eclipse is 69°.0 when $\omega = 340°$ and 50°.8 when $\omega = 0°$; for $i = 65°$ it is 67°.2 when $\omega = 340°$ and 49°.4 when $\omega = 0°$. There is a continuous change in this mean anomaly with the inclination, and in principle the inclination could be determined from the spectroscopic elements and the time of the eclipse Owing to the limited accuracy of the spectroscopic elements (largely because of the irregular fluctuations in velocity, hereinbefore mentioned), this is not feasible in practice.

If we adopt 70° as the most probable inclination and 350° as the most probable longitude of periastron, the mean anomaly at mid-eclipse is 59°.4; and from the photometric ephemeris, $P = 1929^{d}.326 +$

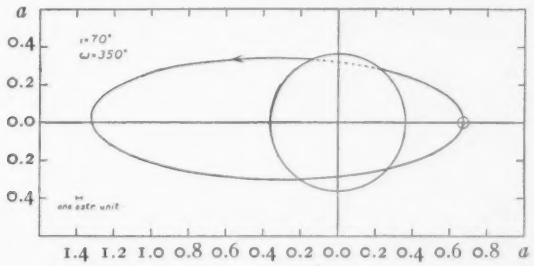

FIG. 1.—The projected orbit of ε Aurigae

$27^{d}.077E$, the epoch of periastron is found to be $T = 1924.86$. The fair agreement of the spectroscopic determination $T = 1924.2$ with the photometric determination shows that the spectroscopic and the photometric elements are consistent.

We shall now examine the consequences of the conclusion that the orbital inclination is close to 65° or 70°. The eclipse produced in this way is a grazing one, as is seen from the fourth column of Table 1, or from Figure 1, which is drawn for $i = 70°$. For this inclination the maximum value of the dip of the center of the F star below the limb of the I star is only 0.097 R_I when $\omega = 340°$ and 0.143 R_I when $\omega = 0°$; for 65° it is 0.063 R_I when $\omega = 340°$ and 0.098 R_I when $\omega = 0°$. This means that only the outermost layers of the I star are responsible for the observed eclipse. It seems possible, therefore, that these layers should be semitransparent, so that the F star is still visible during the minimum But the approximate constancy

of the minimum seems to contradict this possibility. It is clear that a homogeneous sphere with a constant mass-absorption coefficient cannot produce a constant minimum. If there were an increase of density toward the center, the condition would be still more unfavorable. *Only a shell of absorbing material surrounding the I star* will be able to produce the type of minimum observed.

We have therefore to examine whether the physical conditions in the system will give rise to such a shell. This appears to be the case. The two stars have nearly equal mass, and probably comparable luminosity. If anything, the F star is slightly more massive and probably more luminous. The dimensions in the system are such that an element in the atmosphere of the I star on the side of the F star is nearly at the same distance from both stellar centers. Hence the amounts of radiation received from the two stars will be comparable. But the quality of the two radiations is very different, since the effective temperatures of the sources are about 6300° and 1300°, respectively. The ionization of the atmosphere of the I star, as far as it is exposed to the F star, will be almost completely governed by the radiation of the F star. It seems likely that a shell of ionized material will be formed in the exposed part of the atmosphere of the I star which, by electron scattering, reduces the intensity of the continuous light of the F star, seen through it. This explains why the visual and the photoelectric observations show the same depth of minimum, about 0.8 mag.: charged particles scatter in a nonselective manner. Furthermore, it seems probable that this ionized layer is in such a condition that it can enhance the intensity of a number of absorption lines of the F2 spectrum. In this way both the character of the photometric minimum, and the spectral changes, are at least qualitatively accounted for.

In Sections II and III a quantitative treatment of these problems is given. The dimensions of the system may be taken from Table 1, and to these may be added the distance of the center of the F star to the terminator of the illuminated part of the I star. From the mean anomaly at mid-eclipse for $i = 70°$ and $\omega = 350°$, viz., 59°, we find for the distance between the centers of the stars at mid-eclipse, $0.93a$. For that same inclination, $R_I = 0.37a$ and $R_F = 0.026a$ (Table 1). Hence, the distance of the center of the F star

to the terminator is $0.85a$, and the radius of the F star, as seen from the terminator, is 0.0306 radians = 1°.8. In other words, the diameter is seven times that of the sun as seen from the earth, and the surface temperature is slightly higher.

As we shall see, Section II leads to the same hypothesis which has been put forward here, and Section III is also consistent with it. We may, therefore, conclude that the model given follows logically from the observational data: the spectroscopic orbit, the light-curve, and the spectral type; that it removes the apparent contradictions found previously and explains the known phenomena satisfactorily; and that it presents us with a new astronomical phenomenon, an eclipse by a stellar Heaviside layer.

II

The elements of the orbit were derived[9] from the radial velocities plotted in Figure 2*a*. Open circles represent Potsdam results, while dots represent velocities obtained at the Yerkes Observatory. Each value represents the mean of several plates; an attempt was made to group the observations in such a way that the short-period oscillation would be smoothed out.

The spectroscopic phenomena during the eclipse have already been described.[10] A short time before the first contact nearly all strong lines of the F2 star become slightly unsymmetrical on the red side. This is accompanied by an appreciable increase in the equivalent widths of these lines. The asymmetry—never very large—reaches a maximum roughly at second contact. It diminishes rapidly and becomes zero at mid-eclipse. However, the intensities of the lines at mid-eclipse are somewhat stronger than those outside of eclipse. After mid-eclipse the lines become again unsymmetrical, with a strong core on the violet side. This asymmetry increases rapidly until it is very large at about third contact. Some of our best plates, taken in November and December, 1929, show the lines clearly double; but no attempt has been made to measure the com-

[9] Miss Frances Sherman assisted in this work.

[10] Struve and Elvey, *Ap. J.*, **71**, 136, 1930; Frost, Struve, and Elvey, *Pub. Yerkes Obs.*, **7**, 81, 1932; Adams and Sanford, *Pub. A.S.P.*, **42**, 203, 1930; McLaughlin, *Ap. J.*, **79**, 235, 1934; *ibid.*, **82**, 95, 1935.

ponents separately because the wings always overlap. The measures by Adams and Sanford prove that the duplicity is real. Our measures refer to the deepest point of the blended contour. After the end of the eclipse the strong violet components gradually fade out, and the spectrum resumes its normal aspect. The equivalent breadths reach a maximum near third contact.

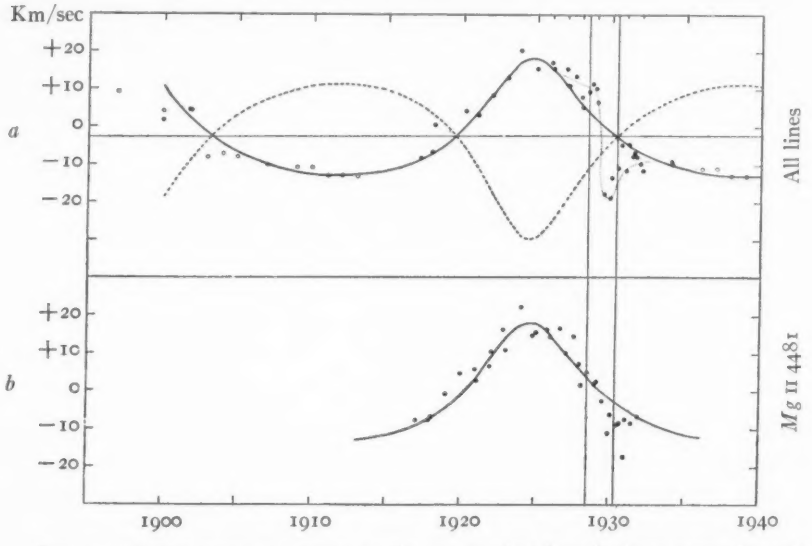

FIG. 2.—Velocity-curve of ϵ Aurigae. The two vertical lines indicate approximately the first and last contacts of the eclipse.

Since we do not know whether there are any lines of the F2 star which are unaffected at eclipse, we have derived the spectrographic elements from that part of the velocity-curve which lies outside the ranges 1927–1932 and 1900–1905. The elements are given in Section I. The velocity-curve of the F2 star, shown in Figure 2, represents these elements. The velocity-curve of the I star is shown for comparison. A mass ratio of $m_F/m_I = 1.3$ was assumed. The eccentricity is well determined, but the longitude of periastron is less certain. It must lie between 340° and 0°. The most probable value is 350°.

Figure 2*b* shows the velocities derived from the line *Mg* II 4481. The systematic departures preceding and following mid-eclipse are less marked, but the large negative residuals in 1930 and 1931 sug-

gest that, although this line is less affected by the asymmetries, it does not exactly follow the velocity-curve. It is, therefore, useless to refer all measures to *Mg* II 4481, as was done in our former work.[10] Instead, the departures must be measured from the ephemeris.

We interpret the spectrographic phenomena in the following way:

1. When the F2 star begins to encroach upon the atmosphere of the I star, new lines, due to the latter, appear in the spectrum.

2. These lines are approximately—but not identically—the same as the normal lines of the F2 star. The strong ionized lines of *Fe* II and *Ti* II are strong in the atmosphere of the I star. *Mg* II is relatively weak. All faint lines are very weak in the I star; *Sr* II is probably relatively weaker in the I star. These phenomena can be explained as a combination of two effects: greater turbulence in the atmosphere of the I star than in that of the F2 star,[11] and a small real difference in spectrum. It is significant also that *Mg* II was absent in the expanding shells of 17 Leporis.[12]

3. Axial rotation shifts the lines of the I star from their normal position on the velocity-curve of this component of the binary. The rotation is therefore direct. The fact that the new lines fall above the velocity-curve of the F2 star in the first half of the eclipse is irrelevant: it simply means that the component of rotation in the line of sight at the proper latitude of the I star is larger than the orbital velocity of the F2 star.

4. The visibility of the rotationally displaced lines of the I star during the phase of the total eclipse proves that the continuous spectrum of the F2 star remains visible even at total phase.

5. The visibility of the normal F2 lines throughout eclipse also proves that the I star is semitransparent.

6. The beginning of the partial phase of the photometric eclipse does not coincide with the date of the first appearance of the additional lines. This suggests the existence in the I star of an outer atmosphere which produces appreciable line absorption but practically no continuous absorption.

7. The total equivalent widths of the blended lines vary continu-

[11] *Ap. J.*, **79**, 409, 1934. [12] Struve, *ibid.*, **76**, 85, 1932.

ously, reaching a maximum near third contact. This seems at first sight to be in contradiction to the flat minimum of the photometric curve. In reality it is a consequence of the difference in velocity between the F2 lines and the rotationally displaced I lines. If the normal contour of an F2 line is $i_1(\lambda)$ and that of the I line is $i_2(\lambda + \Delta\lambda)$, where $\Delta\lambda$ is the velocity shift between the two lines, then the equivalent width of the blended line is

$$E = \int_{-\infty}^{+\infty} [1 - i_1(\lambda) i_2(\lambda + \Delta\lambda)] d\lambda .$$

Only when $\Delta\lambda$ is large, does

$$E = \int_{-\infty}^{+\infty} [1 - i_1(\lambda)] d\lambda + \int_{-\infty}^{+\infty} [1 - i_2(\lambda + \Delta\lambda)] d\lambda = E_1 + E_2 .$$

For overlapping lines, $E < (E_1 + E_2)$. The instrumental contour produced by the three-prism Bruce spectrograph of the Yerkes Observatory is easily obtained with the help of the curves published by Ornstein and Minnaert.[13] The focal length of the collimator is 100 cm, and its focal ratio is 1:19. Consequently, the parameter, σ, equals 5.8π. The corresponding intensity-curve for an infinitely narrow line may then be used to derive from the observed contour of a line in ϵ Aurigae the corresponding true contour. The theoretical contour for an infinitely narrow line is found to lie between the curves drawn by Ornstein and Minnaert for $\sigma = (16/3)\pi$ and $\sigma = (20/3)\pi$. This curve is almost to its full extent contained between the limits of $\pm 0.20A$. Even allowing for additional broadening caused by imperfections in the optical parts of the spectrograph, the entire

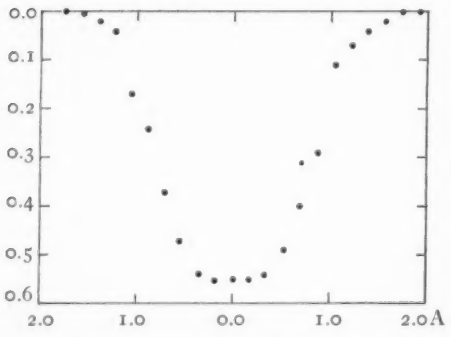

FIG. 3.—Contour of the absorption line *Ti* II 4400 in ϵ Aurigae, outside of eclipse.

[13] *Zs. f. Phys.*, **44**, 404, 1927. Unpublished data by Messrs. Rust and Ebbighausen indicate that the labels for σ in Fig. 2 of the paper quoted should be multiplied by 0.5.

instrumental contour should lie within the limits of $\pm 0.25A$. The observed contour of the line *Ti* II 4400 (outside of the eclipse) is shown in Figure 3. The true contour differs so little from the observed contour[14] that it has not been drawn separately. It is clear that the contour has the typical shape of a line produced largely by turbulence,[11] and we shall therefore assume for the F2 star that

$$i_1 = 1 - ae^{-u\lambda^2},$$

where we shall understand under λ the difference $(\lambda - \lambda_0)$ measured from the center of the line due to the F star. The contours of the I lines are not accurately known, but it is probable that they are also dominated by turbulence. Accordingly,

$$i_2 = 1 - be^{-v(\lambda+\Delta\lambda)^2}.$$

The total equivalent breadth is

$$E = a\int_{-\infty}^{+\infty} e^{-u\lambda^2}d\lambda + b\int_{-\infty}^{+\infty} e^{-v(\lambda+\Delta\lambda)^2}d\lambda$$
$$- ab \cdot e^{-v\Delta\lambda^2}\int_{-\infty}^{+\infty} e^{-(u+v)\lambda^2-2v\Delta\lambda\cdot\lambda}d\lambda = E_1 + E_2 - E_3.$$

The last term is

$$E_3 = \sqrt{\frac{\pi}{u+v}}\, ab \cdot e^{-[(uv)/(u+v)]\Delta\lambda^2}.$$

Let us use a specific line, the central intensity of which is 0.4 in the F2 star and 0.2 in the I star. Let the total equivalent breadth of the F2 line be about 0.7A. Then $a = 0.6$, $u = 1.2$, and

$$E_1 = 0.6\sqrt{\frac{\pi}{2.1}} = 0.73\text{A}.$$

The contour of the I line is not known. From the measured contours it seems probable that, although the central absorption is

[14] This is also apparent from a comparison of the width of the absorption line λ 4400 in Plate III, *Pub. Yerkes Obs.*, **7**, Part II, 1932, with the widths of faint comparison lines.

greater than that of the F2 line, the equivalent breadth is not larger. If we assume that $E_2 = E_1$, we have $b = 0.8$, $v = 3.8$, and

$$E_2 = 0.8\sqrt{\frac{\pi}{3.8}} = 0.73A .$$

We now compute E_3 for different values of $\Delta\lambda$:

$\Delta\lambda$	0.0	0.1	0.2	0.3	0.4	0.5	0.6	0.7	0.8	0.9A
E_3	0.25	0.25	0.24	0.22	0.20	0.18	0.16	0.13	0.11	0.08A
$\Delta\lambda$	1.0	1.1	1.2	1.3	1.4	1.5	1.6	1.7	1.8A	
E_3	0.07	0.05	0.04	0.03	0.02	0.01	0.01	0.00	0.00A	

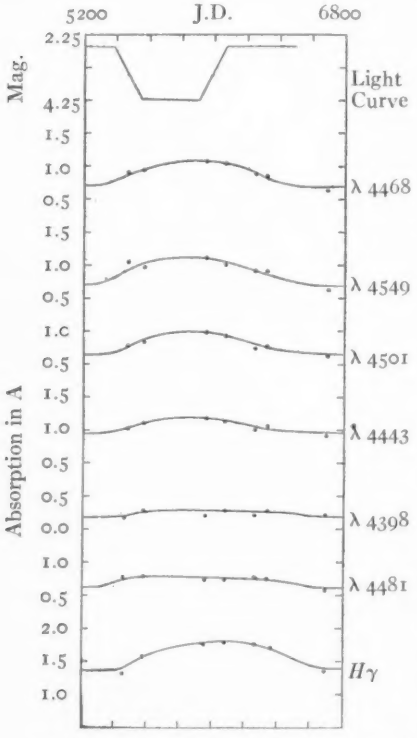

FIG. 4.—Equivalent breadths of typical lines in ε Aurigae, during the eclipse.

When $\Delta\lambda = 0$, the total equivalent breadth is $E = E_1 + E_2 - E_3 = 1.21$A. When the separation of the two lines corresponds to about 0.5A (or 33 km/sec) the total equivalent breadth increases to about 1.28A. This agrees fairly satisfactorily with the intensity curve[15] of *Ti* II 4468 in Figure 4. We observe from Figure 2*a* that $\Delta\lambda$ is of the order of 0.1A before mid-eclipse but reaches about 0.5A after mid-eclipse. The computed increase in the equivalent breadth of 0.07A between the beginning and the end of the eclipse is a little less than the actual amount observed for lines which outside of eclipse have equivalent breadths of about 0.7A. But by making the contours of both

[15] The equivalent breadths of all lines shown on our three-prism spectrograms have been measured during the eclipse and after its end. The lines in Figure 4 have been chosen at random to illustrate the behavior of strong and of weak lines.

lines narrower and deeper, we could have easily obtained a close approximation to the observed curves.

An entirely similar result is obtained if, by following Elvey, we use triangular contours for the two lines. By adjusting the available constants, we can fit, as accurately as we wish, the curves in Figure 4.

8. Figure 5 shows, for four inclinations, the projection of the orbit of the F2 star upon the disk of the I star. The component of axial

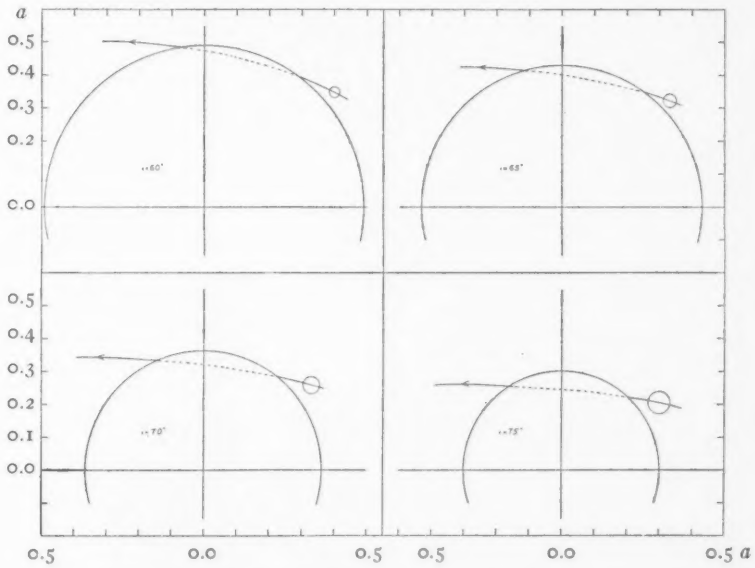

FIG. 5.—Illustration of the asymmetry in the rotation effect for $\omega = 350°$

rotation at the points of intersection is proportional to the x-coordinate of each point, provided the rotation is parallel to the plane of the orbit. The rotational effects with respect to the center of the I star are unsymmetrical. If $\omega = 350°$, we find[16] the ratio of the components of rotational velocity as shown in the following table. Since m_F/m_I depends upon i, we determine separately for

[16] The following figures refer to the points at which the center of the F2 star crosses the limb of the I star. These points are quite close to the times of maximum departures from the velocity-curve. Similar results would have been obtained if, instead of determining the rotational components for the times of disappearance and appearance of the center of the F2 star, we had determined them for second and third contact, respectively.

each value of the inclination the corresponding departure of the measured I line from the corresponding velocity-curve. If we assume

i	Ratio of Components of Rotational Velocity	i	Ratio of Components of Rotational Velocity
60°	4.1:1	70°	1.6:1
65	2.3:1	75	1.3:1

that the Yerkes measures refer to the I lines, corresponding to the deepest point on the contour, we find from the dotted curve in Figure 2*a* that the maximum residuals with respect to the center of the I star are in the ratio of 1.4:1, which would support a value of i close to 70°.

Adams and Sanford's measures gave:

	I Lines	F2 Lines
Nov. 15, 1929	−36 km/sec	+4 km/sec
Feb. 5, 1930	−35	+6

At the same time, the Yerkes measures for the blended lines gave −19 km/sec. It is probable, however, that Adams and Sanford's measures should be corrected for the effect of overlapping wings. We shall adopt −30 km/sec for the velocity of the I lines.

The Mount Wilson plates do not separate the components before mid-eclipse. We are therefore forced to adopt a somewhat arbitrary correction for the Yerkes measures. After mid-eclipse (December, 1929), we have:

Computed velocity of F2 star *minus* Yerkes measure of blended line	+20 km/sec
Computed velocity of F2 star *minus* Mount Wilson measure of I line	+31

The ratio is 1.55. Before mid-eclipse we have:

Computed velocity of F2 star *minus* Yerkes measure of blended lines	−6 km/sec

The factor of correction before mid-eclipse should be $1.55 < f < 2$, since with decreasing displacement between two unequal lines the

blended wave length will lie more and more nearly halfway between the two centers. Adopting $f = 1.8$, we find, for the true difference, 11 km/sec. Referring these velocities now to the center of the I star, we compute for the times of the disappearance and reappearance of the centers of the F2 star the velocity of the center of the I star, making due allowance for the fact that m_F/m_I depends upon i and also upon ω. The measured components, corrected as has been explained, *minus* the velocity of the center of the I star are shown in Table 2. Almost the same effect would have been obtained if we had computed the departures, not for the times of appearance and disappearance of the center of the F2 star, but for second and third contact. The asymmetry is in the right direction, and its amount seems to favor $i = 70°$ or $75°$. But this result depends upon our assumption that the axis of rotation of the I star is perpendicular to the plane of the orbit. The velocities are not sufficiently precise to determine i accurately, but $i = 70°$ is probably a good compromise.

TABLE 2

	$\omega = 340°$	$\omega = 0°$
$i = 60°$ Disappearance	+31 km/sec	+34 km/sec
$i = 60°$ Reappearance	−26	−27
$i = 65°$ Disappearance	+31	+35
$i = 65°$ Reappearance	−26	−26
$i = 70°$ Disappearance	+32	+36
$i = 70°$ Reappearance	−26	−26
$i = 75°$ Disappearance	+33	.....
$i = 75°$ Reappearance	−26	.....

9. The spectral lines of the F2 star outside of eclipse are relatively deep. The central intensity of $H\beta$ is of the order of 0.3. At the node the velocity shift between the two components should be about 50 km/sec. Accordingly, if the conventional photometric solution were correct, the lines of the F2 star should be appreciably filled in by the continuous spectrum of the other component. The fact that there is no such filling-in proves that the continuous spectrum of the companion does not contribute an appreciable fraction of the light.

10. A new search for the lines of the second component has been made on good three-prism spectrograms at and near the time of passage through the ascending node of the F2 star. No trace of such lines could be found.

It is clear that the hypothesis of a semitransparent infrared star explains all spectrographic observations. The equatorial rotational velocity of this star is about 50 km/sec if $i = 70°$ and if the axis is perpendicular to the plane of the orbit. It is surprising that, although the atmosphere of the I star is ionized by the F2 star, the spectral type of the rotational I lines is somewhat similar to that of the F2 star. But we have an analogous phenomenon in the expanding shells of 17 Leporis, P Cygni stars, and novae. In all of these objects the absorption lines adjust themselves rather closely to that spectral type which we would expect from the energy-curves of the stars.

III

As has been shown in the preceding sections, the analysis of the photometric and spectroscopic observations of ϵ Aurigae leads to the following conclusions:

1. Throughout the entire eclipse the light observed is due to the F component.

2. At light minimum about one-half of the light of the F component is absorbed during its passage through the outer part of the I component. In the visual and photographic regions the absorption is approximately independent of the wave length.

3. Within a certain range of dip of the F component under the effective boundary of the I component, corresponding to the phase of constant minimum, the absorption is, to a close approximation, independent of the dip.

It has been pointed out in Section I that, on the surface of the I star, owing to its very low temperature, the flux of ultraviolet radiation from the F star is very much greater than the corresponding flux from the F star. It was further pointed out that this circumstance might be expected to lead to the formation of a semiopaque layer in the outer part of the I star, of such a nature as to produce absorption of the visual and photographic light of the F star, as described in the foregoing summary.

A complete theory of the atmospheres of the components of a stellar system like ε Aurigae would necessarily be very complex. An attempt is made in this section to explain the problem of the absorption of the light of the F star in the atmosphere of the I star, through a discussion of certain simplified models. Though we cannot yet claim to know with certainty the details of the mechanism of absorption, we believe that the main features of the situation have been correctly understood.

We shall consider primarily the following mechanism of absorption of the light of the F star in the I star. The ultraviolet radiation of the F star produces ionization in a region of the I star that would, if the F star were not present or if it were at a much greater distance, be only slightly ionized and practically transparent to visual and photographic light. As the ultraviolet radiation penetrates farther into the I star, it is gradually absorbed. Thus, the region of the I star, ionized by the ultraviolet radiation of the F star, is limited as a consequence of the absorption of the ultraviolet radiation. The free electrons in the ionized region of the I star weaken the passing light of the F star. The weakening, due to electron scattering, is the same for all wave lengths.

In order to see whether this is a true picture in the case of ε Aurigae, we must investigate the following questions:

1. Does the picture lead to a sufficiently wide range in dip, within which the absorption is amply independent of the dip?

2. Is the absorption in visual and photographic light of the correct magnitude?

3. Would the region of the I star, to which the absorption has to be attributed, be transparent to visual and photographic light if the F star were absent (i.e., is the region of the I star between the ionized region and the observer transparent to visual and photographic light)?

4. Is electron scattering, influenced by the diluted radiation of the F star, the main cause of visual and photographic opacity in the region of the I star considered?

We shall now deal with these questions. The result is that the picture considered may be true if certain assumptions, which, of

necessity, are as yet somewhat arbitrary, are taken for granted. Other possible mechanisms are also discussed in less detail.

Before developing the theory of the mechanism of absorption described, we shall discuss a few features of the situation in the case of ϵ Aurigae, making use of the data of the system derived in Section I. Only rough numerical values are needed for our purposes. In our calculations we shall use the following numerical values, which correspond to a value of the inclination of the orbit of 70°:

$R_I = 2.10^{14}$ cm	$T_I = 1400°$
Maximum dip of center of F star $= d = 2.4 \times 10^{13}$ cm	$\log m_I = 1.42$
$R_F = 1.4\ 10^{13}$ cm	$\log R_I = 3.46$

From the values of m_I and R_I we can calculate the density gradient of the outer, practically isothermal, part of the atmosphere of the I star, assuming that it is given by the well-known relation valid for the case of hydrostatic equilibrium:

$$N = N_0 e^{a_s h}, \tag{1}$$

$$a_s = \frac{m_H \mu g}{kT}. \tag{2}$$

Here N denotes the number of particles per unit volume; h, the depth below a certain arbitrary boundary sphere where the value of N is N_0; μ, the mean molecular weight of the gas; g the surface gravity, i.e., Gm/R^2; k/m_H, the gas constant $(k/m_H = 8.26 \times 10^7)$; and T, the temperature.

With $\mu = 1$, corresponding to a mixture in which hydrogen predominates, the following value of a_s is found from the data given above:

$$\log a_s = -12.2. \tag{3}$$

The assumption of a somewhat greater value of μ would not affect the final conclusions. This value of a_s leads to a density increase along a distance equal to the radius of the F star by a factor of about 10^4, and to a density increase by a factor of about 10^7 along a distance equal to the maximum dip. With the hydrostatic value of a, therefore, the cut-off of the I star is so sharp that the partial phase

of the light-curve is due practically to the extent of the F star, while the change of density within the region which obstructs the light of the F star during the constant minimum is so high as to correspond to a factor of 10^7.

It is well known that the gradient in tenuous atmospheres due to turbulent motions or other deviations from the static case may be considerably smaller than the hydrostatic gradient. The sun's chromosphere is one example. Supergiant atmospheres have been considered recently from this point of view by Menzel[17] and by Pannekoek.[18] We describe the density distribution approximately with the aid of an exponential relation, as in the hydrostatic case:

$$N = N_0 e^{\alpha h} . \tag{4}$$

The value of α may be considerably smaller than α_s. Menzel and Pannekoek consider values of α about one hundred times smaller than α_s. Now, in the case of ζ Aurigae, which is considered by Menzel, the assumption of an α-value that is so small apparently contradicts the photometric data, leading, when combined with the known radius of the B star of the system, to a duration of the partial phase which is too long (cf. Kuiper[19]). Still, a diminution factor, say of the order of magnitude 10, is entirely possible.

In the case of ϵ Aurigae the known duration of the partial phase similarly sets a lower limit to the density gradient, which can be assumed. This again leads to a minimum value of the density variation in the region through which the F star shines during the constant minimum. This density variation can hardly be assumed less than, say, 20.

We have thus made one of our problems (cf. 1, p. 588) more definite. The absorption has to be constant for a range in dips that corresponds to a range of density of the gas passed by at least a factor of 20.

From the foregoing considerations it follows that the numerical value of the constant α in (4), which governs the density distribution, probably lies somewhere between 10^{-12} and 10^{-13}.

It will appear from the following analysis that the accuracy with

[17] *Harvard Circ.*, No. 417.

[18] *B.A.N.*, **8**, 175, 1937.

[19] *Ap. J.*, unpublished.

which a is thus known is sufficient for the purposes of numerical discussion of the theory, the constant a being, in the final equations in question, only raised to the power of $\frac{1}{4}$.

We shall now develop the theory of ionization in the atmosphere of the I star by the ultraviolet radiation of the F star and of the electron scattering opacity thereby produced.

The order of magnitude of the electron pressure in the region with which we shall be concerned can be estimated at once. The electron-scattering coefficient is 0.4 m_H, or 7×10^{-25}, per electron. The optical depth corresponding to the electron scattering along the path of the radiation from the F star through the I star must be of the order of magnitude 1 in order to produce the observed absorption. On the other hand, the path along which the electron density is appreciable will be considerably smaller than the radius of the I star. It will be of the order of magnitude of the maximum dip. With a geometrical path of 10^{13} cm we find that a mean absorption coefficient of the order of 10^{-13} is required, and hence a mean number of electrons of the order of magnitude 10^{11} per cm^{-3}. The corresponding electron pressure is of the order of 10^{-1} dynes, or 10^{-7} atmospheres.

The number of free electrons and ions is therefore so high that the ionization equilibrium in a given element of volume is reached practically instantaneously when the radiation field changes. This simplifies the discussion of the ionization of the atmosphere of the I star by the radiation of the F star. The order of magnitude of the degree of ionization can also be estimated at once. As the ionizing radiation of the F star penetrates into the I star, it is gradually absorbed. At an optical depth in the wave lengths of the ionizing radiation (which we shall refer to as "ultraviolet" for the sake of brevity) of the order of magnitude 10, the ionizing radiation will be cut down so much that the ionization is inappreciable. We thus see that the ultraviolet absorption coefficient must not be more than about ten times larger than the absorption coefficient corresponding to electron scattering; otherwise the ionized region will not be sufficiently extended to give the required electron-scattering optical depth of the order of magnitude 1.

The ratio of the electron-scattering absorption coefficient to the ultraviolet absorption coefficient is equal to the product of the ratio

of the scattering coefficient per electron, 0.4 m_H, to the ultraviolet absorption coefficient a_u per absorbing atom and the ratio of the number of electrons to the number of absorbing atoms. Now, the numerical value of a_u is of the order of magnitude $10^6 m_H$ (we shall deal with the question of the value of a_u in more detail later). We conclude that the number of absorbing atoms must be less than about 10^{-5} times the number of free electrons in order that the ratio of ultraviolet and electron scattering absorption be smaller than the required limiting value. The degree of ionization in the region which obstructs light by electron scattering must therefore be quite high.

It is clear that the derived value of the electron pressure, together with the degree of ionization just found, gives the order of magnitude of the amount of ionizing ultraviolet radiation from the F star which is required in order to produce the observed opacity in the visual and photographic regions.

We now proceed to the analytical discussion of the problem. We shall consider first the case that the ionizing F star, which is also the star for which we want to find the light loss in the visual and photographic region, is practically a point source as seen from the other star (the I star). Consider a ray from the point source through the atmosphere of the I star. The degree of ionization at any point along the ray is given with sufficient accuracy for our purpose by the following equation:

$$\frac{N''N_e}{N'} = 10^{15.4-\theta I} T^{3/2} w e^{-\tau_u} . \qquad (5)$$

The notation used is explained below:

N'' = Number of ions per unit volume
N' = Number of neutral atoms per unit volume
N_e = Number of free electrons per unit volume
T = Temperature
$\theta = 5040°/T$
I = Ionization potential
w = The dilution factor of the ionizing star as seen from the I star
τ_u = The ultraviolet optical depth along the ray from the ionizing star to the point considered

Equation (5) is the ionization equation of the thermodynamical equilibrium modified to take account of dilution in the usual way and, further, to take account of the reduction of the ionizing radiation due to its passage through part of the I star.

For our purpose it will be sufficiently accurate to lump the metals together into one group with a certain mean ionization potential. Hydrogen is practically nonionized in the region in question. The role played by the ionization potential and the abundance of an element in the problem will become more clear at a later point in the discussion.

Let N be the sum of the number of ions N'' and the number of atoms N'; and let x, as usual, denote the degree of ionization:

$$\left.\begin{aligned} N'' &= xN \\ N' &= (1 - x)N \\ N_e &= xN \end{aligned}\right\} . \tag{6}$$

Introducing, further, the constant C,

$$C = 10^{15.4-\theta I} T^{3/2} w , \tag{7}$$

we can write equation (5) in the form

$$\frac{x^2}{1 - x} N = Ce^{-\tau_u} . \tag{8}$$

The optical depth τ_u in the ionizing ultraviolet region can be expressed in terms of the absorption coefficient in the ultraviolet a_u per atom and the number of neutral atoms $N' = (1 - x)N$ per unit volume, which absorb the ionizing radiation:

$$d\tau_u = (1 - x)Na_u ds . \tag{9}$$

Here ds is the line element along the ray considered. Equations (8) and (9) now enable us to find the degree of ionization x as a function of position s on the ray considered. The analytical process of finding $x(s)$ is simplified by the following circumstance. As was shown by the qualitative discussion of the problem, the ionization in the region of the I star, where the ultraviolet radiation of the F star has not yet

suffered serious loss by absorption, must be quite high. In fact, $1 - x$ must be as low as about 10^{-5}. According to equation (8), this means that e^{τ_u} is of the order of magnitude 10^4 before x begins to differ appreciably from 1. When e^{τ_u} has reached this magnitude, the absorption coefficient in the ultraviolet is so high [cf. (8 and 9)] that a relatively very small advance Δs along the ray cuts the ultraviolet radiation down so much that the degree of ionization x is practically zero. Consequently, the transition region in which x falls from a value practically equal to 1 to a value practically equal to zero is relatively very narrow. In calculating the optical depth due to electron scattering, we therefore obtain sufficient accuracy by dividing the path along the ray considered in two parts: one, $s \leqq s_0$, for which $x = 1$; and the other, $s > s_0$, for which $x = 0$.

These considerations can easily be put into an analytical form. Writing equation (8) in the form

$$1 - x = \frac{1}{C} N x^2 e^{\tau_u} \tag{10}$$

and substituting this expression for $1 - x$ in (9), we find

$$d\tau_u = \frac{a_u}{C} N^2 x^2 e^{\tau_u} ds \,. \tag{11}$$

Upon separation of the variables τ_u and s and upon integration this becomes

$$\int_0^{\tau_u} \frac{1}{x^2} e^{-\tau_u} d\tau_u = \frac{a_u}{C} \int_0^s N^2 ds \,. \tag{12}$$

The integral on the left-hand side of (12) increases with τ_u. We know that x does not differ appreciably from 1 until e^{τ_u} has reached a value of the order of magnitude 10^4. Hence we have

$$\int_0^{\tau_u} \frac{1}{x^2} e^{-\tau_u} d\tau_u = 1 - e^{-\tau_u} \,, \qquad \text{for} \qquad 1 \geqq e^{-\tau_u} > 10^{-4} \,. \tag{13}$$

For values of $e^{\tau_u} > 10^4$, x begins to decrease, and hence $1/x^2$ begins to exceed 1. While x decreases to $1/10$, the integrand stays less than 10^{-2}, and hence the increase of the integral is inappreciable com-

pared with the value of the integral itself, which is very close to 1. When $x < (1/10)$ it is sufficiently accurate to put $1 - x = 1$ in (10), which gives

$$\frac{1}{x^2} = \frac{1}{C} N e^{\tau_u}, \qquad \text{for} \qquad x < \tfrac{1}{10}. \tag{14}$$

Inserting this in the integral on the left-hand side of (12), we find for this integral

$$\int_{\tau'_u}^{\tau_u} \frac{1}{x^2} e^{-\tau_u} d\tau_u = \int_{\tau'_u}^{\tau_u} \frac{N}{C} d\tau_u, \qquad \text{for} \qquad x < \tfrac{1}{10}. \tag{15}$$

Now N/C is of the order of magnitude, say, $10^{-5} - 10^{-3}$ [cf. (10)], and, consequently, the integral increases extremely slowly with τ_u. In fact, even an increase of, say, 20 in τ_u, which, according to (14), will reduce x from a quantity less than $1/10$ to a quantity less than $(1/10)e^{-10}$, or less than 10^{-5}, will not increase the value of the integral appreciably.

We therefore see that, as the integral on the right-hand side of (12) increases with s, x remains practically equal to 1, until the value of that integral becomes very nearly equal to 1. Let us define s_0 so that

$$1 = \frac{a_u}{C} \int_0^{s_0} N^2 ds. \tag{16}$$

Then x remains practically equal to 1 until s is practically equal to s_0. A very small increase of s, leading to a very small increase of the integral on the right-hand side and, hence, of the integral on the left-hand side in (12), corresponds to a large increase in τ_u and a very rapid reduction of x from 1 to a value practically equal to 0.

Thus, the result of the analysis is that

$$\left.\begin{aligned} x &= 1 \text{ for } s \leqq s_0 - \epsilon_1 \\ \text{and} \qquad & \\ x &= 0 \text{ for } s \geqq s_0 + \epsilon_2 \end{aligned}\right\}, \tag{17}$$

where s_0 is defined by (16) and ϵ_1 and ϵ_2 are so small as to be entirely negligible in our problem.

We can now calculate the optical depth τ corresponding to the electron scattering. We have

$$d\tau = 0.4 m_H x N ds , \tag{18}$$

or

$$\tau(s) = 0.4 m_H \int_0^s x N ds . \tag{19}$$

From (17) and (19) we now find

$$\tau(s) = 0.4 m_H \int_0^{s_0} N ds , \qquad \text{for} \qquad s \geqq s_0 , \tag{20}$$

which, in particular, gives the optical depth τ along the total path through the atmosphere of the I star:

$$\tau = 0.4 m_H \int_0^{s_0} N ds . \tag{21}$$

Equations (16) and (21) contain the solution of our problem. For any given density distribution $N(s)$, equation (16) determines s_0 and equation (21) then determines τ.

In order to get a general insight into the problem we shall now, with the aid of equations (16) and (21), study three models of different density distributions. The last of these models probably corresponds rather closely to the atmosphere of the I component of ϵ Aurigae.

First, let us consider a region of constant density N, of arbitrary shape, subject only to the conditions that the region should be practically opaque in the ultraviolet for all the traversing rays considered. For this model, (16) becomes

$$1 = \frac{a_u}{C} N^2 s_0 , \tag{22}$$

and (21)

$$\tau = 0.4 m_H N s_0 . \tag{23}$$

From (22) we find

$$s_0 = \frac{C}{a_u} \frac{1}{N^2} . \tag{24}$$

Inserting in (23), we get

$$\tau = 0.4 m_H \frac{C}{a_u} \frac{1}{N} . \tag{25}$$

The opacity due to the electron scattering is then the same for all directions. It is inversely proportional to the density. Thus, the decrease of the number of electrons per unit volume with decreasing density is more than compensated by the increase in the extent of the ionized region with decreasing density. The opacity τ is further proportional to the constant C, which, according to (7), is a measure of the amount of ionizing radiation and is inversely proportional to the atomic absorption constant a_u in the ultraviolet.

It should be noted that the variation of τ with N is in the opposite direction to the usual one and is also less pronounced than the ordinary exponential variation.

For a given region, when N tends toward zero, the region will ultimately become transparent in the ultraviolet. Then the opacity τ is no longer given by (25) but decreases with the density, ultimately becoming proportional to it.

Next we consider a model of plane-parallel stratification of the matter, with a density increasing exponentially in the direction of the normal to the stratification. Along a ray making the angle θ with the normal, the relation between s and N is then

$$N = N_0 e^{\alpha \cos \theta \cdot s} , \tag{26}$$

the geometrical path being counted from some point on the ray where the density N_0 is negligibly small, compared with the other densities that may enter into the problem. For this model equation (16) becomes

$$1 = \frac{a_u}{C} \int_0^{s_0} N_0^2 e^{2\alpha \cos \theta \cdot s} ds , \tag{27}$$

or

$$1 = \frac{a_u}{C} \frac{1}{2\alpha \cos \theta} N_0^2 (e^{2\alpha \cos \theta \cdot s_0} - 1) . \tag{28}$$

Neglecting N_0^2 in comparison with $N^2(s_0)$, this becomes

$$1 = \frac{a_u}{C} \frac{1}{2a \cos \theta} N^2(s_0) . \tag{29}$$

Equation (21) takes the form

$$\tau = 0.4 m_H \int_0^{s_0} N_0 e^{a \cos \theta \cdot s} ds , \tag{30}$$

or, again neglecting N_0 in comparison with N,

$$\tau = 0.4 m_H \frac{1}{a \cos \theta} N(s_0) . \tag{31}$$

Eliminating $N(s_0)$ in (31), with the aid of (29), we get

$$\tau = 0.4 m_H \sqrt{\frac{C}{a_u}} \frac{\sqrt{2}}{\sqrt{a \cos \theta}} . \tag{32}$$

The opacity τ is now proportional to the square root of the constant C, measuring the amount of impinging ionizing radiation. The opacity increases with the angle between the ray and the normal, but only as $\sqrt{\sec \theta}$.

Finally, we consider a model which probably corresponds rather closely to the actual conditions in the atmosphere of the I component of ϵ Aurigae. We assume that the density distribution is symmetrical around a center and falls off exponentially with the distance r from the center:

$$N = N_0 e^{-ar} . \tag{33}$$

The region corresponding to the atmosphere is the only region of the model that interests us. The numerical value of the constant a is limited to the range $10^{-12} - 10^{-13}$ cm^{-1} (cf. p. 591).

Consider, now, a ray which traverses the atmosphere in such a way that the minimum distance from the center of the star to the ray is y. For the rays that interest us, y will not be very different from the radius of the I star. A change in the dip of the ray is

equivalent to a change in y of the same amount. Let s be counted along the ray from the point of smallest distance from the center, positive in the direction toward the observer. Then it follows from (33) that the dependence of N upon s is given by the relation

$$N = N_0 e^{-a\sqrt{y^2+s^2}} . \tag{34}$$

Introducing

$$N_c = N_0 e^{-ay} , \tag{35}$$

the maximum density on the ray, and

$$t = \frac{s}{y} , \tag{36}$$

we can write (34) in the form

$$N = N_c e^{-ay(\sqrt{1+t^2}-1)} . \tag{37}$$

We now have to introduce this relation between N and s into the general equations (16) and (21). We thus find:

$$1 = \frac{a_u}{C} N_c^2 \int_{-\infty}^{s_0} e^{-2ay(\sqrt{1+t^2}-1)} ds , \tag{38}$$

or

$$1 = \frac{a_u}{C} N_c^2 y \int_{-\infty}^{t_0} e^{-2ay(\sqrt{1+t^2}-1)} dt , \tag{39}$$

and

$$\tau = 0.4 m_H N_c y \int_{-\infty}^{t_0} e^{-ay(\sqrt{1+t^2}-1)} dt . \tag{40}$$

Now, the smallest possible value of ay is about 20, corresponding to $a = 10^{-13}$. This means that the integrands of the integrals in (39) and (40) fall off rapidly with t. In fact, for $t = 1$, they are at most of the order of magnitude 10^{-7} and 3×10^{-4}. This means that the effective extent of the atmosphere along the rays considered is small compared with the radius of the I star. Analytically, it means that we can obtain useful asymptotic expansions of the integrals in

(39) and (40) by expanding $\sqrt{1 + t^2}$ in the exponents in powers of t. In fact, the first term of the asymptotic expansion gives sufficient accuracy. (A similar asymptotic expansion has been used by Menzel[17] to evaluate an extinction integral occurring in the discussion of ζ Aurigae.) In this way we find, from (39) and (40),

$$1 = \frac{a_u}{C} N_c^2 y \int_{-\infty}^{t_0} e^{-ayt^2} dt \tag{41}$$

and

$$\tau = 0.4 m_H N_c y \int_{-\infty}^{t_0} e^{-\frac{1}{2}ayt^2} dt \,. \tag{42}$$

Using $erf(x)$ to denote the error function:

$$erf(x) = \frac{2}{\sqrt{\pi}} \int_0^x e^{-x^2} dx \,, \tag{43}$$

we finally get from (41)

$$N_c = \sqrt{\frac{C}{a_u}} \frac{1}{\sqrt{y}} (ay)^{1/4} \frac{\sqrt{2}}{\pi^{1/4}} \frac{1}{\sqrt{1 - erf(-\sqrt{ay}\, t_0)}} \,, \tag{44}$$

and from (42)

$$\tau = 0.4 m_H N_c y \frac{\sqrt{2}}{\sqrt{ay}} \frac{\sqrt{\pi}}{2} [1 - erf(-\sqrt{\tfrac{1}{2}}\sqrt{ay}\, t_0)] \,. \tag{45}$$

Equation (44) relates the maximum density N_c along the ray with $t_0 = s_0/y$, which measures the relative extent of the ionized region, while equation (45) allows τ to be found from N_c and t_0. Remembering that N_c is a function of the dip of the ray under the surface of the I star, we see that (44) and (45) determine the opacity τ as a function of the dip. Eliminating N_c from (45) with the aid of (44), we find

$$\tau = 0.4 m_H \sqrt{\frac{C}{a_u}} \sqrt{y} \frac{1}{(ay)^{1/4}} \pi^{1/4} \frac{1 - erf(-\sqrt{\tfrac{1}{2}}\sqrt{ay}\, t_0)}{\sqrt{1 - erf(-\sqrt{ay}\, t_0)}} \,. \tag{46}$$

Let us now consider τ as a function of the dip. When the dip increases, N_c increases according to (35). The minimum distance y from the center of the I star for the ray considered is decreased; however, the relative variation of y is small, the maximum dip being small compared to the radius of the I star (cf. p. 590). For our purposes it is sufficiently accurate to consider y in equations (44), (45), and (46) as a constant equal to R_{I}. Equation (44) then gives t_0 as a function of N_c, and equation (46) gives τ as a function of t_0.

TABLE 3

$\sqrt{\alpha y}\, t_0$	$[1 - erf(-\sqrt{\alpha y}\, t_0)]^{-\frac{1}{2}} \sim N_c$	$\frac{1 - erf(-\sqrt{\frac{1}{2}}\sqrt{\alpha y}\, t_0)}{\sqrt{1 - erf(-\sqrt{\alpha y}\, t_0)}} \sim \tau$
−3.0	210.	0.57
−2.5	50.	0.60
−2.0	14.5	0.65
−1.5	5.6	0.73
−1.0	2.5	0.81
−0.5	1.4	0.90
0.0	1.00	1.00
+0.5	0.81	1.12
+1.0	0.74	1.24
+1.5	0.71	1.33
+2.0	0.71	1.38
∞	0.71	1.41

Table 3 gives the quantities $[1 - erf(-\sqrt{\alpha y}\, t_0)]^{-(1/2)}$ and $[1 - erf(-\frac{1}{2}\sqrt{\alpha y}\, t_0)]\,[1 - erf(-\sqrt{\alpha y}\, t_0)]^{-(1/2)}$ as a function of $\sqrt{\alpha y}\, t_0$. According to (44), N_c is proportional to the first of these quantities, while, according to (46), τ is proportional to the latter.

It appears from Table 3 that the opacity decreases with increasing dip, contrary to the case of normal extinction. Furthermore, it is seen that the range of variation of τ is only by a factor of 2.4, corresponding to a range in N_c of 300. In the case of normal extinction, τ would have been proportional to N_c, leading to a tremendous variation in the extinction. We thus see that the decrease of the thickness of the ionized region with increasing density approximately compensates—in fact, slightly overcompensates—the increase in the absorption per unit volume with the density.

Before completing the discussion of equations (44) and (46) we shall consider briefly the influence of the finite disk of the F star, as

seen from the ionized region of the I star considered, upon the resulting opacity in the visual and photographic regions.

Let us consider for a moment the case that the ionizing radiation came from the half of the disk of the F star highest above the horizon of the considered region of the I star, and that the obstruction of the photographic and visual light from the lower half was being studied. The ionized region would then extend farther into the I star, and the opacity τ would be increased. This effect would be the more marked the greater the dip. In this way we see that for the lower half of the disk, owing to the effect studied, there will be an increase of opacity and a tendency for the march of τ with N_e to be reversed. For the upper half of the disk the effect will lead to the opposite result. The net result for the whole disk will probably be in the same direction as for the lower half of the disk. It is easy to show that for an angular radius of the F star as seen from the region of the I star considered, equal to $1^\circ.8$ (cf. p. 579), the result cannot differ very much from the case of a point source. The sign of the change of τ with N_e could hardly be reversed, and the opacities given in Table 3 could hardly be increased by more than a factor of 2. It would not present great difficulties to treat the case of an extended disk rigorously.

Returning now to the discussion of equations (44) and (46), we next find the value of C/a_u required to give the observed opacity in visual and photographic light. The observed value of τ is 0.7. With $y = R_I = 2.10^{14}$ and $ay = 50$, and with the last factor in (46) equal to 2 to allow for the effect of the finite disk, we find that the required value of $\sqrt{C/a_u}$ is about 6.10^{16}, and thus C/a_u is about 4.10^{33}.

The atomic absorption coefficient a_u for the ionizing radiation can be estimated as follows: Taking sodium as a typical atom and using the Coulomb-field formula to derive a_u (cf., for instance, Unsöld[20]), a value of the order of 10^{-16} is found. In the case of sodium it is well known, however, that the Coulomb-field formula gives a value that is considerably too great, when applied to the continuum originating from the *ground state*. In fact, the application of the sum rule, as well as direct experimental and theoretical determinations of the

[20] *Zs. f. Ap.*, **8**, 225, 1934.

absorption coefficient in question, gives a value about one hundred times smaller than the Coulomb-field value (cf. Trumpy[21]). The situation is not so clear for other atoms involved. We shall assume that the correction to the Coulomb-field value is of the same order of magnitude in these cases also. More accurate values naturally would be of great value. Hence, we shall adopt a_u as of the order of magnitude 10^{-18}.

With $a_u = 10^{-18}$, we find $C = 4.10^{15}$. We have now to compare this value with the value found from (7). Choosing Ca with $I = 6.1$ as a typical element, we find from (7), with $T = 6300°$ and $w = 2.5 \times 10^{-4}$, a value of C equal to 10^{13}. We thus find that the value of C required to give the observed opacity is between one hundred and one thousand times larger than the value computed from (7). We conclude that the amount of ultraviolet ionizing radiation of the F star at the surface of the I star is between one hundred and one thousand times greater than the amount calculated from Planck's formula with $T = 6300°$. The same fact may also be expressed by saying that the opacity corresponding to the Planck radiation is about twenty times smaller than the opacity observed.

The value of C found above is naturally rather uncertain, but it seems difficult to escape the conclusion that, if the picture of the mechanism of light obstruction considered here is correct, the ultraviolet radiation of the F star at the I star must be very considerably higher than the Planck value.

A priori, it is not impossible that an excess of ionizing radiation such as has just been considered is really present. The presence of hydrogen emission lines in the spectrum of ϵ Aurigae at the time of the eclipse (cf. Adams and Sanford[10]) is an indication in that direction. Also, in the case of the sun, as is well known, many anomalies can be explained by the assumption of an excess of ultraviolet radiation, though here this assumption is not the only one possible.

We conclude, therefore, that the result obtained from the discussion of the value of C derived from the observed opacity does not rule out the picture that we are discussing here in the greatest detail. On the other hand, we cannot be certain that this picture is

[21] *Zs. f. Phys.*, **71**, 720, 1931.

the correct one; and, therefore, all other possibilities have to be considered carefully.

With the value of C/a_u derived from (46), we now find N_e as a function of t_0 with the aid of (44). The numerical value of the multiplier of the quantity $[1 - erf(-\sqrt{a}y\, t_0)]^{-(1/2)}$ given in Table 3 is found to be 1.10^{10}. To $t_0 \to \infty$, then, corresponds the density $N_e = 7.10^9$. This means that for a ray with the maximum density $N_e = 7.10^9$ the ionized region just extends along the whole of the ray through the atmosphere of the I star. For a smaller value of N_e, that is, for a smaller dip, the I star is no longer opaque to the ionizing radiation. The ionization is complete ($x = 1$) along any ray with $N_e < 7.10^9$. The opacity τ, due to electron scattering, is now [cf. (42)]:

$$\tau = 0.4 m_H N_e y \int_{-\infty}^{+\infty} e^{-\frac{1}{2}ay^2 t^2} dt\,, \qquad \text{for} \qquad N_e < 7.10^9 \qquad (47)$$

or

$$\tau = 0.4 m_H N_e y \frac{\sqrt{2\pi}}{\sqrt{a}y}\,, \qquad \text{for} \qquad N_e < 7.10^9\,. \qquad (48)$$

Hence, τ decreases proportionally to N_e for $N_e < 7.10^9$. The approximately constant minimum thus begins when the dip has been reached for which $N_e = 7.10^9$. As N_e increases with increasing dip, τ, according to Table 3, now decreases slowly. The range of increase of N_e during the constant minimum is, as we have seen (cf. p. 591), at least about 20. The corresponding change of τ, according to Table 3, is by a factor of 2. Even an increase of N_e by a factor of 300 above the limit $N_e = 7.10^9$ changes τ by a factor of 2.4 only.

Now a change of τ by a factor of 2, although very much smaller than the change corresponding to ordinary extinction, contradicts the observed constant minimum. As we have seen, the effect of the finite size of the disk tends to diminish the variation of τ with N_e. The effect of the presence of several elements with different ionization potentials goes in the same direction. Further, as we shall see, with increasing N_e other sources of opacity become of importance, hence tending to compensate the small remaining variation. It may well be possible that a sufficiently constant minimum is produced in

this manner, so that the picture considered cannot be said to be contradicted by the observational evidence of a very nearly constant minimum.

We now have to investigate whether the region of the I star here considered is practically transparent when the influence of the F star is absent, that is, on the nonionized part of the rays considered. The temperature of that region is about 1400°, the number of free electrons per unit volume being about $10^{10} - 10^{12}$. An inspection of the tables by Unsöld[20] and Pannekoek[22] for the opacity due to photoelectric absorption from excited states shows that it is so low for $T = 1400°$ and electron pressure P_e from 10^{-3} to 10^{-1} dynes that it can be neglected. We shall see, however, that there is one source of opacity which becomes appreciable as the density increases from the limit $N = 7.10^9$ to values that are, say, from ten times to one hundred times higher, namely, Rayleigh scattering due to neutral hydrogen atoms.

The atomic absorption coefficient corresponding to Rayleigh scattering for wave lengths that are large compared to the dispersion wave length is known to be

$$a = \frac{128\pi^5}{3}\, a'^2 \cdot \frac{1}{\lambda^4}, \tag{49}$$

where a' is the polarizability of the atom and state considered. For the ground state of hydrogen we have $a' = 6.63 \times 10^{-25}$ (cf. van Vleck).[23] Thus, we find

$$a_H = 1 \times 10^{-27}\left(\frac{5000\,\mathrm{A}}{\lambda}\right)^4. \tag{50}$$

Now, owing to the high ionization potential of hydrogen, the region of ionization of hydrogen in the I star is negligible. We then find [cf. (48)] that the opacity τ_H, owing to Rayleigh scattering along a ray, on which the maximum number of hydrogen atoms per unit volume is $N_{c,H}$, is given by

$$\tau_H = 1 \times 10^{-27}\left(\frac{5000\,\mathrm{A}}{\lambda}\right)^4 N_{c,H}\, y\, \frac{\sqrt{2\pi}}{\sqrt{ay}}. \tag{51}$$

[22] *Astr. Inst. Amsterdam*, No. 4, 1935.

[23] J. H. van Vleck, *The Theory of Electric and Magnetic Susceptibilities*, Oxford, 1932.

For $\lambda = 5000$ A, with $y = 2.10^{14}$ and $ay = 50$ as before, we find from (51) that

$$\tau_H = 2.5 \times 10^{-13} N_{c,H} . \tag{52}$$

Therefore, when $N_{c,H}$ is, say, $1 \times 10^{12} - 2 \times 10^{12}$, Rayleigh scattering becomes quite appreciable. Now, as we have seen, the constant minimum sets in for $N_c = 7.10^9$, the dip increasing until a value of at least $1 \times 10^{11} - 2 \times 10^{11}$ has been reached. We now see that, unless the ratio of the number of hydrogen atoms N_H per unit volume to the number of atoms in the group of ionizable elements N per unit volume is less than about 10, the Rayleigh scattering would become appreciable to such an extent as to destroy the constant minimum. It may be noted that an appreciable obstruction of a smaller part of the disk of the F star by Rayleigh scattering would only tend to flatten the minimum (cf. p. 605).

With the upper limit of the relative hydrogen abundance just mentioned, it is further found that the influence of Rayleigh scattering in the wave-length region of the ionizing radiation is not appreciable in the density region in question [$N > 7 \times 10^9$].

The numerical value 10, which we have found for the upper limit of N_H/N is, of course, subject to some uncertainty. The order of magnitude, however, should be right. The relative abundance of hydrogen thus turns out to be considerably smaller than is now usually assumed for the atmospheres of normal stars of the main sequence. It is not impossible, however, that the true value of the relative hydrogen abundance in the atmosphere of a supergiant like the I component of ε Aurigae is as low as, or lower than, the required limit.

We are now in a position to discuss the question mentioned on page 594, which elements contribute appreciably to the opacity in the visual and photographic regions, according to the mechanism under discussion. From equations (7) and (46) we see that elements of high ionization potential are ionized in such a narrow region only that the resulting τ becomes very small. On the other hand, we now see that elements of small relative abundance reach the required N_c for the element [cf. (44) and (46)] only at such depths that Rayleigh scattering of the neutral hydrogen would prevent the occur-

rence of any constant minimum. Probably, therefore, the opacity is largely due to such elements as *Na*, *Al*, *Ca*, and possibly *Mg* and *Fe*. Doubly ionized ions are probably present in a very narrow region only, and thus the singly ionized ions do not contribute an appreciable amount of free electrons.

We have seen that the density of the region responsible for the light obstruction, to which the picture under discussion leads, is low enough to insure that the constant minimum is not distorted by other sources of opacity, provided the relative hydrogen abundance does not exceed a certain limit. We shall next consider the density arrived at from another point of view. From Table 3 it is apparent that in the denser part of the obstructing region most of the traversing rays go through nonionized matter. It is, therefore, to be expected that the corresponding absorption lines due to resonance lines of neutral atoms would be very strong. In fact, combining the value of the density arrived at with the length of the path through nonionized matter [cf. (48)], we find that the strength of a line such as the resonance line of *Ca* would be extremely strong—much stronger than observed. In order to avoid contradiction with the observations it is, therefore, necessary to assume that the abundances and the amount of ionizing radiation are such as to shift the obstruction effect to elements with higher ionization potentials that have their resonance lines in the unobservable ultraviolet region. This would require an even higher excess of the ionizing radiation over Planck radiation, though the ratio of the ionizing radiation to the total radiation of the F star would not be very much changed.

It will be seen that we have now dealt with the first three of the points mentioned on page 589. We shall finally consider the last point, whether other sources of opacity are of importance in the region of the I star that is influenced by the radiation of the F star. In order to investigate this we shall have to find the state of excitation of the matter in the ionized region. Comparing this with a region in thermodynamical equilibrium at the same density and at a temperature equal to that of the F star, we see that the number and the velocity distribution of the ions and the free electrons are practically the same in the two cases. The number of neutral atoms in the ground state is extremely low in the ionized region but still high-

er than in thermodynamical equilibrium by a factor equal to the reciprocal of the dilution factor. At the surface of the I star the number of processes of radiation excitation of excited states is about the same as in thermodynamical equilibrium, because the reduction of the intensity of the exciting radiation is compensated by the greater number of atoms in the ground state. Scattering of the exciting radiation will very soon reduce it, however. The contribution of electron captures to the population in the excited state, on the contrary, is practically the same as in thermodynamical equilibrium, throughout the ionized region. The population of the excited states will, therefore, correspond very nearly with that in the highest layers of the F star itself. The opacity due to photoelectric absorption from the excited states will be equal to the value found for thermodynamical equilibrium at the same pressure and at a temperature equal to that of the F star, reduced by a factor approximately equal to the residual intensity of the lines corresponding to transitions between the ground state and the excited states in question.

The absorption coefficient $\kappa_\nu\rho$ per unit volume, owing to photoelectric transitions, is given by the well-known expression (cf., for instance, Unsöld[20])

$$\kappa_\nu\rho = \frac{16\pi^2}{3\sqrt{3}} \frac{e^6}{hc(2\pi m_e)^{3/2}} Z_{eff}^2 \frac{e^{h\nu/kT} - 1}{\nu^3} \frac{1}{(kT)^{1/2}} N'' N_e , \qquad (53)$$

or

$$\kappa_\nu\rho = c_1 N'' N_e , \qquad (54)$$

that is, cf. (6),

$$\kappa_\nu\rho = c_1 x^2 N^2 . \qquad (55)$$

With $Z_{eff} = 1$, $\lambda = 5000$ A, and $T = 6300°$, the constant c_1 is 1×10^{-36}. We thus see that in thermodynamical equilibrium the photoelectric absorption coefficient per free electron in a practically completely ionized gas ($x = 1$) is smaller than the free-electron scattering coefficient 0.4 m_H when the density N is smaller than $10^{11} - 10^{12}$.

Now, in the ionized region considered, the opacity, as we have seen, is reduced by a factor of the order of the residual line inten-

sities. Therefore, even allowing for a considerable increase in the photoelectric opacity due to a value of Z_{eff} larger than 1, the photoelectric opacity in the ionized region of the I star with $N < 1\text{-}2 \times 10^{11}$ would not be comparable with electron scattering.

It may be noted that the contribution of photoelectric opacity to the obstruction of photographic and visual light is independent of the dip, for a certain range of dips. In fact, the optical depth τ_p corresponding to this process, is [cf. (21)]

$$\tau_p = c_1 \int_{-\infty}^{s_0} N^2 ds \,. \tag{56}$$

Now, according to (16), for all dips for which the I star is opaque to the ultraviolet [$N > (7.10^9)$], this is equal to

$$\tau_p = c_1 \frac{C}{a_u} \,, \tag{57}$$

which is, in fact, constant.

It is interesting to note that in the ionized region of the I star, as we have seen, the distribution over the excited states corresponds closely to that in the highest layers of the F star. We shall not, however, enter here into the rather complicated problem of the influence of the I star upon the intensities of the corresponding lines.

Summarizing the discussion of the mechanism of electron scattering in a region of the I star ionized by the radiation of the F star, we can say that this picture may be the correct one but that we have met with certain difficulties: the required amount of ultraviolet radiation; the required, rather low, upper limit to the hydrogen abundance; and the necessity of avoiding too great a strength of resonance absorption lines in the observable wave-length region, or of the extreme edges of such lines beyond that region (Rayleigh scattering).

In investigating other possibilities of mechanisms to explain the observed obstruction effect, the following considerations may be of importance. With a mechanism that would give a higher mass-absorption coefficient than electron scattering, the obstructing region would be shifted toward smaller densities. The required ultraviolet radiation would be smaller, the influence of hydrogen Rayleigh scat-

tering would also be smaller, and the strength of the resonance lines of neutral atoms would be smaller—possibly very much smaller. In fact, all three difficulties would be lessened.

In investigating the general problem of stellar atmospheres, the author of this section has been led to consider the effect of two-quantum absorption processes on opacity in the continuous spectrum. Without entering into a detailed discussion of the possibility of the importance of this effect in the present connection, we shall show that the mechanism of two-quantum absorption processes leads to constant obstruction for a certain range of dip. Let the absorption coefficient in a frequency of the visual and photographic regions be proportional to the intensity of ultraviolet radiation, not necessarily of the same wave-length region as that considered before:

$$d\tau = c_l N e^{-\tau_{u'}} ds \,, \tag{58}$$

with

$$d\tau_{u'} = c_{u'} N ds \,. \tag{59}$$

It follows from (58) and (59) that

$$d\tau = \frac{c_l}{c_{u'}} e^{-\tau_{u'}} d\tau_{u'} \,, \tag{60}$$

or

$$\tau(s) = \frac{c_l}{c_{u'}} (1 - e^{-\tau_{u'}}) \,, \tag{61}$$

which means that

$$\tau = \frac{c_l}{c_{u'}} \tag{62}$$

when the region considered is opaque to the ultraviolet radiation in question.

This example, together with the discussion of the opacity due to electron scattering and also of the opacity due to photoelectric absorption, shows that the independence (or practical independence) of opacity of dip in a certain range of dips is a very general feature when the cause of the opacity is outside radiation. Therefore, though

we cannot claim that we yet know the mechanism of the light obstruction in the case of ϵ Aurigae with certainty, it does seem certain that an important characteristic of that mechanism has been established.

In concluding, it may be mentioned that the general discussion given on page 593, of the extent of the region of ionization as a function of the amount of ionizing radiation and the absorption coefficient of that radiation, has, with an obvious modification, an application also to another problem, namely (cf. Eddington[24]), that of the ionization of hydrogen in interstellar space.

YERKES OBSERVATORY
November 1937

[24] *Observatory*, **60**, 99, 1937.

Note added in proof.—The computations given in Table 1, page 575, are based on the elements of Huffer's light-curve. If Miss Güssow's elements ($D = 714$ days, $d = 330$ days) are used, which are based on a somewhat larger number of observations, the entries in Table 1 are slightly reduced. For ω 350° and $i = 70°$ we find

$$R_F = 0.025a\,, \quad R_I = 0.357a\,, \quad \frac{m_F}{m_I} = 1.47\,, \quad \log R_F = 2.28\,, \quad \log R_I = 3.43\,,$$

$$\log m_F = 1.56\,, \quad \log m_I = 1.39\,, \quad M_F = -7.2\,, \quad T_e(I) = 1350°\,.$$

These figures make the stability argument given on page 576 slightly more favorable.

Since $m_v = 3.27$ P.D. (Güssow), or 3.10 IPv, the distance modulus of ϵ Aurigae is 10.3 mag. Allowing for a visual space absorption of 0.4 mag. per 1000 parsecs, the parallax is found to be 0".0010. The total amplitude of the orbital motion of the F component projected on the sky is very nearly $2a_1$, or 0".030. A verification of this value would at the same time verify the high luminosity of the F component, found in this paper; a lower luminosity would lead to a larger displacement, by a factor of 1.6 for each magnitude.

A NEW SLIT SPECTROGRAPH FOR DIFFUSE GALACTIC NEBULAE

OTTO STRUVE

ABSTRACT

A spectrograph has been constructed which consists of a wide slit, attached to the outside of the upper end of the tube of the 40-inch telescope, and an f:1 Schmidt camera of 94 mm aperture with two 60° quartz prisms. Very faint nebulae can be observed with this instrument, provided their diameters exceed 11′.

In the course of recent work at the McDonald Observatory on diffuse galactic nebulae it was found necessary to determine the spectra of a number of objects which had not previously been observed. In 1933 Hubble[1] summarized all observations then available, including his own. The latter were obtained with six different instruments, five of them being objective prisms, and only one a focal plane spectrograph with the slit removed, attached to the 60-inch reflector and equipped with collimator and camera lenses of about 6-inch focus.

Wolf succeeded in obtaining the spectrum of the narrow southern part of the North America nebula (NGC 7000) with an objective prism.[2]

The principal problem at this time was to find a method suitable for obtaining the spectrum of the faint nebulosities near γ Cygni. I have already shown[3] from direct photographs that these nebulae are strong in *Hα* and are, therefore, of the emission type.

Preliminary experiments with an objective prism in front of our f:2 Schmidt camera were disappointing. Even with emulsions of great contrast, such as Eastman Process, the nebulae were lost in the background illumination of the night sky. Since the latter gives essentially white light and is not reduced in intensity, the nebulae lose enormously in contrast when their light is split up into numerous images. Conditions are even more hopeless when the spectrum of the nebula is continuous.

[1] *Ap. J.*, **56**, 173 and 176, 1922.

[2] *Sitz. Heidelberg*, No. 27, 1910.

[3] *Ap. J.*, **86**, 95, 1936.

A fast slit spectrograph equipped with a short camera and a strong dispersing unit offers better promise. The new f:1 Schmidt camera, in conjunction with the two quartz prisms of the McDonald Observatory Cassegrain spectrograph, is ideal for this purpose.

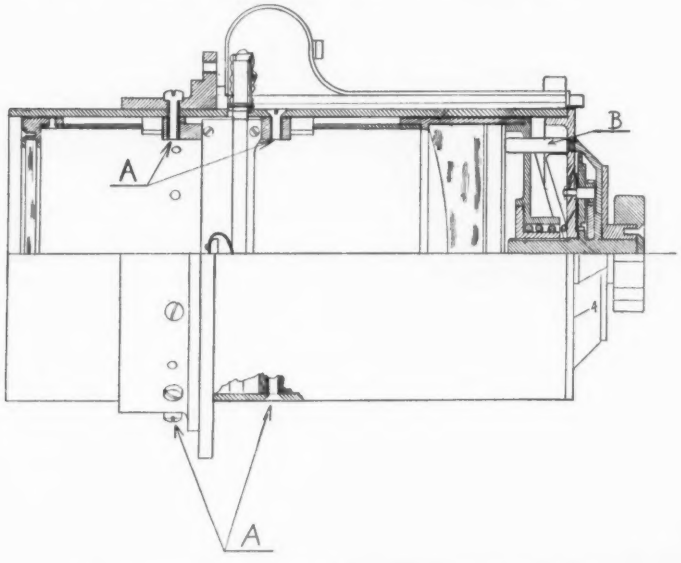

FIG. 1.—Schmidt camera of the McDonald Observatory

The optical parts of the camera, made by C. H. Nicholson, of DuQuoin, Illinois, have the following specifications:

Aperture of correcting plate made of Jena UV glass	94 mm
Thickness of correcting plate	4 mm
Aperture of aluminized spherical mirror	110 mm
Focal ratio of camera	f:1

The specifications for the quartz prisms (made by Bausch and Lomb) are:

Type of prisms	Cornu
Refracting angle of each prism	62°11′
Length of edge of each prism	80 mm
Length of face of first prism	130 mm
Length of face of second prism	140 mm
Total deviation of system	90°
Linear dispersion in the region of $H\delta$	250 A/mm

PLATE XXIX

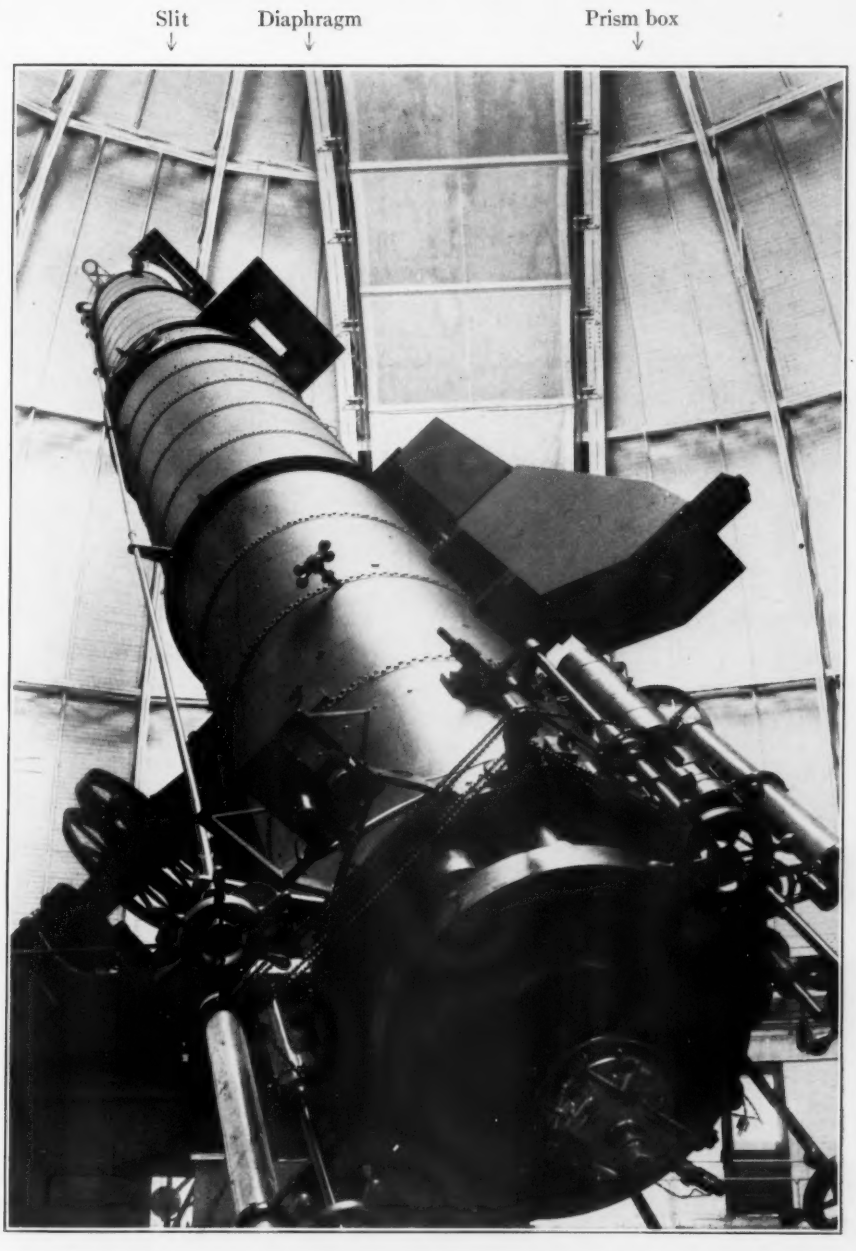

THE SPECTROGRAPH ATTACHED TO THE TUBE OF THE 40-INCH REFRACTOR

The slit is at the upper end of the tube. A diaphragm in the middle of the tube blocks out the sky. The wooden box at the lower end carries the two quartz prisms. The Schmidt camera projects outside, at right angles to the tube.

It is important in nebular work of this type to achieve the greatest possible speed. If the object under observation is sufficiently large to cover the entire solid angle subtended by the collimator lens at the slit, this can best be accomplished by omitting the telescope lens or the mirror system. An ordinary collimator of the type used in stellar spectrographs is much too short: for example, in our Cassegrain spectrograph the length of the collimator is 1 meter and the aperture is 76 mm. The angle is, therefore, 4°. Few nebulae are larger than 4° in diameter; therefore the method cannot be used.

To avoid this difficulty, we have placed a relatively wide slit on the outside of the upper end of the 40-inch telescope of the Yerkes Observatory. The camera and the quartz prisms are mounted in a wooden box at the lower end of the tube. In order to block out the entire direct light of the sky, a diaphragm was placed about halfway up the tube.

The collimator lens has been omitted: it is not required because the slit is so far from the prisms that the beam is sufficiently near parallelism when it strikes the first prism-surface. Rayleigh's formula[4] for the longitudinal aberration produced by a prism at minimum deviation, in the case of a diverging beam, is

$$\delta\nu = \frac{3y \sin \phi \, (\mu^2 - 1)}{\mu^2 \cos^2 \phi'} ,$$

where y = linear semiaperture of prism face, μ = index of refraction, ϕ = angle of incidence of axial ray on first surface, and ϕ' = angle of incidence of axial ray on second prism-surface. If u is the distance between the slit and the prism, we obtain for the total angular broadening of an infinitely narrow slit:

$$2\omega = 2\delta\nu \frac{\theta}{u} ,$$

where

$$\theta = \frac{y \cos \phi}{u} .$$

[4] *Phil. Mag.* (3d ser.), **9**, 40. See also Wadsworth, *Ap. J.*, **16**, 2, 1902, and **17**, 12, 1903.

Accordingly,

$$2\,\omega = \frac{6\theta^2(\mu^2 - 1)\sin\phi}{\mu^2 \cos\phi \cos^2\phi'} .$$

For a single 60° prism of flint glass, Wadsworth[4] finds

$$2\omega = 6.50\,\theta^2 .$$

In our case, $u = 17.70$ m, and

$$\theta = 2.2 \times 10^{-3} \text{ rad.} ; \qquad 2\omega = 3 \times 10^{-5} \text{ rad} .$$

On the photographic plate the broadening will be

$$x = 3 \times 10^{-3} \text{ mm} ,$$

and this can be safely neglected. The quartz prisms will produce nearly the same effect. We are, therefore, quite safe in omitting the collimator lens.

The angle subtended by the instrument in the sky is

$$\Omega = \text{Aperture of correcting plate} = 2\,\theta = 16' .$$

If the nebula is at least 16′ in diameter,[5] the new instrument is the fastest that can be designed for the given combination of camera and prisms. The advantage over a focal-plane spectrograph consists in the elimination of light losses in the telescope objective and in the collimator lens. For the 40-inch telescope we would have eight reflections (or twelve reflections if the photographic correcting lens is used). Using the expression

$$T = \left[1 - \left(\frac{\mu - 1}{\mu + 1}\right)^2\right]^8 ,$$

we find with an average index of refraction a transmission of 0.66. The total thickness of glass in the lenses is about 10 cm. For our combination of glasses the transmissions are roughly:

Wave length.....	λλ 5000–7000	λ 4500	λ 4000	λ 3750	λ 3500
Transmission.....	0.9	0.8	0.7	0.5	0.0

[5] Strictly speaking, the instrument covers an area bounded by the edges of the prism, the projection of which is 80×80 mm, and of the correcting plate, which has a diameter of 94 mm.

In the ordinary photographic region the combined transmission[6] is, therefore, approximately 0.5, while in the ultraviolet the 40-inch objective is practically opaque. Accordingly, the new spectrograph is at least twice as fast as a similar spectrograph would be in the focal plane of the 40-inch telescope, and it gives us the additional advantage of reaching into the ultraviolet region.

The slit width can be varied. Most of the preliminary photographs have a slit of 25 mm. On the plate this corresponds to 0.14 mm. With a dispersion of 250 A/mm this is equivalent to 35 A. We can measure with a precision of a fraction of an angstrom unit.

If the nebula is not as large as 16′, the method is less satisfactory. Since the transmission of the telescope and collimator is 0.5, the focal plane spectrograph and our new instrument would be equally efficient when the diameter of the nebula is about 11′. For still smaller objects, the focal plane spectrograph has the advantage in the ordinary photographic region.

The advantages of our instrument over an objective prism of similar specifications are enormous. The slit resolves the spectrum of the sky into a series of strong auroral emission lines and a weak continuous spectrum. The nebular emission lines are projected upon this faint background. With an exposure of from three to four hours the principal nebular lines of the North America nebula—$H\alpha$, $N_1 + N_2$, $H\beta$, and λ 3727—are very strong. The strongest emission lines in the nebula, $H\alpha$ and λ 3727, could have been detected with a much shorter exposure—perhaps one of thirty minutes. Consequently, a much fainter nebula could have been detected. In fact, the method is by far the most powerful in existence for the discovery of faint emission nebulae: with long exposures we can detect emission lines of nebulae which are too faint to be photographed directly on the background of the night sky.

In principle, the limit is now set by the weak continuous spectrum of the sky. If the nebula has, in effect, the equivalent of three equally strong emission lines between λ 3500 and $H\alpha$, it is divided into three images. With a slit-width of 0.14 mm on the plate, the spectrum of the sky, if it were all continuous, would be spread over about 7 mm, giving us an increase in contrast by a factor of 17. But

[6] See also G. E. Hale, *Ap. J.*, **5**, 127, 1897.

the sky gives mostly emission lines. Assuming that 0.75 of the total light of the sky is concentrated in the auroral lines, the factor becomes 68. In other words, if we push our exposure sufficiently to place the continuous spectrum of the night sky upon the most favorable part of the characteristic curve of our plate, we can detect emission nebulae which are sixty-eight times fainter than those detectable with the same emulsion on a direct photograph. Since our spectrograph integrates the light from an area of 16′ in diameter, this computation assumes that the nebula is of uniform surface brightness.

In practice the present equipment would require exposures of some ten to fifteen hours to reach this limit. Direct photographs on fast emulsions give a sufficiently dark background in about two minutes. According to our assumptions, with a plate for which the reciprocity relation holds we would require an exposure of four hundred minutes to obtain the same blackening in the continuous spectrum, if loss of light in the prisms is neglected. Allowing for it, the exposure would have to be of the order of ten to fifteen hours.

The principal interest of the method lies in the fact that it requires no large telescope. A relatively inexpensive camera with an objective prism and a long arm carrying the slit, equatorially mounted and driven by a clock (or fed by a coelostat),[7] is sufficient to give important results. An even shorter Schmidt camera, with a correspondingly stronger dispersion in the prisms, would be an advantage. A long slit permits the exploration of a considerable section of the sky. Our slit of 25 inches covers a section in the sky 15′ wide and about 2° long.

It should be pointed out that the camera is focused at the slit and that the stars form on the plate little disks 16′, or 0.5 mm, in

[7] A stationary instrument for nebular spectroscopy is now being built for the McDonald Observatory, under the supervision of Messrs. G. Van Biesbroeck and L. Henyey. A polar axis driven by a small synchronous motor carries on one side a plane mirror, 120 cm × 25 cm., and a wide slit, and on the other side a box containing the Schmidt camera and the quartz prisms. A stationary plane mirror having a diameter of 60 cm is mounted separately on the continuation of the polar axis, at a distance of about 23 m. The total length of the spectrograph is therefore about 46 m. and the area in the sky which is integrated by the instrument has a diameter of 6′. The slit does not rotate with respect to the sky, and the arrangement has certain advantages over an ordinary coelostat.

diameter. The outlines of the nebulae are, of course, diffused by the same amount, but this does not seriously interfere with their identification. The fact that the stars are out of focus tends to make their spectra sufficiently wide for measurement. But it increases the difficulty of avoiding bright stars in the field. The unresolved faint stars contribute, of course, only a very small fraction to the light of the sky, and their effect is included in the continuous background which we have discussed.

The flexure of the 40-inch tube would be serious if it were not so small. A complete reversal over 180° corresponds to a shift in the optical axis of about 2 cm. This is less than our slit-width; even for long exposures the effect is negligible.

The emission lines of the sky form a useful set of comparison lines for measurements of wave lengths. Since we suspect that large areas of the Milky Way give hydrogen emission lines and perhaps also λ 3727, we shall mount an aluminized plane mirror in front of a small portion of the slit. This will give us a comparison spectrum of the sky from a region which lies outside the Milky Way.

The first results, obtained by Messrs. Henyey and Greenstein, are described in the following paper.

The mechanical parts of the Schmidt camera were designed by Dr. G. W. Moffitt, and the photographs used in this article were made by Mr. E. L. McCarthy. It is a pleasure to acknowledge a grant from the American Academy of Arts and Sciences, which was used for the construction of some of the mechanical parts of the Schmidt camera.

YERKES OBSERVATORY
November 3, 1937

NOTES

THE SPECTRA OF THE NORTH AMERICA NEBULA AND OF THE γ CYGNI NEBULA

In the preceding paper Struve has described a new fast spectrograph suitable for obtaining spectra of large nebulous objects. In this report we give a preliminary account of the important features of some spectra now available. We have used the f/1 Schmidt camera with Agfa Supersensitive Panchromatic film, covering the spectral range from 3200 A to 6600 A.

A spectrum of three hours' exposure on the North America nebula, NGC 7000, is shown in Plate XXX. The slit was centered at α 20^h52^m, $\delta + 44^\circ.2$ (1875). The length of the slit, approximately 2°, crosses the brightest portion of the nebula at the given declination. The lines in the radiation from the night sky traverse the entire spectrum, in contrast to the lines originating in the nebula, which show a density gradient along the slit because of the structural features of the nebula. These lines, marked on the plate, are $H\alpha$, $H\beta$, $H\gamma$, $H\delta$, $H\epsilon$, and the nebular lines λ 5007 [*O* III] and λ 3727 [*O* II]. It is possible that a blend of $H\zeta$ and λ 3889 of *He* is also present. There is a marked difference in the distribution of density along the lines $H\beta$, λ 5007, and λ 3727, implying a variation of excitation over the surface of the nebula. A weak continuum appears with no obvious absorption lines. Wolf[1] has observed the emission spectrum of this object with an objective prism.

In Plate XXX is reproduced a spectrum of a faint nebulous patch at α $20^h12.6^m$, $\delta + 41^\circ.4$ (1875), which is part of IC 1318, the large nebulous mass surrounding γ Cygni. The exposure was 161 minutes. A photograph of this object, found on Plate 44 of Barnard's *Atlas of the Milky Way*, shows that the brightest portion is $0^\circ.5$ in diameter. As before, the lines crossing the entire spectrum have their origin in the night sky, while the shorter lines, marked on the plate, arise in the nebula. They are $H\alpha$, $H\beta$, $H\gamma$, and the nebular line λ 3727 of

[1] *Mitt. Heidelberg Sternwarte*, No. 22, 1910.

PLATE XXX

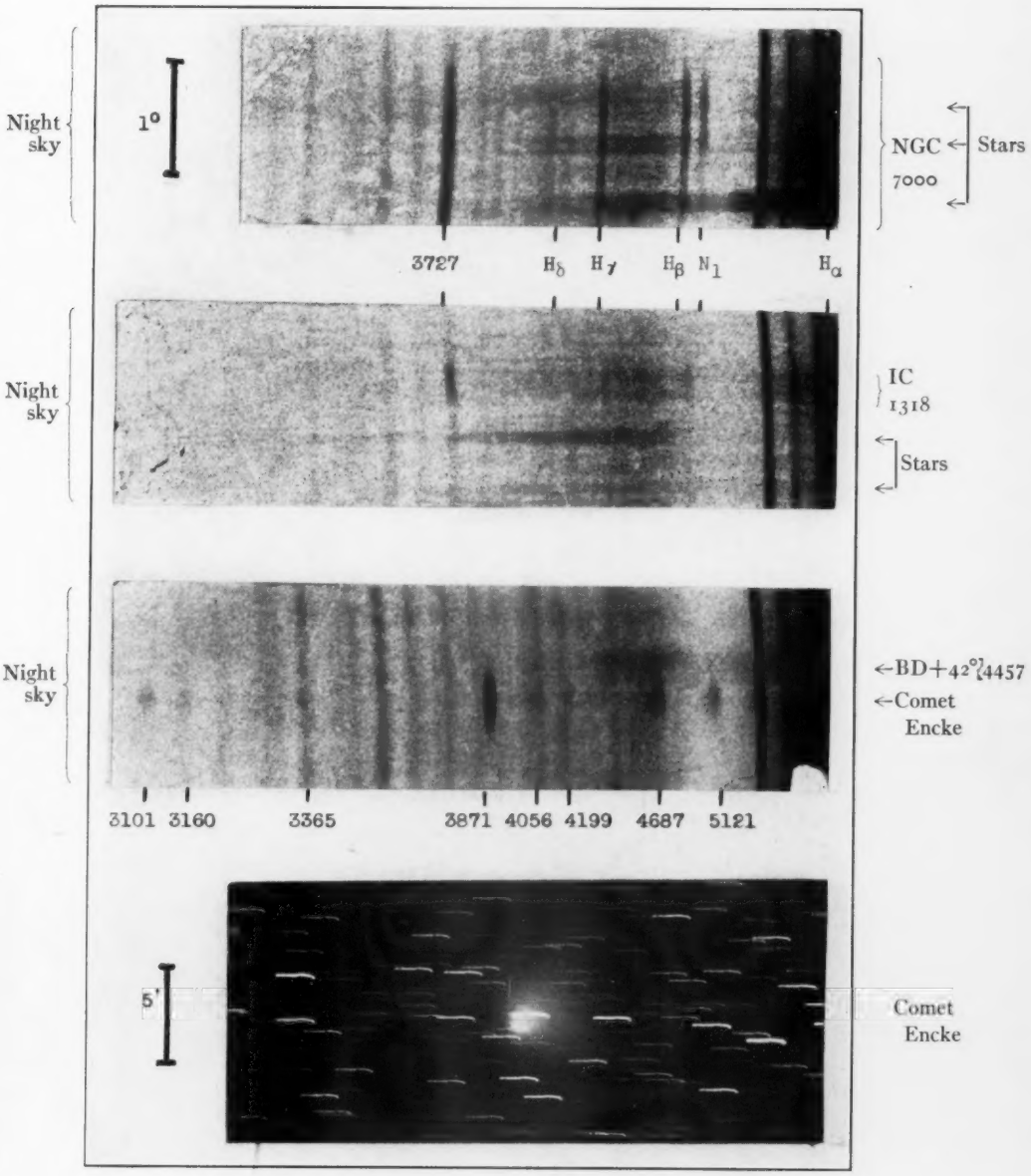

SPECTRA OF NEBULAE AND OF COMET ENCKE

Attention is called to the distribution of light in the continuous spectrum of IC 1318, near γ Cygni. The brighter of the two stars below it is of spectral type B8; the nebula is much redder than this star.

[*O* II]. There is a well-defined continuous spectrum which is superposed on the continuous spectra of the night sky and of unresolved starlight. Struve[2] has predicted the existence of $H\alpha$ in emission on the basis of the strength of the nebula indicated on direct photographs taken in the red.

All exposures show the spectrum of the night sky, even on nights without conspicuous aurora. Approximately twenty lines in a four-hour exposure have been identified with known lines or bands. The green auroral line appears in a ten-minute exposure.

The emission spectra of the two nebulae discussed distinguish these objects as unusual. Hubble[3] found that the larger majority of diffuse nebulae illuminated by stars of spectral type later than B1 have continuous spectra. Emission-line nebulae are associated with stars of earlier type. The North America nebula is probably illuminated by α Cygni (A2p) and IC 1318 by γ Cygni (F8p), two well-known supergiant stars. It is possible that the excitation of these nebulae is, in fact, dependent on the supergiant character of the exciting stars. The theory of extended stellar atmospheres developed by Kosirev[4] and Chandrasekhar[5] predicts such an effect. It appears in the form of an excess of ultraviolet radiation over the black-body energy distribution corresponding to the excitation temperatures of the stars. It should be possible to use the relative intensities of the emission lines and of the continuous spectrum to evaluate this excess and to study the structure of extended stellar atmospheres.

We intend to carry through such an investigation for these and other nebulae, as well as a comparison of the energy distribution in the continuous spectra of nebulae and of associated stars, in order to determine the scattering properties of the interstellar particles. It should be possible, in addition, to investigate the spectra of various extended objects, such as globular clusters, extragalactic nebulae, dark nebulae, and Milky Way star clouds.

JESSE L. GREENSTEIN[6]
L. G. HENYEY

YERKES OBSERVATORY
November 6, 1937

[2] *Ap. J.*, **86**, 94, 1937.

[3] *Ibid.*, **56**, 162 and 400, 1922.

[4] *M.N.*, **94**, 430, 1934.

[5] *Ibid.*, p. 444.

[6] National Research Council Fellow.

NOTE ON THE SPECTRUM OF PERIODIC COMET ENCKE

Visual examination of this comet with the 40-inch telescope on November 3 showed that it had developed a broad diffuse tail visible to a distance of five minutes from the nucleus. This nucleus was perfectly stellar in appearance, and it was estimated to be of the thirteenth magnitude. Plate XXX (in preceding note) contains a reproduction of a twenty-minute exposure taken with the 24-inch reflector on November 6. This plate and the visual observation on November 3 reveal that it is difficult to distinguish between the coma and the tail, since the nebulous patch is directed very nearly in the direction of the sun (position angle 270°), and since there is no apparent nebulosity on the opposite side.

Since the comet was bright enough to be seen in the four-inch finder, it was thought that there was a possibility of obtaining its spectrum with the instrument described in the preceding notes. Plate XXX shows the result of the attempt. The exposure was taken on November 4 from 2^h12^m to 5^h57^m U.T. through a very transparent atmosphere. The heliocentric distance at that time was 1.18 astronomical units, and the geocentric distance was 0.30 astronomical units. The guiding was done with the 40-inch telescope. The star BD + 42°4457 (7^M1, K5), near which the comet passed one hour before the exposure was started, remained sufficiently close to have its spectrum recorded. The long spectral lines, as seen in the plate, are those of the night sky; while the short ones are the cometary bands. The original plate was measured, and the wave lengths of the centers of the bands were deduced by means of a Hartmann formula derived from the auroral lines.

The bands are given in the accompanying table. The band at

λ Measured	Identification	λ Measured	Identification
5121	Third *C* band	3871	Third *CN* band
4687	Fourth *C* band	3365	N_2 ?
4198	Second *CN* band	3160	? New
4056	?	3103	? New

λ 3365 is probably the same as that recently suspected by Wares,[1] while the ones at λ 3103 and λ 3160 probably have not been observed previously.

An attempt will be made to observe the spectrum of Comet Encke when it becomes brighter, in order that faint bands may be separated from the auroral lines and that any other bands existing in the ultraviolet may be found.[2]

G. VAN BIESBROECK
L. G. HENYEY

YERKES OBSERVATORY
November 10, 1937

PARTIALLY DEGENERATE STELLAR CONFIGURATIONS

As the author has shown,[1] the structure of completely degenerate configurations can be fully described by the differential equation

$$\frac{1}{\eta^2}\frac{d}{d\eta}\left(\eta^2\frac{d\varphi}{d\eta}\right) = -\left(\varphi^2 - \frac{1}{y_0^2}\right)^{3/2}. \qquad \text{(I)}$$

This equation describes exactly the structure of stellar configurations based on the exact equation of state of a degenerate electron gas, and in particular takes into account the gradual change of the equation of state from the law $p = K_1\rho^{5/3}$ to the law $p = K_2\rho^{4/3}$, with increasing density. On the theory of white dwarfs based on equation (I), the gaseous fringe is neglected as being insignificant, as may indeed be readily verified.[2] However, for such stars in the interior of which we have only partial degeneracy at not too high densities, the relativistic effects can be properly neglected; and the problem now is to take into account the gradual change of the equa-

[1] Unpublished; verbally reported at the meeting of the American Astronomical Society in September, 1937.

[2] Such attempts were made on November 21 and 23, when the comet was brighter, but at a considerably lower altitude. The band at λ 3365 is present on both plates; λ 3160 is suspected on the first one only.

[1] *M.N.*, **95**, 207, 1934.

[2] B. Strömgren, *Erg. d. Exact. Natur.*, **16**, 508, 1937.

tion of state from the law $p = K_1\rho^{5/3}$ to the law $p = (k/\mu H)\rho T$. The exact equation of state, neglecting relativity effects, can be written as

$$\rho = 2\frac{(2\pi mkT)^{3/2}}{h^3}\mu H\, U_{1/2}(A)\,, \tag{1}$$

$$p = 2\frac{(2\pi mkT)^{3/2}}{h^3}kT\, U_{3/2}(A)\,, \tag{2}$$

where $U_\rho(A)$ is a function of A defined by

$$U_\rho = \frac{1}{\Gamma(\rho+1)}\int_0^\infty \frac{u^\rho du}{\frac{1}{A}e^u + 1}\,. \tag{3}$$

To be able to study the structure of stellar configurations based on the equation of state parametrically expressed by (1) and (2), we should have to make an assumption concerning the circumstances determining the temperature gradient and the energy-source distribution. We shall consider two cases: (*a*) an isothermal gas sphere, and (*b*) the standard model.

a) We can show that the structure of an isothermal gas sphere based on (1) and (2) is governed by the differential equation

$$\frac{1}{\xi^2}\frac{d}{d\xi}\left(\xi^2\frac{d\psi}{d\xi}\right) = -U_{1/2}(e^\psi)\,, \tag{II}$$

where

$$\psi = \log A \tag{4}$$

and ξ is the radius vector in a suitably chosen scale. We easily verify that, as $A \to 0$, equation (II) reduces to the usual Emden isothermal equation. On the other hand, if $\log A \gg 1$, equation (II) reduces to the Emden equation of index $n = 3/2$. A study of the configurations based on (II) should be of importance in following up certain cosmological speculations by Eddington.[3]

[3] *Proc. Roy. Soc., London*, A, **111**, 424, 1925.

b) For the "standard model" ($p_{\text{gas}} : p_{\text{rad}} = \beta : 1 - \beta = \text{Constant}$), we find that the structure will be governed by solutions of the differential equation

$$\frac{1}{\xi^2}\frac{d}{d\xi}\left(\xi^2 U_{3/2}^{2/3}\frac{d\psi}{d\xi}\right) = -U_{3/2}U_{1/2}\,, \tag{III}$$

where ψ is defined as in (4) and ξ in a suitably chosen scale is the radius vector. Again one can show that, as $A \to 0$, equation (III) reduces to the Emden equation of index 3; while for $\log A \gg 1$, equation (III) reduces to the Emden equation of index $n = 3/2$. Equation (III), then, generalizes the usual standard model for stars of small mass and with incipient degeneracy in the central regions.

Finally, we may consider an isothermal gas sphere at such high temperatures that, if and when degeneracy sets in, it is already relativistic. For such configurations we can show that the differential equation governing the structure is

$$\frac{1}{\xi^2}\frac{d}{d\xi}\left(\xi^2\frac{d\psi}{d\xi}\right) = -U_2\,. \tag{IV}$$

Configurations described by (IV) may be of importance in considerations relating to the ultimate fate of massive stars.

The problems suggested in this preliminary note will be examined in detail in a future communication.

S. CHANDRASEKHAR

YERKES OBSERVATORY
November 1937

REVIEWS

Cosmological Theory. By G. C. McVittie. London: Methuen & Co., 1937. Pp. viii+103. 2*s.* 6*d.*

Dr. McVittie has here presented the relativistic theory of cosmology, together with its observational and theoretical background, in a little monograph of one hundred pages. The observational data on extra-galactic nebulae, chiefly from the work of Hubble, Humason, and Shapley, are sketched in the ten pages of chapter i. This is followed in chapter ii with a twenty-page exposition of tensor analysis and its application to Riemannian geometry, and by a short chapter iii on the principles of general relativity. The twenty-odd pages of chapter iv are devoted to the main purpose of the book—a concise account of the theory of the expanding universe of general relativity and a comparison of the resulting observational relations with the empirical data. It is rather surprising to find here no mention of the important pioneer work of Friedmann in this field. The final chapter, v, of the book presents the essential elements of Milne's kinematical theory of the universe in terms of a model whose space-time structure is that of one of the less well-known forms of the De Sitter universe, and concludes with an impartial statement of the aims and difficulties of Milne's proposed theory of gravitation.

With certain reservations Dr. McVittie's monograph may be recommended as an admirable presentation of cosmological theory with a minimum of mathematical equipment. For the most part the exceptions are perhaps mere matters of taste—as, for example, the inclusion of two sections on absolute parallelism in chapter ii and the presentation of Milne's theory in terms of the more complicated De Sitter universe in place of the simpler Minkowski space-time. A more thorough discussion of co-ordinates and measurement in special relativity might profitably have replaced the oversimplified, and even misleading, treatment of these matters in general relativity. But the only serious criticism is to be leveled against McVittie's treatment of Hubble's $N(m)$ relationship, giving the number N of nebulae up to limiting apparent magnitude m. This treatment, which is essentially that of his recent paper in *M.N.*, **97**, 163, 1937, completely ignores the dispersion in absolute magnitude of the nebulae,

and has subsequently been answered in detail by Hubble in *ibid.*, page 506, 1937. In this respect McVittie, in common with Eddington, Vogt, and most others who have criticized Hubble's treatment of the observational data, fails adequately to take into account the developments contained in the fundamental paper by Hubble and Tolman, in *Ap. J.*, **82**, 391, 1935, on observational relations in relativistic cosmology.

H. P. ROBERTSON

Princeton University

Die mathematischen Hilfsmittel des Physikers. By E. MADELUNG: 3d ed. Berlin: Springer, 1936. Pp. xiii+381. $10.

The introduction of more and more complex mathematical manipulations into the domain of physics is partly responsible for the popularity of handbooks of mathematical formulae. Though many mathematicians will continue to look askance at possessors of handbooks, there are many physicists who find Madelung's *Hilfsmittel* indispensable. They will welcome the third edition of this book with its one hundred additional pages, its thoroughly revised section on quantum mechanics, and its chapter on group theory.

One suggestion is made here for improving this very useful book. In addition to the excellent general references at the end of the present edition more page references might be included in the body of the book.

W. B.

ERRATUM

The scale of Plate VII, Volume **86**, of this *Journal*, accompanying the article by Harlow Shapley and John S. Paraskevopoulos on "The Nuclear Star Cluster in 30 Doradus," is incorrectly given as 1 mm = 70″.2. It should be 1 mm = 9″.7.

INDEX TO VOLUME 86

SUBJECTS

AUTHORS